Resonanztunneln in mesoskopischen Systemen

Diplomarbeit
von
Jürgen König

Institut für Theoretische Festkörperphysik
Universität Karlsruhe
Oktober 1995

Referent: Prof. Dr. Gerd Schön
Korreferent: Prof. Dr. Gergely Zimanyi

Contents

Chapter 1

Introduction

Electronic quantum transport through mesoscopic islands has been the subject of extensive experimental and theoretical research [1, 2, 3]. It includes transport through discrete energy levels in quantum dots [4, 5, 6, 7, 8, 9, 10, 11, 12, 13, 14, 15, 16, 17] as well as transport through a continuum of energy levels in small metallic islands [1, 2, 3, 18, 19, 20, 21, 22]. Structured two-dimensional electron gases (2 DEG) in semiconductor heterostructures ($GaAs/Al_xGa_{1-x}As$) provide a realization of a quantum dot [13, 14, 15, 16]. Recently, it has become possible to fabricate tunnel systems with ultra small metallic particles which show discrete electronic states [17].

Model systems are the electron box and the single electron transistor. The box consists of a small island coupled via a tunnel junction to a lead. It is further coupled capacitively to a voltage source, the gate. The single electron transistor consists of a small island coupled via tunnel junctions to two leads. An applied transport voltage V drives a current through the system. Here as well, the island is coupled capacitively to a further voltage source, the gate. The small size of the systems implies a small island capacitance C. Therefore, the Coulomb interaction of the electrons on the island becomes relevant. This interaction is described in terms of the electrostatic energy of the whole system, the *charging energy* $E_{ch}(n) = E_C(n - n_x)^2$ with $E_C \equiv e^2/2C$ [1, 2, 3]. The charging energy depends on the number of excess electrons n on the island and on the continuously varying variable n_x which can be tuned by the gate voltage. At low temperature the electron number on the island takes the value which minimizes the charging energy. It, therefore, increases in steps of unity when the gate voltage is increased.

Tunneling processes in the transistor are only possible in lowest order perturbation theory if either the temperature or the transport voltage is sufficient to overcome the energy difference of two adjacent charge states. Therefore, transport at low temperatures and voltages (i.e. for $k_BT \ll E_C$ and $eV \ll E_C$) depends strongly on the gate voltage. It can be allowed or suppressed (*Coulomb blockade*). As a consequence, the differential conductance shows in linear response a series of peaks as a function of the gate voltage (*Coulomb oscillations*). In nonlinear response, i.e., at larger transport voltage, these peaks show further structure.

A master-equation description of sequential tunneling [1, 2, 3, 4, 5, 6, 7] is sufficient as long as the coupling of the leads to the island is weak and the temperature and transport voltage are not too small. In this regime, transport occurs in sequences of uncorrelated tunneling processes. In one process an electron enters the island from the lead with higher electrochemical potential and then, in a second process, an electron goes from the island to the lead with lower electrochemical potential. Thus, electrons are transferred one by one while two adjacent charge states are involved. The corresponding rates are obtained in lowest-order perturbation theory in the tunneling amplitudes. The master equation allows us then to evaluate the probabilities for different island states and the current through the system.

In general, quantum fluctuations and higher-order coherent tunneling processes should be considered [8, 9, 10, 11, 12, 19, 20, 21, 22]. This includes "cotunneling" [23], in which in a second-order coherent process electrons tunnel via a virtual state of the island directly from one lead to the other, thus avoiding the Coulomb blockade. Furthermore, "resonant tunneling" plays a role. It contains coherent processes with an arbitrary number of tunneling events in both junctions. In comparison to the well known phenomenon of resonant tunneling of single electrons one encounters two complications. One lies in the fact that metallic systems with a continuous excitation spectrum contain many electrons, and therefore with overwhelming probability, different electron states are involved in the different transitions of one coherent process. The second arises because the influence of the Coulomb interaction is strong and, hence, cannot be accounted for in perturbation theory.

We distinguish two classes of higher-order tunneling processes: if no electron-hole excitation remains on the island after the whole process then we call it *elastic*, otherwise we call it *inelastic*. While in metallic systems inelastic processes dominate, in quantum dots with high level spacing elastic processes are more important.

The quantum dot with only one energy level is equivalent to the Anderson model. For a low lying level, the Anderson model can be mapped by a Schrieffer-Wolff transformation onto the Kondo model which describes scattering of electrons in a metal by the spin of magnetic impurities. At low temperatures, the interaction of the spin of the conductance electrons with the spin of the impurity leads to an increase of the resistivity (Kondo effect). In the Anderson model the Kondo effect shows up as an increase of the transmittivity through the dot, expressed by a spectral density with sharp resonances near the Fermi levels of the leads. The understanding of this effect requires an investigation beyond perturbation theory, i.e., only resonant tunneling processes are sufficient for an explanation.

A description is called for which allows a systematic classification of all these processes. In the case of a single energy level, furthermore, the description of the Kondo effect, generalized to nonequilibrium situations, should be included.

The purpose of this work is to develop a systematic diagrammatic technique to identify the processes of single electron tunneling, cotunneling and resonant tunneling and to examine their influence on the transport properties of the single electron transistor [22, 24, 25, 26, 27]. The description of the system is based on a standard

tunneling Hamiltonian. We study the reduced propagator, which governs the time evolution of the density matrix, by using a many-body expansion technique. For metallic systems we also use an alternative approach in a real-time path-integral representation. The latter is similar to techniques used in Refs. [28, 29], in which a quantum system coupled to a harmonic oscillator bath has been considered and in Refs. [18, 30], in which electron tunneling has been described.

The quantum fluctuations represented by resonant tunneling processes influence the spectral density which describes the excitations of the system. The real and imaginary part of an energy-dependent self-energy causes renormalization and finite life-time broadening effects. The system exhibits Kondo physics, which is indicated by logarithmic singularities in the real part of the self-energy. The physical quantities of interest, the probability distribution of the island states and the current through the system can be expressed in terms of the spectral density and, therefore, display renormalization and broadening effects as well.

This thesis is organized as follows:

A description of the single electron transistor as well as a qualitative picture of its transport properties is given in Chapter 2. We introduce the tunneling Hamiltonian for the two limiting cases of a discrete excitation spectrum and a continuous one.

In Chapter 3, we expand the reduced propagator in the tunneling part of the Hamiltonian and describe each term of the expansion in a diagrammatic language. All tunneling processes mentioned above can then be related to corresponding diagrams.

In Chapter 4 and Chapter 5, we derive analytic formulas for the spectral density and, thus, for the average charge on the island and the current through the system. To do so, we use a systematic criterion to select the most important class of diagrams and then sum up all these contributions.

The influence of renormalization and broadening effects on the physical quantities of interest is discussed in Chapter 6. As a result, the plots of the average charge on the island and the differential conductance as a function of the gate voltage are washed out. Furthermore, for systems with discrete energy levels the whole curve is shifted. In this case the quantum fluctuations give rise to the Kondo effect. For a low-lying energy level, we see sharp resonances near the Fermi levels. They lead to a maximum [11, 12, 41] of the conductance at zero transport voltage (zero-bias maximum). Interestingly, however, we find that for the level lying near or above the Fermi levels the logarithmic terms in the real part of the self-energy are still important and lead to an inversion of the whole structure in the conductance, i.e., to a zero-bias minimum.

The diagrammatic technique presented here is very general and can therefore be applied to more complex systems. As an example, we discuss in Chapter 7 an extension of the method to a quantum dot including bosonic interactions [26, 27, 31, 32, 33, 34, 35]. The bosons lead to a further splitting of the Kondo peaks, the conductance as a function of the gate voltage shows new side peaks and the zero-bias extrema are accompanied by side extrema. Remarkably, we find Kondo peaks due

to different emission and absorption probabilities of the bosons even in the case of a nondegenerate level.

Some technical details concerning the derivation of the effective action for metallic systems, the solution of the integral equation appearing in Chapter 4, the calculation of the self-energy and the special case of a dot with one non-degenerate level are presented in the appendices.

In order to keep all formulas transparent, we put $\hbar = 1$ throughout this work.

Chapter 2

Quantum Transport through the Single Electron Transistor

We start with a description of the system of interest, the single electron transistor. Then the concept of charging energy, which describes the electrostatic energy of the system, is introduced. With the help of this concept, we can draw a qualitative picture of the transport properties through the transistor. We identify several different processes contributing to the current as single electron tunneling (SET), cotunneling and resonant tunneling. A more quantitative understanding of the current-voltage characteristic can only be achieved, if one has more information about the excitation spectrum of the island. We consider the two limiting cases of a discrete excitation spectrum or a continuous one, which is usually realized in quantum dots or metallic islands, respectively. In the second part of this chapter, we introduce the model Hamiltonian for each case and consider then the reduced propagator, which determines the time evolution of the density matrix.

2.1 The Single Electron Transistor

The single electron transistor consists of a small island which is coupled via tunnel junctions to two leads (see Fig. 2.1). An applied transport voltage V drives a current through the island. Electrons from the lead with higher electrochemical potential, say the left one, reach the other, the right one. The simplest process contributing to the current is the tunneling of one electron through one junction. This process is called "single electron tunneling" (SET). For a complete transport cycle we need two single electron tunneling events: an electron enters the island via the the left tunnel junction and then an electron (the same or an other one) leaves the island via the right tunnel junction. Afterwards, the next cycle can start. Thus, electrons are transferred one by one, and therefore this situation is called "sequential tunneling". An important condition to allow these processes is, that the number of electrons in the island can change. To decide if this is possible, we have to compare the relevant

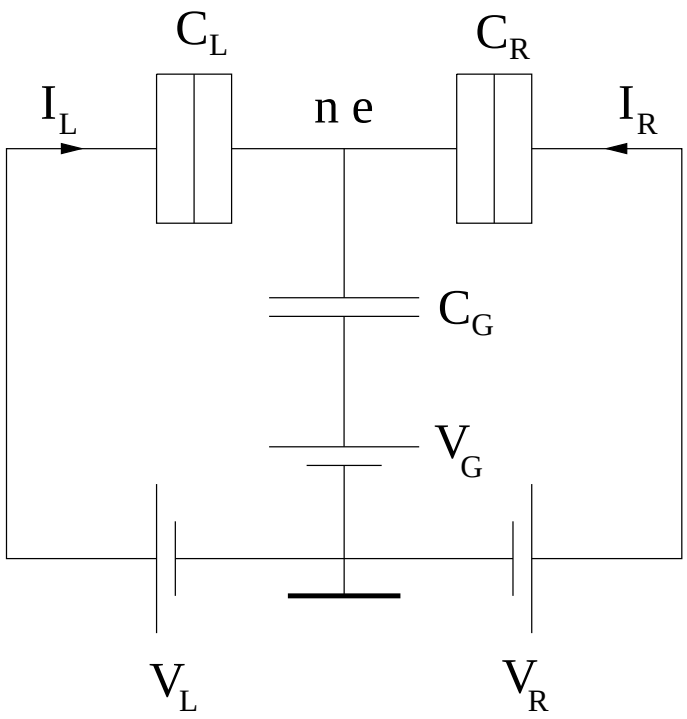

Figure 2.1: The SET transistor.

energies. The electrostatic energy of the system, the charging energy, plays a central role.

2.2 Charging Energy and Coulomb Oscillations

The Coulomb interaction of the electrons has to be accounted for in some way. This is done here within a capacitive model. In addition to the ability to transmit electrons, the tunnel junctions are characterized by a capacitance C_r, where $r = L, R$ denotes the left and right lead, respectively. Furthermore, the island is coupled capacitively via C_G to a third electrode, the gate. The charge on the island, described by the number of excess electrons n, is distributed among the three capacitors, which, therefore, contain energy. The relevant free energy is a Legendre transform of this energy, which also includes the work done by the voltage sources. The result, up to a contribution which does not depend on the variable n, is [1]

$$E_{ch}(n) = E_C(n - n_x)^2 \,, \tag{2.1}$$

which is called *charging energy*. Here, $en_x = C_L V_L + C_R V_R + C_G V_G$ is independent of n and can be tuned continuously by the gate voltage V_G. The total island capacitance $C = C_L + C_R + C_G$ defines the energy scale for the charging energy

$$E_C \equiv \frac{e^2}{2C} \,. \tag{2.2}$$

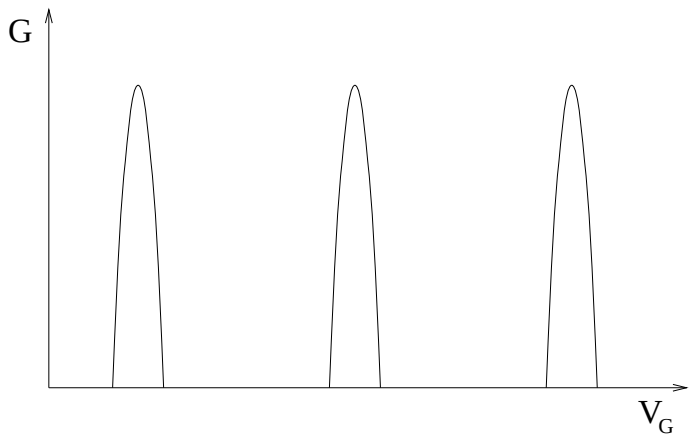

Figure 2.2: The Coulomb oscillations: the differential conductance shows a periodic structure as a function of the gate voltage.

In addition to the charging energy, one has to account for the single particle energy of the levels on the island. We denote the energy of the l-th electron state with ϵ_l.

Other energy scales are provided by the temperature, k_BT, and the transport voltage, eV. Besides the ground state of the system, in which the electron number n takes the value which minimizes the charging energy, other charge states m are allowed only if either the temperature or the transport voltage can overcome the difference $E_{ch}(m) - E_{ch}(n) + \sum_{l=n+1}^{m} \epsilon_l$. (Typically, the energy scale of the single particle energies is much smaller than E_C. Therefore, the main features are determined by the charging energy. The single particle energies of the level on the island lead only to minor corrections.) For small systems the Coulomb interaction becomes relevant. In our model this is expressed by small capacitances. It is clear from Eq. (2.1) that for

$$E_C \gg \max\{k_BT, eV\} \tag{2.3}$$

only two situations are possible, depending on the gate voltage:
(i) the island charge is fixed or
(ii) two adjacent electron numbers n and $n+1$ are allowed.
In the first case, the simplest process described above gives no contribution to the current. The transport is suppressed (*Coulomb blockade*), since the intermediate state with increased or decreased island charge is energetically forbidden. In the second case, a current flows by electrons entering and leaving the island alternately. Since at most two charge states are allowed, the electrons have to pass one by one. There are no processes with two or more electrons entering or leaving the island simultaneously. By tuning the gate voltage, one can decide which situation is realized. The current and therefore the conductance $G = \partial I/\partial V$ shows a periodic structure as a function of V_G (see Fig. 2.2), called *Coulomb oscillations*. These features justify the name *single electron transistor*.

2.3 Higher-Order Contributions

Besides single electron tunneling (see Figs. 2.3a and 2.4a) there are more complicated processes of higher order, which become crucial if single electron tunneling is suppressed by Coulomb blockade. An electron enters and an electron leaves the island within one coherent process, during which the island charge is never increased or decreased *really* but only *virtually*. This process, called "cotunneling", is responsible for the current in the Coulomb blockade regime (see Figs. 2.3b and 2.4b).

In general, there are coherent processes with an arbitrary number of tunneling events at both junctions. The sum of all these contributions (including single electron tunneling and cotunneling) is called "resonant tunneling" (for illustration see Figs. 2.3c and 2.4c).

The purpose of this work is to describe the effect of resonant tunneling in situations near the resonances in Fig. 2.2. Then, only two charge states need to be considered, i.e., in addition to the condition (2.3) the energy difference of two adjacent charge states has to be small compared to E_C.

2.4 The Two Limits: Quantum Dot and Metallic Island

The concept of charging energy is sufficient to explain the Coulomb oscillations. Detailed features of the transport characteristics, however, are determined by the properties of the island, especially the excitation spectrum. In the following, we consider the two limiting cases of
(i) a discrete spectrum with high level spacing and
(ii) a spectrum with small level spacing, so that the spectrum can be assumed to be continuous.

The first case is given in quantum dots consisting of a structured 2 DEG (two-dimensional electron gas) in semiconductor heterostructures. It is possible to manufacture dots with a lateral dimension in the order of the Fermi wave length ($\lambda_F \approx$ 50nm) and therefore to see a finite level spacing.

The second case is realized in systems with small metallic islands, where the size of the system typically exceeds the Fermi wave length ($\lambda_F \approx$ 1nm). Recently, it became possible to fabricate tunnel systems with metallic islands which are small enough to show discrete energy levels [17], so that this system belongs to the first case. Nevertheless, we use here the expression "metallic island" as a synonym for a tunnel system with a continuous spectrum.

The leads are macroscopic and therefore have always a continuous spectrum.

2.4.1 Discrete Spectrum (Quantum Dot)

If the level spacing exceeds the temperature and the transport voltage, only one level on the island is involved in resonant tunneling processes. (This level can be degenerate, e.g. due to spin degrees of freedom.) Fig. 2.3 shows some possible processes at zero temperature using an energy diagram. On the left and right hand side, describing the left and right lead, respectively, there is a continuum of states which are filled up to the Fermi level. Due to an applied transport voltage, the Fermi level of one lead is higher than the Fermi level of the other lead. In the middle part of the diagram, describing the island, we draw only one energy level. The position of the level describes the energy of an occupied dot, including the charging energy.

Single Electron tunneling is possible, if the level lies within the energy window given by the transport voltage (Fig. 2.3a).

Otherwise, the simplest process is cotunneling, in which an electron tunnels through in a coherent way (Fig. 2.3b). Entering the island from one lead costs energy (indicated by the arrow going up), but this will be regained after leaving the island to the other lead (indicated by the arrow going down). After the whole process, energy is conserved.

In generalization, an arbitrary number of tunneling events are involved in a resonant tunneling process (Fig. 2.3c). Also here, energy conservation of the *whole* process must hold.

This picture remains valid at finite temperature, with the modification that there are some occupied states above and unoccupied states below Fermi level.

Transport through the dot is trivially *elastic*, since only one level is involved and therefore no electron-hole excitations can remain on the island.

2.4.2 Continuous Spectrum (Metallic Island)

In the other limiting case, the level spacing on the island is less than any other energy scale. Then, the states in the island build up a continuum like in the leads. Like above, it is possible to visualize processes with the help of an energy diagram, in which the position of the levels in the island includes the charging energy (Fig. 2.4).

Single Electron tunneling, cotunneling and resonant tunneling are described in a similar way as before. But now in higher-order processes, with overwhelming probability, different states on the island are involved. This leads to electron-hole-excitations on the island. Such processes are therefore called *inelastic*.

2.5 Hamiltonian and Density Matrix

The single electron transistor is described by the standard tunneling Hamiltonian $H = H_0 + H_T$, in which H_0 describes the decoupled system and H_T the tunneling between the leads and the island. We calculate physical quantities like current

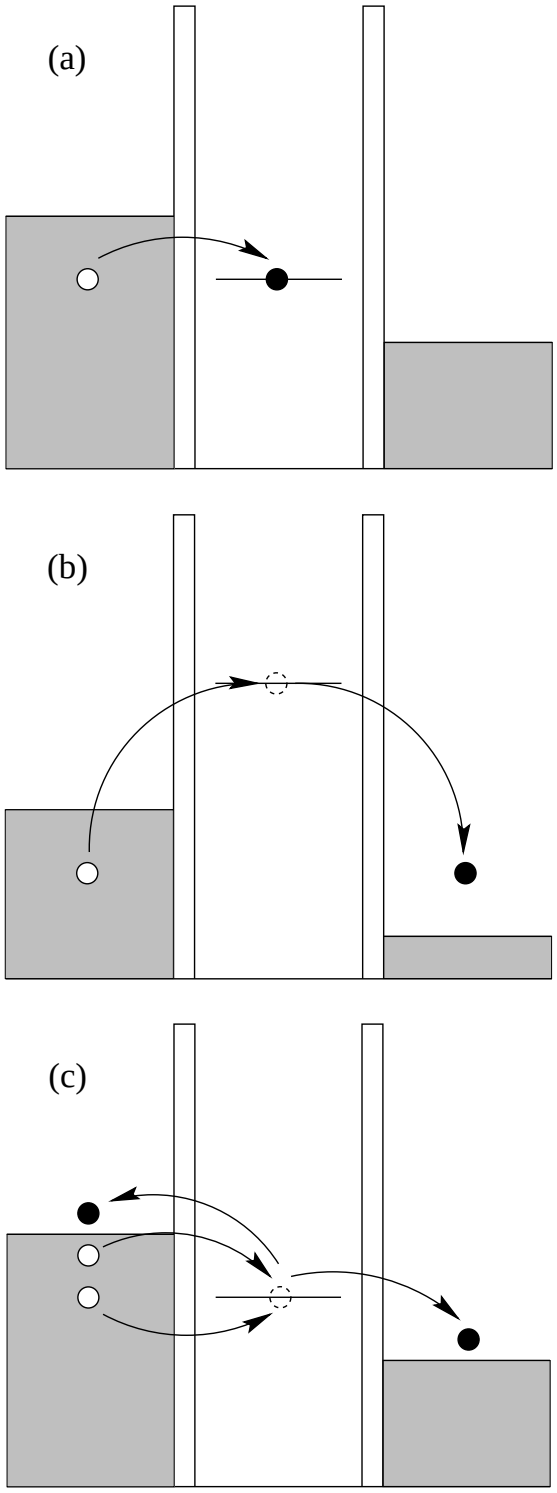

Figure 2.3: Different processes contributing to the current through a quantum dot: an example of a) single electron tunneling, b) cotunneling and c) resonant tunneling. All processes are elastic since only one level is involved and therefore no electron-hole excitation remains on the island.

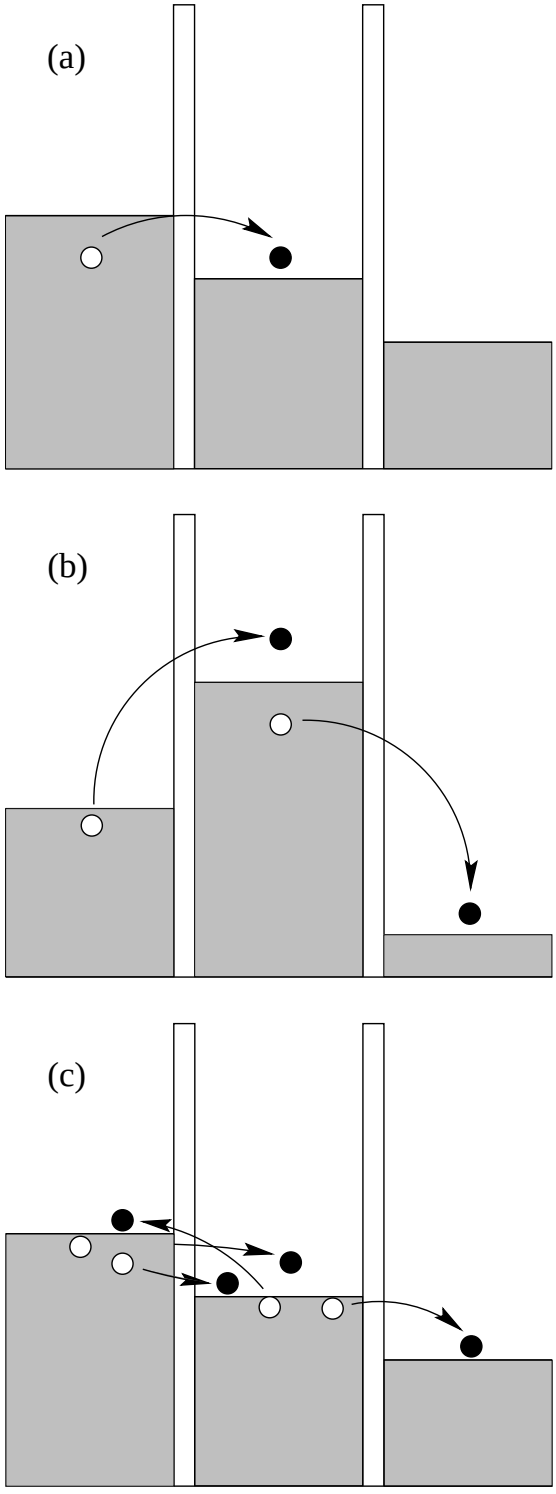

Figure 2.4: Different processes contributing to the current through a metallic island: an example of a) single electron tunneling, b) cotunneling and c) resonant tunneling. All processes are inelastic.

and occupancy probabilities as quantum statistical expectation values of the corresponding operators using the density matrix and its time evolution. However, the density matrix provides much more information than it is needed to examine transport properties. Therefore, we partially trace out most degrees of freedom and obtain a reduced density matrix, which describes only the state of the island.

2.5.1 Discrete Spectrum: Anderson Model

Since in our considerations only one level in the dot is involved, we describe here the system by an Anderson Hamiltonian

$$H = H_L + H_R + H_D + H_{T,L} + H_{T,R} \tag{2.4}$$

in which

$$H_r = \sum_{k\sigma} \epsilon_{k\sigma r} a^\dagger_{k\sigma r} a_{k\sigma r} \tag{2.5}$$

describes noninteracting electrons in the left and right lead, for $r = L, R$ respectively, and the dot Hamiltonian is given by

$$H_D = \epsilon_0 \sum_\sigma c^\dagger_\sigma c_\sigma + U \sum_{1\le\sigma<\sigma'\le M} n_\sigma n_{\sigma'}. \tag{2.6}$$

We have used here creation (annihilation) operators for the leads $a^\dagger_{k\sigma r}$ ($a_{k\sigma r}$) and for the dot $c^\dagger_\sigma$ (c_σ), and $\sigma = 1, \ldots, M$ denotes the spin and k labels the states. Furthermore, $n_\sigma = c^\dagger_\sigma c_\sigma$ is the number of electrons with spin σ on the dot, ϵ_0 is the level position and U describes the Coulomb repulsion. The influence of the gate voltage in the capacitance model is absorbed into the level position ϵ_0. For this reason, there is no explicit term for the gate. The terms (2.5) and (2.6) are collected in $H_0 = H_L + H_R + H_D$. The other part of the Hamiltonian $H_T = H_{T,L} + H_{T,R}$ couples the dot with the left and right lead:

$$H_{T,r} = \sum_{k\sigma} \left(T^r_k a^\dagger_{k\sigma r} c_\sigma + h.c. \right) \tag{2.7}$$

with spin independent tunneling matrix elements T^r_k for barrier $r = L, R$.

A quantum-statistical expectation value of an operator A at time t is given by

$$\langle A(t) \rangle = \mathrm{tr}[\rho_0 A(t)_H], \tag{2.8}$$

where $A(t)_H = \exp(iHt) A \exp(-iHt)$ is the operator in Heisenberg picture. Permutation under the trace yields

$$\langle A(t) \rangle = \mathrm{tr}[\rho(t) A] \tag{2.9}$$

with A in Schrödinger picture. The density matrix $\rho(t)$ evolves in time via

$$\rho(t) = e^{-iHt} \rho(t_i) e^{iHt}. \tag{2.10}$$

We assume that the initial density matrix $\rho_0 = \rho(t_i)$ factorizes into three parts for the left and right lead and the dot:

$$\rho_0 = \rho_0^L \rho_0^R \rho_0^D . \tag{2.11}$$

The leads are treated as large equilibrium reservoirs with fixed electrochemical potentials $\mu_r = -eV_r$, $r = L, R$. Therefore, we describe the electrons in the leads by Fermi functions $f_r(E) = 1/[\exp(\beta(E - \mu_r)) + 1]$ and the density matrix reads

$$\rho_0^r = \frac{1}{Z_0^r} \exp\left[-\beta(H_r - \mu_r n_r)\right] \tag{2.12}$$

where $\beta = 1/k_B T$ and $n_r = \sum_{k\sigma} a^\dagger_{k\sigma r} a_{k\sigma r}$ the number of electrons in the lead r with $r = L, R$. The normalization factor Z_0^r is determined by $\operatorname{tr} \rho_0^r = 1$. For the initial distribution of the dot states we assume that it is diagonal in the occupation numbers:

$$\rho_0^D = \sum_\chi P_\chi^0 |\chi\rangle\langle\chi| \tag{2.13}$$

with $\sum_\chi P_\chi^0 = 1$, where the many-body *dot* states are labeled by $|\chi\rangle$. We will see later, that in the stationary limit, i.e., when t_i is shifted to minus infinity, all the physical quantities are independent of the choice of P_χ^0.

In the following, it is convenient to change to the interaction picture with respect to H_0. This implies $A(t)_I = \tilde{T} \exp\left(-i \int_t^{t_i} dt' \, H_T(t')_I\right) A(t)_H \, T \exp\left(-i \int_{t_i}^t dt' \, H_T(t')_I\right)$ in which the time-ordering operator T orders the operators in such a way that each operator lies on the right hand side of all operators with a later time. The anti-time-ordering operator orders the operators in the opposite way. Then we find

$$\langle A(t)\rangle = \operatorname{tr}\left[\rho_0 \, T_K \exp\left(-i \int_K dt' H_T(t')_I\right) A(t)_I\right] . \tag{2.14}$$

Here, we wrote the two integrals $\int_{t_i}^t dt' \ldots$ and $\int_t^{t_i} dt' \ldots$ as one contour integral $\int_K dt' \ldots$ (over the *Keldysh contour*), forward from t_i to t and then backward from t to t_i. We furthermore introduced the Keldysh time-ordering operator T_K, which orders all following operators such that the leftmost operator is the one with the latest "time" with respect to the Keldysh contour and the rightmost is the earliest one. The "time" now labels the physical time and in addition the information, on which part of the contour the corresponding operator lies.

The only part of the system which is not in equilibrium is the dot. Therefore, we are only interested in operators A which do not depend on electron operators of the leads, i.e. $A = A(c, c^\dagger)$. The trace over the leads does not influence $A(t)_I$ in this case and we can write

$$\langle A(t)\rangle = \operatorname{tr}_D[\rho_0^D \Pi A(t)_I] = \sum_\chi P_\chi^0 \langle\chi|\Pi A(t)_I|\chi\rangle \tag{2.15}$$

in which

$$\Pi = \mathrm{tr}_L \ \mathrm{tr}_R \left[\rho_0^L \rho_0^R \, T_K \exp\left(-i \int_K dt' H_T(t')_I \right) \right] \tag{2.16}$$

describes the propagation of the reduced system (the dot), including a forward and a backward propagator in time, which become coupled due to the trace over the leads. As we will see in Chapter 3, when we derive the diagrammatic rules, we can perform this trace using Wick's theorem, since the Hamiltonian H_0 is bilinear in the lead electron operators. The Coulomb interaction is expressed in terms of dot electron operators and therefore poses no problem. Notice, that the time-ordering operator acts on *all* operators on the right, i.e., it acts on $A(t)_I$ as well.

The matrix element which describes the propagation from the dot state χ_1 at time t_i forward to state χ_1' at time t and then backward from χ_2' to χ_2 is

$$\Pi^{\chi_1,\chi_1'}_{\chi_2,\chi_2'} = \langle \chi_2 | \Big[\Pi(|\chi_2'\rangle\langle\chi_1'|)(t)_I \Big] |\chi_1\rangle = \tag{2.17}$$
$$\mathrm{tr}_L \ \mathrm{tr}_R \left[\langle \chi_2 | \, \tilde{T} \exp\left(-i \int_t^{t_i} dt' H_T(t')_I \right) |\chi_2'\rangle\langle\chi_1'| \, T \exp\left(-i \int_{t_i}^{t} dt' H_T(t')_I \right) |\chi_1\rangle \right] .$$

In order to calculate the current through the dot, we will make use of correlation functions $\langle A(t_1)B(t_2)\rangle$, in which A and B are independent of lead electron operators. The ordering of the operators implies $t_1 > t_2$ with respect to the Keldysh contour. Very analogous to the quantum-statistical expectation value of one operator we get

$$\begin{aligned} \langle A(t_1)B(t_2)\rangle &= \mathrm{tr}[\rho_0 A(t_1)_H B(t_2)_H] \\ &= \mathrm{tr}_D[\rho_0^D \Pi A(t_1)_I B(t_2)_I] \\ &= \sum_\chi P_\chi^0 \langle \chi | \Pi A(t_1)_I B(t_2)_I | \chi \rangle . \end{aligned} \tag{2.18}$$

2.5.2 Continuous Spectrum: Path-Integral Approach

For a continuous spectrum on the island the Hamilton reads

$$H = H_0 + H_T \tag{2.19}$$
$$H_0 = H_L + H_R + H_I + H_{ch} \tag{2.20}$$
$$H_T = H_{T,L} + H_{T,R} \tag{2.21}$$

with

$$H_r = \sum_{kn} \epsilon_{knr} a^\dagger_{knr} a_{knr} \tag{2.22}$$

for the left and right lead, $r = L, R$ respectively,

$$H_I = \sum_{qn} \epsilon_{qn} c^\dagger_{qn} c_{qn} \tag{2.23}$$

for the electrons on the island and

$$H_{T,r} = \sum_{kqn} \left(T^{rn}_{kq} a^\dagger_{knr} c_{qn} + h.c. \right) \tag{2.24}$$

for the tunneling between island and leads, $r = L, R$. The tunnel matrix elements $T^{rn}_{kq} = T^{rn}$ are considered independent of the states k and q. They can be related to the tunnel resistances R_r of the left and right junction

$$\frac{1}{R_r} = \frac{2\pi e^2}{\hbar} \sum_n N^n_r(0) N^n_I(0) |T^{rn}|^2, \tag{2.25}$$

where $N_I(0)$ is the densities of states of the island and $N_r(0)$ are the density of states of the leads, $r = L, R$.

We assume that the junctions, although small, still accommodate many transverse channels labeled by the index n, which includes the spin. From a comparison of Andreev reflection and single electron tunneling in small normal-superconducting junctions one can conclude that for a typical system the number of channels is $N_{ch} \geq 10^3$.

The Coulomb interaction is described in our model by an effective capacitive interaction. The charging energy Hamiltonian is just the operator form of Eq. (2.1)

$$H_{ch} = \frac{e^2}{2C} \left(\sum_{qn} c^\dagger_{qn} c_{qn} - n_x \right)^2 . \tag{2.26}$$

Here, we used $n = \sum_{qn} c^\dagger_{qn} c_{qn}$.

Since the gate only influences the charging energy and does not participate in tunneling, we need no term describing the gate electrons.

Now, in contrast to the Anderson model, the labels describing the many-body eigenstates of the island provides much more information than necessary to examine transport properties through the whole system. The only information we need is the number of excess electrons on the island. Furthermore, the Hamiltonian describing Coulomb interaction contains quartic terms in the island electron operators. Therefore, we cannot proceed like above for the Anderson model and trace out the microscopic degrees of freedom using Wick's theorem.

Instead, we consider the propagator

$$\mathbf{1} = T_K \exp\left(-i \int_K dt\, H(t) \right) . \tag{2.27}$$

In order to handle the interaction, we perform a Hubbard-Stratonovich transformation. It introduces the electrostatic potential of the island $V(t)$ as a macroscopic field. The capacitive interaction between electrons is replaced in this way by an interaction of the electrons with the collective variable. We can, therefore, treat the island as well as the leads as large equilibrium reservoirs with fixed electrochemical potentials $\mu_r = -eV_r$ for $r = L, R, I$. We define $\mu_I = 0$. The only fluctuating field is $V(t)$. The definition

$$V(t) \equiv -\frac{\dot{\varphi}(t)}{e} \tag{2.28}$$

relates $V(t)$ to the phase $\varphi(t)$. Its quantum mechanical conjugate, the number of excess electrons $n(t)$ on the island, is a macroscopic field, which is treated independently of the degrees of freedom described by c_{qn} and $c_{qn}^\dagger$.

At this stage, the electronic degrees of freedom can be traced out. After this step, the system can no longer be described by a Hamiltonian. Instead, the reduced propagator is written as a path integral over the collective variable $\varphi(t)$

$$\Pi = \mathrm{tr}\left[\rho_0\, T_K \exp\left(-i\int_K dt H(t)\right)\right] = \int \mathcal{D}[\varphi(t)] \exp\left(iS[\varphi(t)]\right) . \tag{2.29}$$

Here, we used the effective action (for some details of the calculation see Appendix A)

$$S[\varphi(t)] = S_{ch}[\varphi(t)] + S_T[\varphi(t)] . \tag{2.30}$$

The first term represents the charging energy

$$S_{ch}[\varphi(t)] = \int_K dt \left(\frac{C}{2}\left(\frac{\dot\varphi(t)}{e}\right)^2 + n_x\dot\varphi(t)\right) . \tag{2.31}$$

We can write this term in the form

$$S_{ch}[\varphi(t)] = \sum_{r=L,R,G}\int_K dt\,\frac{C_r}{2}\left(V_r + \frac{\dot\varphi(t)}{e}\right)^2 , \tag{2.32}$$

which displays clearly how the expression for a single junction [18] has to be extended for the transistor: the effective action is the sum of the three contributions for a single capacitor with capacitance C_r, $r = L, R, G$ for the left and right lead and the gate. The voltage across the capacitor is $V_r - V(t) = V_r + \dot\varphi(t)/e$.

Electron tunneling is described by

$$S_T[\varphi(t)] = i\sum_{m=1}^{\infty}\sum_{r_1=L,R}\cdots\sum_{r_m=L,R}(2\pi)^{2m-1}\int_K dt_1\int_K dt_1'\ldots\int_K dt_m\int_K dt_m' \\ \underset{t_1<t_2,\ldots,t_m}{} \\ \alpha^K_{r_1,\ldots,r_m}(t_1,t_1',\ldots,t_m,t_m')e^{i\varphi(t_1)}e^{-i\varphi(t_1')}\ldots e^{i\varphi(t_m)}e^{-i\varphi(t_m')} , \tag{2.33}$$

in which $t_1 < t_2, \ldots, t_m$ with respect to the Keldysh contour ensures, that all terms of the sum are different. For each term of the sum we will draw in the diagrammatic language (see Fig. 3.2) a loop connecting $2m$ vertices. The tunneling term couples the forward and backward propagators. This arises in the step in which the microscopic degrees of freedom are eliminated. The value of $\alpha^K_{r_1,\ldots,r_m}(t_1,t_1',\ldots,t_m,t_m')$ is given in Appendix A. Because it is roughly proportional to the number of channels N_{ch}, the iteration of the simplest loop ($m = 1$) will dominate over more complicated loops for a wide junction with a large number of channels. In this case

$$S_T[\varphi(t)] = 2\pi i\sum_{r=L,R}\int_K dt\int_K dt'\alpha_r^K(t,t')e^{i\varphi(t)}e^{-i\varphi(t')} , \tag{2.34}$$

with $\alpha_r^K(t,t') = \alpha_r^+(t-t')$ for $t < t'$ and $\alpha_r^K(t,t') = \alpha_r^-(t-t')$ for $t > t'$ with respect to the Keldysh contour, and $\alpha_r^\pm(t)$ can be calculated from

$$\alpha_r^\pm(\omega) = \pm\alpha_0^r \frac{\omega - \mu_r}{\exp[\pm\beta(\omega-\mu_r)] - 1} \tag{2.35}$$

via Fourier transformation $\alpha_r^\pm(t) = \frac{1}{2\pi}\int d\omega e^{-i\omega t}\alpha_r^\pm(\omega)$.

The dimensionless parameter

$$\alpha_0^r = \frac{h}{4\pi^2 e^2 R_r} \tag{2.36}$$

measures the coupling strength of the island with lead $r = L, R$.

To evaluate the matrix element which describes the propagation from the state φ_1 at time t_i forward to state φ_1' at time t and then backward from φ_2' to φ_2, we fix the phases at these times in the path integral:

$$\Pi_{\varphi_2,\varphi_2'}^{\varphi_1,\varphi_1'} = \int_{\varphi_2,\varphi_2'}^{\varphi_1,\varphi_1'} \mathcal{D}[\varphi(t)] \exp\left(iS[\varphi(t)]\right) \ . \tag{2.37}$$

In order to calculate an expectation value of $A = A(\varphi)$ which depends only on the collective variable, we fix the phases φ_0 at time t_i and integrate then over all values of φ_0, weighted by an initial distribution P_{φ_0}

$$\langle A(t)\rangle = \int d\varphi_0 P_{\varphi_0} \Pi_{\varphi_0}^{\varphi_0} A \,. \tag{2.38}$$

An important step for a systematic description of tunneling processes is the change from the phase to a charge representation. I.e., quantum-statistical expectation values of $A = A(n)$ are calculated according to

$$\langle A(t)\rangle = \sum_{n_0} P_{n_0} \Pi_{n_0}^{n_0} A \,, \tag{2.39}$$

with an initial distribution P_{n_0} for the excess electron number on the island. The propagation from n_1 forward to n_1' and then from n_2' backward to n_2 is given by the matrix element

$$\begin{aligned}\Pi_{n_2,n_2'}^{n_1,n_1'} = \int d\varphi_1 \int d\varphi_1' \int d\varphi_2' \int d\varphi_2 \, e^{in_1\varphi_1} e^{-in_1'\varphi_1'} e^{in_2'\varphi_2'} e^{-in_2\varphi_2} \\ \int_{\varphi_2,\varphi_2'}^{\varphi_1,\varphi_1'} \mathcal{D}[\varphi(t)] \int \mathcal{D}[n(t)] \exp\left(-iS_{ch}[n(t)] + iS_T[\varphi(t)] + i\int_K dt\, n(t)\dot{\varphi}(t)\right) \ .\end{aligned} \tag{2.40}$$

The charging energy is now described by

$$S_{ch}[n(t)] = \int_K dt \, \frac{e^2}{2C}(n(t) - n_x)^2 \,. \tag{2.41}$$

Here, we have modeled the Coulomb interaction by a capacitive interaction between electrons and then performed a Hubbard-Stratonovich transformation, which introduced a collective variable φ. Due to this transformation, we arrived at a real-time path-integral formulation. In the next section we follow an alternative approach, which leads to the same diagrammatic rules.

2.5.3 Continuous Spectrum: Operator Approach

We separate the charge and fermionic degrees of freedom at the very beginning by introducing the phase operator φ, which is the canonical conjugate to the operator describing the number of excess electrons on the island n, i.e. $[\varphi, n] = i$. These operators, describing the charge degrees of freedom, are treated independently of the fermionic degrees of freedom, the field operators c_{ln} and $c_{ln}^\dagger$. The Hamiltonian is then given by

$$\begin{aligned} H &= H_0 + H_T && (2.42)\\ H_0 &= H_L + H_R + H_I + H_{ch} && (2.43)\\ H_T &= H_{T,L} + H_{T,R}\,, && (2.44) \end{aligned}$$

in which H_0 is the same as in the previous section. But now, the tunneling Hamiltonian includes a factor $e^{\pm i\varphi}$ which increases or decreases the number of excess electrons at each tunneling process,

$$H_{T,r} = \sum_{kqn} \left(T_{kq}^{rn} a_{knr}^\dagger c_{qn} e^{-i\varphi} + h.c. \right) \tag{2.45}$$

for $r = L, R$. This Hamiltonian is just the operator form of the corresponding expression in the path-integral approach (see A.10).

The path-integral approach is sufficient to describe the single electron transistor. We reformulate the problem within an operator approach since we are then able to proceed in the same way as for the Anderson model. Furthermore, we avoid path integrals and, therefore, all formulas become more compact.

An expectation value of an operator $A = A(\varphi)$ or $A = A(n)$ at time t is given by

$$\langle A(t) \rangle = \mathrm{tr}[\rho_0 A(t)_H]\,, \tag{2.46}$$

where we assume the initial density matrix $\rho_0 = \rho(t_i)$ to factorize into four parts for the left and right lead, the island fermionic degrees of freedom and the charge degrees of freedom:

$$\rho_0 = \rho_0^L \rho_0^R \rho_0^I \rho_0^n. \tag{2.47}$$

The leads and the island are treated as large equilibrium reservoirs with fixed chemical potentials $\mu_r = -eV_r$, $r = L, R, I$. We define $\mu_I = 0$. Therefore, we describe the electrons in the leads by Fermi functions $f_r(E) = 1/[\exp(\beta(E - \mu_r)) + 1]$ and the density matrix reads

$$\rho_0^r = \frac{1}{Z_0^r} \exp\left[-\beta(H_r - \mu_r n_r)\right]\,. \tag{2.48}$$

For the initial distribution of the dot states we assume only that it is diagonal in the occupation numbers:

$$\rho_0^n = \sum_n P_n^0 |n\rangle\langle n| \tag{2.49}$$

with $\sum_n P_n^0 = 1$.

Then we change to interaction picture with respect to H_0 and get

$$\langle A(t)\rangle = \mathrm{tr}\left[\rho_0\, T_K \exp\left(-i\int_K dt' H_T(t')_I\right) A(t)_I\right]. \tag{2.50}$$

In the next step, we trace out all fermionic degrees of freedom. The trace does not influence $A(t)_I$ and therefore we can write

$$\langle A(t)\rangle = \mathrm{tr}_n[\rho_0^n \Pi A(t)_I] = \sum_n P_n^0 \langle n|\Pi A(t)_I|n\rangle \tag{2.51}$$

where

$$\Pi = \mathrm{tr}_L\ \mathrm{tr}_R\ \mathrm{tr}_I\left[\rho_0^L \rho_0^R \rho_0^I\, T_K \exp\left(-i\int_K dt' H_T(t')_I\right)\right] \tag{2.52}$$

describes the propagation of the reduced system (the charge degrees of freedom on the island), including a forward and a backward propagator in time, which become coupled due to the trace over the leads. Due to the separation of fermionic and charge degrees of freedom the Hamiltonian H_0 is bilinear in the electron operators. For this reason Wick's theorem does apply and the performance of the trace poses no problem.

The matrix element which describes the propagation from the charge state n_1 at time t_i forward to state n_1' at time t and then backward from n_2' to n_2 is

$$\Pi_{n_2,n_2'}^{n_1,n_1'} = \langle n_2|\Big[\Pi(|n_2'\rangle\langle n_1'|)(t)_I\Big]|n_1\rangle = \tag{2.53}$$
$$\mathrm{tr}_L\ \mathrm{tr}_R\ \mathrm{tr}_I\left[\langle n_2|\,\tilde{T}\exp\left(-i\int_t^{t_i} H_T(t')_I dt'\right)|n_2'\rangle\langle n_1'|\,T\exp\left(-i\int_{t_i}^{t} H_T(t')_I dt'\right)|n_1\rangle\right].$$

Correlation functions $\langle A(t_1)B(t_2)\rangle$, in which A and B are independent of the electron operators, are given by

$$\begin{aligned}\langle A(t_1)B(t_2)\rangle &= \mathrm{tr}[\rho_0 A(t_1)_H B(t_2)_H] \\ &= \mathrm{tr}_n[\rho_0^n \Pi A(t_1)_I B(t_2)_I] \\ &= \sum_n P_n^0 \langle n|\Pi A(t_1)_I B(t_2)_I|n\rangle. \end{aligned}\tag{2.54}$$

Chapter 3

Diagrammatic Expansion

In this chapter, we derive the diagrammatic rules for the evaluation of the transport properties. We expand the reduced propagator introduced in the previous chapter with respect to the tunneling part of the Hamiltonian. Each term of the expansion can be visualized by a diagram. Rules for the evaluation of the diagrams are formulated in time space and, in the stationary limit, in energy space. The propagator can be expressed as an iteration in the style of a Dyson equation using irreducible self-energy parts. In the stationary limit, we derive a Master equation for the distribution function of the island states. The irreducible self-energy parts play the role of the transition rates. In order to determine the current through the system, we will make use of correlation functions. These are related to the spectral density, which describes the excitation of the whole system.

3.1 Diagrammatic Rules in Time Space

3.1.1 Quantum Dot

In a first step, we expand the reduced propagator

$$\Pi = \mathrm{tr}_L \, \mathrm{tr}_R \left[\rho_0^L \rho_0^R \, T_K \exp\left(-i \int_K dt' H_T(t')_I \right) \right] . \tag{3.1}$$

with respect to the tunneling Hamiltonian, i.e., we expand the exponential

$$\begin{aligned} & T_K \exp\left(-i \int_K dt' H_T(t')_I \right) = \\ & \sum_{m=0}^{\infty} (-i)^m \int_K dt_1 \int_K dt_2 \ldots \int_K dt_m \, T_K \left\{ H_T(t_1)_I H_T(t_2)_I \ldots H_T(t_m)_I \right\} \\ & \qquad\qquad t_1 > t_2 > \ldots > t_m \end{aligned} \tag{3.2}$$

in which the relation $t_1 > t_2 > \ldots > t_m$ has to be understood with respect to the Keldysh contour. The time-ordering operator T_K puts the operators behind the propagator on the right place between the tunneling Hamiltonians. Then, we

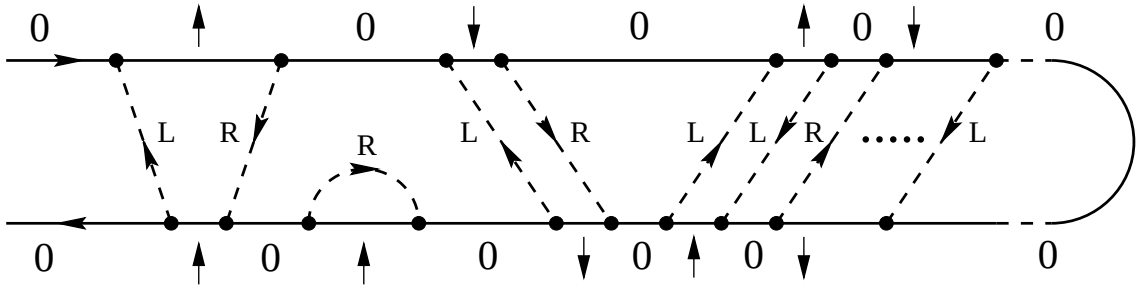

Figure 3.1: A diagram showing various tunneling processes in the quantum dot case (with $M = 2$, i.e., spin up and spin down are the possible spin states): single electron tunneling in the left and right junction, a term preserving the norm, a cotunneling process, and resonant tunneling.

perform the trace for each term of the sum by applying Wick's theorem for the lead electron operators. This means, that we have to contract the lead electron operators in all possible ways and sum up all contributions. Since the leads are in thermal equilibrium, the value of a contraction is given by

$$\langle a^\dagger_{k\sigma r}(t) a_{k'\sigma' r'}(t')\rangle = \delta_{kk'}\delta_{rr'}\delta_{\sigma\sigma'} e^{-i\epsilon_{k\sigma r}(t-t')} f_r^+(\epsilon_{k\sigma r}) \tag{3.3}$$

$$\langle a_{k'\sigma' r'}(t') a^\dagger_{k\sigma r}(t)\rangle = \delta_{kk'}\delta_{rr'}\delta_{\sigma\sigma'} e^{-i\epsilon_{k\sigma r}(t-t')} f_r^-(\epsilon_{k\sigma r}) \tag{3.4}$$

in which $f_r^+(\epsilon) = f(\epsilon - \mu_r)$ is the Fermi function $f(\epsilon) = 1/[\exp(\beta\epsilon) + 1]$ of reservoir r and $f_r^-(\epsilon) = 1 - f_r(\epsilon)$. We visualize each term of the expansion by a diagram (see Fig. 3.1). There is a forward and a backward propagator symbolized by the upper and lower horizontal line, running from t_i to t_f and back from t_f to t_i, respectively. Along this time path, we arrange internal vertices. Each of them corresponds to a product of a lead and a dot electron operator. The vertices are connected in pairs by directed tunneling lines (dashed lines) $\gamma_r^K(t,t')$ from t' to t, with $\gamma_r^K(t,t') = \gamma_r^+(t-t')$ for $t < t'$ and $\gamma_r^K(t,t') = \gamma_r^-(t-t')$ for $t > t'$ with respect to the Keldysh contour. They include the contractions and furthermore the intrinsic broadening Γ_r of the dot levels due to the coupling to lead r with

$$\Gamma_r(\omega) = 2\pi \sum_k |T_k^r|^2 \delta(\omega - \epsilon_{k\sigma r})\,. \tag{3.5}$$

Here and for the following we define

$$\gamma_r^\pm(t) = \int \frac{d\omega}{2\pi} e^{-i\omega t} \gamma_r^\pm(\omega) \tag{3.6}$$

$$\gamma_r^\pm(\omega) = \frac{1}{2\pi}\Gamma_r(\omega) f_r^\pm(\omega) \tag{3.7}$$

$$\gamma^\pm(\omega) = \sum_{r=L,R} \gamma_r^\pm(\omega) \tag{3.8}$$

and

$$\gamma_r(\omega) = M\gamma_r^+(\omega) + \gamma_r^-(\omega) \tag{3.9}$$
$$\gamma(\omega) = M\gamma^+(\omega) + \gamma^-(\omega) \tag{3.10}$$

as well as

$$\Gamma(\omega) = \sum_{r=L,R} \Gamma_r(\omega)\,. \tag{3.11}$$

Here, M denotes the spin degeneracy.

There are vertices from which a tunneling lines leaves (representing $a^\dagger_{k\sigma r}(t)c_\sigma(t)$ which removes a dot electron with spin σ) and others to which a tunneling line enters (visualizing $c^\dagger_\sigma(t)a_{k\sigma r}(t)$ which adds a dot electron with spin σ). Wick's theorem yields, furthermore, a minus sign for each crossing of tunneling lines.

For the interacting dot electrons, Wick's theorem does not apply. Therefore, a product of dot electrons can not be contracted into pairs, but has to be treated explicitly. In the interaction picture the dot electron operators get exponential factors which contain the energies ϵ_χ of the many-body dot states χ given by $\epsilon_\chi|\chi\rangle = H_D|\chi\rangle$. The order of the dot electron operators may induce furthermore a minus sign.

So far, we have accounted for the propagator. If we evaluate the expectation value of one or a product of various operators, we additionally draw external vertices, where no tunneling line enters or leaves. The only effect is a change of the dot state.

In summary, we get the following rules:

1. Draw all topological different diagrams with directed tunneling lines connecting pairs of internal vertices. Assign states χ and the corresponding energy ϵ_χ to each element of the propagators. The propagation from t' to t with $t' < t$ on the Keldysh contour implies a factor $\exp[-i\epsilon_\chi(t-t')]$.

2. Pairs of internal vertices are connected by a directed tunneling line $2\pi\gamma_r^K(t,t')$ running from t' to t. They correspond to a tunneling process in reservoir $r = L, R$.

3. Each diagram carries a prefactor $(-i)^m(-1)^c$, where m is the total number of internal vertices and c the number of crossings of tunneling lines. There may be a further minus sign due to the order of dot electron operators.

4. Integrate over the internal times along the Keldysh contour without changing their ordering and sum over the reservoirs.

3.1.2 Metallic Island

For the metallic island the propagator can be described using a path-integral or an operator approach for the collective variable φ (or n). These approaches are

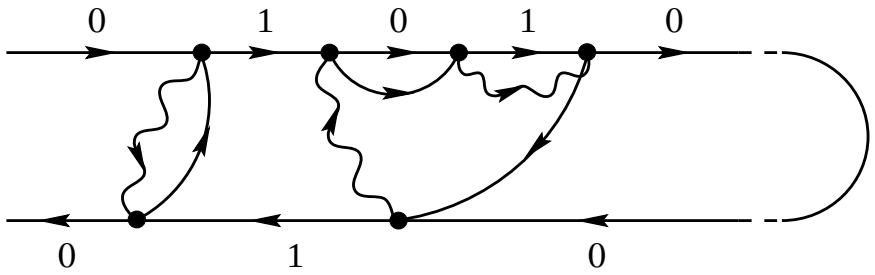

Figure 3.2: A diagram in the metallic case: loops with alternating lead and island lines.

equivalent, i.e., they lead to the same diagrammatic rules. The diagrams are very similar to those for the quantum dot. There is a forward and a backward propagator visualized by two horizontal lines. But now, we have to draw two classes of lines connecting the vertices: lines for the leads (solid lines) and lines for the island (wiggly lines). They build up directed loops in which the lines of the two classes alternate (see Fig. 3.2).

Within the path-integral approach, we start with the reduced propagator given in Eq. (2.40), in which the microscopic degrees of freedom are already traced out. The only task now is to expand $\exp\left(iS_T[\varphi(t)]\right)$ with respect to the effective action describing the tunneling and then to perform the integrals over φ and n. After the expansion we get a product of exponentials $e^{\pm i\varphi}$ at different times on the forward and backward propagator. The integration over φ results in a functional delta-function which fixes the number of excess electrons within a segment of a propagator delimited by two vertices while at a vertex representing $e^{+i\varphi}$ the number of excess electrons on the island increases and at a vertex representing $e^{-i\varphi}$ the number decreases. The integration over n yields $\exp[-iE_{ch}(n)(t-t')]$ for each segment of the propagator between t and t' with $t' < t$ on the Keldysh contour.

If we employ the operator approach, we start with Eq. (2.53), expand the exponential with respect to the tunneling Hamiltonian and then perform Wick's theorem, like we did for the quantum dot. But now, there are, furthermore, contractions between island electron operators

$$\langle c^\dagger_{qn}(t) c_{q'n'}(t')\rangle = \delta_{qq'}\delta_{nn'} e^{-i\epsilon_{qn}(t-t')} f^+(\epsilon_{qn}) \tag{3.12}$$

$$\langle c_{q'n'}(t') c^\dagger_{qn}(t)\rangle = \delta_{qq'}\delta_{nn'} e^{-i\epsilon_{qn}(t-t')} f^-(\epsilon_{qn})\,. \tag{3.13}$$

Each vertex represents a product $a^\dagger c$ where a lead line leaves and an island line enters or $c^\dagger a$ where a lead line enters and an island line leaves. The value of a loop is then calculated as in Appendix A.

Finally, we formulate the rules:

1. Draw all topological different diagrams with loops of directed lead and island tunneling lines connecting internal vertices. Assign charge states n and

the corresponding energy E_{ch} to each element of the propagators. The propagation from t' to t with $t' < t$ on the Keldysh contour implies a factor $\exp[-iE_{ch}(n)(t-t')]$.

2. A loop connecting 2m internal vertices at times $t_1, t_1', \ldots, t_m, t_m'$ contributes $(2\pi)^{2m-1}\alpha^K_{r_1,\ldots,r_m}(t_1, t_1', \ldots, t_m, t_m')$. It corresponds to a tunneling process in which the reservoirs $r_1, \ldots, r_m = L, R$ are involved.

3. Each diagram carries a prefactor $(-i)^m(-1)^c$, where m is the total number of internal vertices and c the number of crossings of tunneling lines.

4. Integrate over the internal times along the Keldysh contour without changing their ordering and sum over the reservoirs.

3.2 Diagrammatic Rules in Energy Space

3.2.1 Quantum Dot

In order to calculate stationary transport properties it is convenient to change to an energy representation. This is achieved by the following transformation: in each diagram we order the times from left to right and label them by t_j with $j = 1, 2, \ldots, m$, irrespective on which branch they are. We further set $t_i = -\infty$ and $t_f = t_{m+1} = 0$.

In the following we develop the diagrammatic rules for the expectation value of one operator at time t_f. In order to calculate correlation functions, i.e. expectation values of a product of operators, these rules are slightly generalized (see Section 3.5).

The Keldysh contour integrals are now written as ordinary integrals. This includes a minus sign for each vertex on the backward propagator. We then encounter expressions of the type

$$\int_{-\infty}^{0} dt_1 \int_{t_1}^{0} dt_2 \ldots \int_{t_{m-1}}^{0} dt_m \, e^{\eta t_1} e^{-i\Delta E_1(t_1-t_2)} e^{-i\Delta E_2(t_2-t_3)} \ldots e^{-i\Delta E_m t_m}$$
$$= \frac{1}{-i\Delta E_1 + \eta} \cdot \frac{1}{-i\Delta E_2 + \eta} \cdots \frac{1}{-i\Delta E_m + \eta} \,. \qquad (3.14)$$

Here ΔE_j is the difference of all energies going to the left minus all energies going to the right in each segment limited by t_j and t_{j+1}. This includes the energies of the propagators and – if present – the energies of the tunneling lines. The convergence factor $e^{\eta t_1}$ $(\eta \to 0^+)$ is related to an adiabatic switching on of the tunneling term H_T. The rules in energy representation read:

1. Draw all topologically different diagrams. These are the same as in time space. In addition to the energy ϵ_χ assigned to the propagators we assign an energy ω to each tunneling line.

2. For each segment derived from $t_j \leq t \leq t_{j+1}$ with $j = 1, 2, \ldots, m$ assign a resolvent $\frac{1}{\Delta E_j + i\eta}$ where ΔE_j is the difference of the leftgoing minus the rightgoing energies (including the energies of the tunneling lines).

3. The prefactor is given by $(-1)^b(-1)^c$, where b is the total number of internal vertices on the backward propagator and c the number of crossings of tunneling lines. There may be a further minus sign due to the order of dot electron operators.

4. For each coupling of vertices write $\gamma_r^+(\omega)$, if the tunneling line of reservoir $r = L, R$ is going backward and $\gamma_r^-(\omega)$, if it is going forward with respect to the closed time path.

5. Integrate over the energies of tunneling lines and sum over the reservoirs.

3.2.2 Metallic Island

In the same way we perform the change to an energy representation for the metallic island. The rules then read:

1. Draw all topological different diagrams. These are the same as in time space. In addition to the energy $E_{ch}(n)$ assigned to the propagators assign an energy ϵ to each lead line and E to each island line.

2. For each segment derived from $t_j \leq t \leq t_{j+1}$ with $j = 1, 2, \ldots, m$ assign a resolvent $\frac{1}{\Delta E_j + i\eta}$ where ΔE_j is the difference of the leftgoing minus the rightgoing energies (including the energies of the tunneling lines).

3. The prefactor is given by $(-1)^b(-1)^c$, where b is the total number of internal vertices on the backward propagator and c the number of crossings of tunneling lines.

4. For each loop connecting $2m$ vertices write $\alpha_{r_1,\ldots,r_m}^{\sigma_1,\eta_1,\ldots,\sigma_m,\eta_m}(\epsilon_1, E_1, \ldots, \epsilon_m, E_m)$, where the sign of σ and η is $+$ if the tunneling line is going backward and $-$ if it is going forward with respect to the closed time path.

5. Integrate over the energies of tunneling lines and sum over the reservoirs.

If we only take into account single loops consisting of one lead and one island line, we can replace the loop by a tunneling line (dashed line) with the same direction as the lead line (see Fig. 3.3) and assign an energy ω. The value of this tunneling line is then $\alpha_r^+(\omega)$, if the tunneling line of reservoir $r = L, R$ is going backward and $\alpha_r^-(\omega)$, if it is going forward with respect to the closed time path. Finally we integrate over all energies of tunneling lines. The number of crossings of lines is then always even and therefore $(-1)^c = 1$. The diagrams look then very similar to those for the quantum dot (see Fig. 3.4).

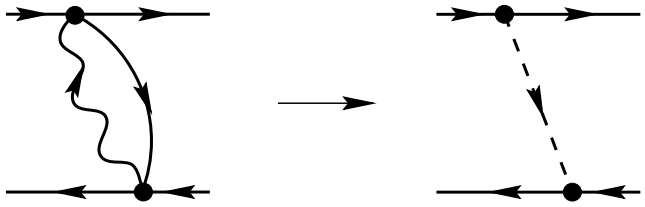

Figure 3.3: Replacement of a simple loop consisting of one lead and one island line by a single (dashed) tunneling line. The arrow direction is the same as the direction of the lead.

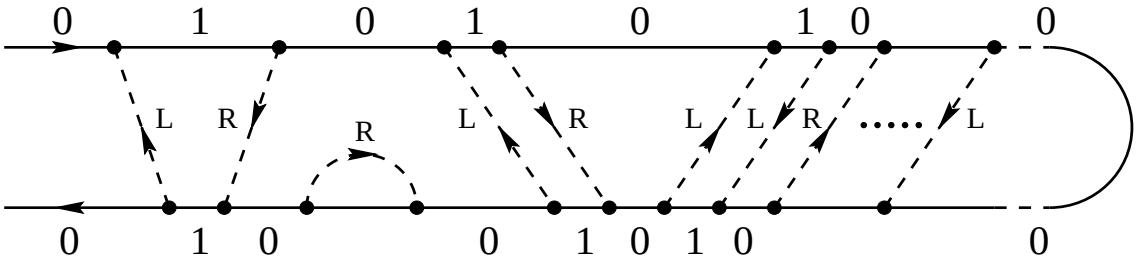

Figure 3.4: A diagram showing various tunneling processes in the metallic case: single electron tunneling in the left and right junction, a term preserving the norm, a cotunneling process, and resonant tunneling.

3.3 Mirror Rule

If we use the diagrammatic technique the first task is to find all contributing diagrams. It is often convenient to combine them into pairs of related diagrams. If we have constructed a possible diagram (or a part of a diagram), then we get another possible diagram by performing the following transformation: (i) exchange the forward and backward propagator, i.e., reflect the diagram horizontally and (ii) change the direction of all tunneling lines. The evaluation of the new diagram is then the same as for the old one, except that the energy difference in each resolvent changes sign, i.e.

$$\frac{1}{\Delta E + i\eta} \to \frac{1}{-\Delta E + i\eta} = -\left(\frac{1}{\Delta E + i\eta}\right)^* , \tag{3.15}$$

and if the total number of internal vertices m is odd, the number of vertices on the backward propagator is changed from odd to even or from even to odd, and therefore we get an extra factor -1. Complex conjugating the value of the old diagram d and eventually multiplying the factor -1 yields the value of the new diagram

$$d \to (-1)^m (-1)^l \, d^* , \tag{3.16}$$

where m is the number of internal vertices and l the number of resolvents. We call this *mirror rule*. It is an useful tool which allows us to derive some general properties of the considered quantities and to simplify their evaluation.

3.4 Master Equation and Stationary Probabilities

The propagator from χ_1 forward to χ_1' and then from χ_2' backward to χ_2 is denoted by $\Pi^{\chi_1,\chi_1'}_{\chi_2,\chi_2'}$. It is the sum of all diagrams with the given states at the ends and can be expressed by an irreducible self-energy part $\Sigma^{\chi_1,\chi_1'}_{\chi_2,\chi_2'}$, defined as the sum of all diagrams in which any vertical line cutting through them crosses at least one tunneling line. The propagator can be expressed as an iteration in the style of a Dyson equation, illustrated in Fig. 3.5

$$\Pi = \Pi^{(0)} + \Pi\,\Sigma\,\Pi^{(0)} \tag{3.17}$$

with self-energy Σ or for the matrix elements

$$\Pi^{\chi_1,\chi_1'}_{\chi_2,\chi_2'} = \Pi^{(0)\,\chi_1}_{\quad\chi_2}\delta_{\chi_1,\chi_1'}\delta_{\chi_2,\chi_2'} + \sum_{\chi_1'',\chi_2''} \Pi^{\chi_1,\chi_1''}_{\chi_2,\chi_2''}\,\Sigma^{\chi_1'',\chi_1'}_{\chi_2'',\chi_2'}\,\Pi^{(0)\,\chi_1'}_{\quad\chi_2'}\,. \tag{3.18}$$

Here $\Pi^{(0)}$ is the free propagator without any tunneling process.

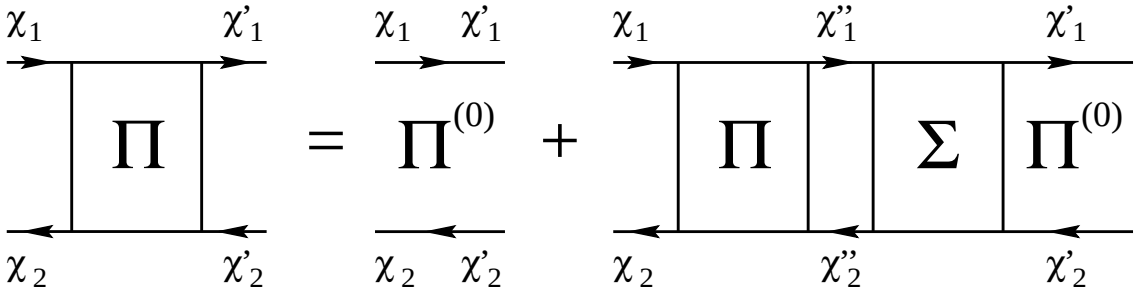

Figure 3.5: The iteration of processes for the propagator Π.

The probability, that the (reduced) system is in state χ at time t, $P_\chi(t)$, is given by the quantum-statistical expectation value of the projector $|\chi\rangle\langle\chi|(t)$

$$P_\chi(t) = \langle(|\chi\rangle\langle\chi|)(t)\rangle\,. \tag{3.19}$$

The stationary distribution follows from

$$P^{st}_\chi = \lim_{t\to\infty} P_\chi(t) = \lim_{t_i\to-\infty} P_\chi(0) \tag{3.20}$$

and is *not* the equilibrium one if the electrochemical potentials of the left and right lead are different.

In order to calculate the stationary probabilities we start from a density matrix which is diagonal, $\rho_0 = \sum_\chi P^0_\chi|\chi\rangle\langle\chi|$. This means that the density matrix remains diagonal except during transitions described by the self-energy Σ. Hence, we consider

$$\Sigma_{\chi,\chi'} \equiv \Sigma^{\chi,\chi'}_{\chi,\chi'} \quad , \quad \Pi_{\chi,\chi'} \equiv \Pi^{\chi,\chi'}_{\chi,\chi'}\ , \quad \text{and} \quad \Pi^{(0)}_\chi \equiv \Pi^{(0)\,\chi}_{\quad\chi}\,. \tag{3.21}$$

Equation (3.18) then reads

$$\Pi_{\chi,\chi'} = \Pi^{(0)}{}_{\chi}\delta_{\chi,\chi'} + \sum_{\chi''} \Pi_{\chi,\chi''}\,\Sigma_{\chi'',\chi'}\,\Pi^{(0)}{}_{\chi'} \ . \tag{3.22}$$

The term $\Pi^{(0)}$ describes a propagation in a diagonal state (i.e. equal energies on the forward and backward propagator) which does not contain a tunneling line. According to the rules in the energy representation this introduces a factor $1/i\eta$ if there is any vertex to the left and 1 if there is none.

After multiplication with P^0_χ from the left and summation over χ, we get

$$P^{st}_{\chi'} = P^0_{\chi'} + \sum_{\chi''} P^{st}_{\chi''}\Sigma_{\chi'',\chi'}\frac{1}{i\eta} \ . \tag{3.23}$$

Performing the limit $\eta \to 0+$ we find

$$\sum_{\chi''} \Pi_{\chi,\chi''}\,\Sigma_{\chi'',\chi'} = 0 \qquad \text{and therefore} \qquad \sum_{\chi'} P^{st}_{\chi'}\Sigma_{\chi',\chi} = 0 \ . \tag{3.24}$$

By attaching the rightmost vertex of each diagram Σ to the upper and lower propagator the minus sign for each vertex on the backward propagator yields (see Fig. 3.6)

$$\sum_{\chi'} \Sigma_{\chi,\chi'} = 0 \, , \tag{3.25}$$

which allows us to rewrite the equation in the form

$$0 = \sum_{\chi'} [-P^{st}_{\chi}\Sigma_{\chi,\chi'} + P^{st}_{\chi'}\Sigma_{\chi',\chi}] \, . \tag{3.26}$$

We recover the structure of a stationary master equation with transition rates given by $\Sigma_{\chi',\chi}$. In general the irreducible self-energy Σ yields the rate of all possible correlated tunneling processes. If we can calculate them, we get the stationary probabilities P^{st}_χ, which are independent of the initial distribution P^0_χ.

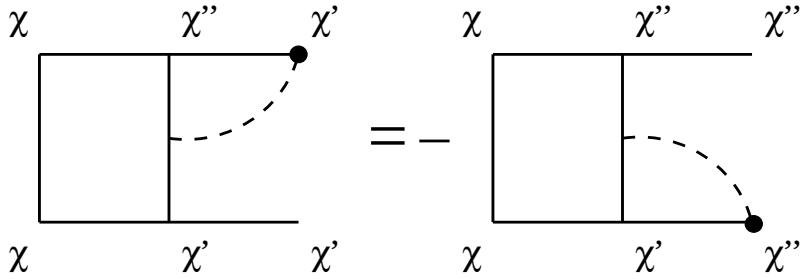

Figure 3.6: Attaching the rightmost vertex of a diagram Σ on the opposite propagator yields the multiplication of a minus sign.

Applying the mirror rule we find

$$\Pi_{\chi,\chi'} = \Pi_{\chi,\chi'}{}^{*} \qquad \text{and} \qquad \Sigma_{\chi,\chi'} = -\Sigma_{\chi,\chi'}{}^{*}\,, \tag{3.27}$$

i.e., $\Pi_{\chi,\chi'}$ is real and $\Sigma_{\chi,\chi'}$ is purely imaginary.

Complicated diagrams are built up by simpler parts. We introduce an irreducible diagram labeled by $\phi^{\chi_1,\chi_1'}_{\chi_2,\chi_2'}(r,\sigma,\omega)$ (see Fig. 3.7a). It has an open tunneling line asso-

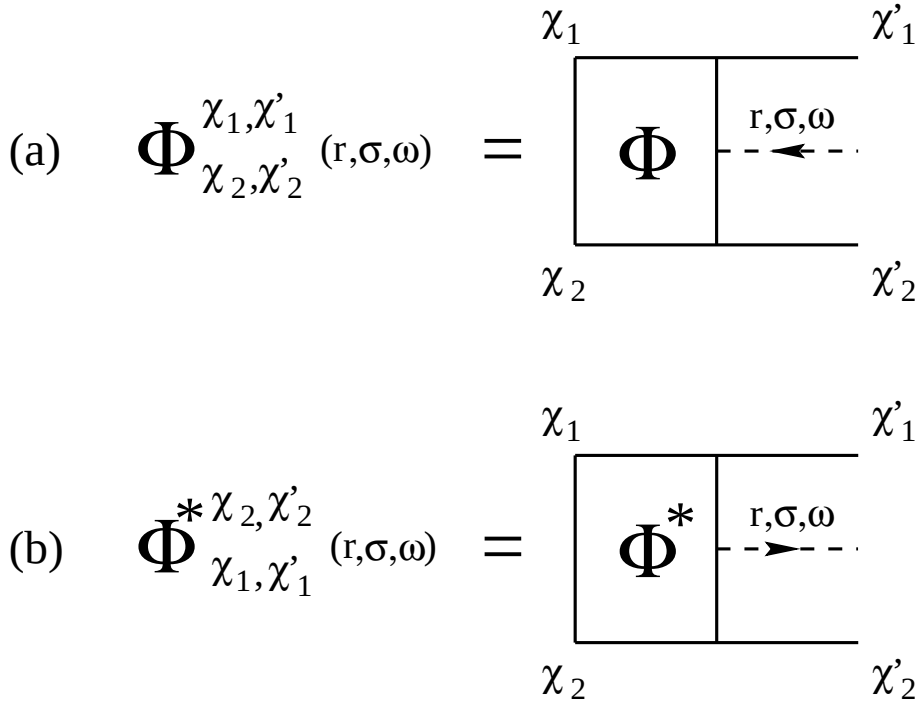

Figure 3.7: a) Definition of Φ. It denotes a part of a diagram with an open tunneling line entering from the right. b) A part of a diagram with an open tunneling line leaving to the right can be calculated with the help of the mirror rule.

ciated with tunneling of an electron (with spin σ in the case of a discrete spectrum) in the junction r carrying the energy ω. The line is directed from the right to the left.

According to the mirror rule, the corresponding diagram with an open tunneling line running from the left to the right has the value $\phi^{*\,\chi_2,\chi_2'}_{\chi_1,\chi_1'}(r,\sigma,\omega)$ (see Fig. 3.7b).

Another important diagram is the propagator $\pi(\omega)$ while a tunneling line with energy ω is running in parallel from the right to the left. Like before, this diagram can be expressed as an iteration in the style of a Dyson equation (see Fig. 3.8)

$$\pi(\omega) = \pi^{(0)}(\omega) + \pi(\omega)\,\sigma(\omega)\,\pi^{(0)}(\omega) \tag{3.28}$$

or for the matrix elements

$$\pi^{\chi_1,\chi_1'}_{\chi_2,\chi_2'}(\omega) = \pi^{(0)}{}^{\chi_1}_{\chi_2}(\omega)\delta_{\chi_1,\chi_1'}\delta_{\chi_2,\chi_2'} + \sum_{\chi_1'',\chi_2''} \pi^{\chi_1,\chi_1''}_{\chi_2,\chi_2''}(\omega)\,\sigma^{\chi_1'',\chi_1'}_{\chi_2'',\chi_2'}(\omega)\,\pi^{(0)}{}^{\chi_1'}_{\chi_2'}(\omega)\,. \tag{3.29}$$

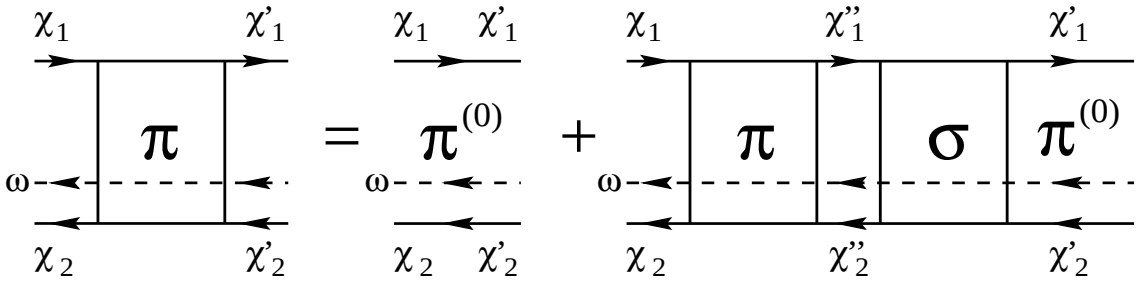

Figure 3.8: The iteration of processes for the propagator π with a tunneling line running in parallel from the right to the left.

In analogy to Σ, the self-energy $\sigma(\omega)$ denotes the sum of all irreducible diagrams with a tunneling line going backward. Here, the free propagator

$$\pi^{(0)\,\chi_1}_{\chi_2}(\omega) = \frac{1}{\omega - (\epsilon_{\chi_1} - \epsilon_{\chi_2}) + i\eta} \tag{3.30}$$

is not singular. Hence, we can solve Eq. (3.28) and find

$$\pi(\omega) = [[\pi^{(0)}(\omega)]^{-1} - \sigma(\omega)]^{-1}\,. \tag{3.31}$$

The corresponding diagrams with an open tunneling line running from the left to the right have the values (mirror rule) $-\pi^{*\,\chi_2,\chi_2'}_{\chi_1,\chi_1'}(\omega)$ and $-\sigma^{*\,\chi_2,\chi_2'}_{\chi_1,\chi_1'}(\omega)$.

3.5 Correlation Functions and Spectral Density

As we will see later (in Chapter 5), the stationary current through the island can be related to the following real-time correlation functions:

$$C^{>}(t,t') = -i\langle c_\sigma(t)_H\, c^\dagger_\sigma(t')_H\rangle \tag{3.32}$$
$$C^{<}(t,t') = i\langle c^\dagger_\sigma(t')_H\, c_\sigma(t)_H\rangle \tag{3.33}$$

for the quantum dot and

$$C^{>}(t,t') = -i\langle e^{-i\varphi(t)} e^{i\varphi(t')}\rangle \tag{3.34}$$
$$C^{<}(t,t') = i\langle e^{i\varphi(t')} e^{-i\varphi(t)}\rangle \tag{3.35}$$

for the metallic island. Here $C^{>}$ and $C^{<}$ are independent quantities since we do not assume equilibrium. These correlation functions are calculated in time space according to the rules in Section 3.1 by correspondingly arranging external vertices.

In the stationary limit, i.e. $t_i \to -\infty$, the correlation functions depend only on the time difference $\tau = t - t'$ and we can define the Fourier transform

$$C^{>}(\omega) = \int d\tau\, e^{i\omega\tau} C^{>}(\tau) = \int_{-\infty}^{0} d\tau \left[e^{-i\omega\tau} C^{>}(0,\tau) + e^{i\omega\tau} C^{>}(\tau,0)\right] \tag{3.36}$$
$$C^{<}(\omega) = \int d\tau\, e^{i\omega\tau} C^{<}(\tau) = \int_{-\infty}^{0} d\tau \left[e^{-i\omega\tau} C^{<}(0,\tau) + e^{i\omega\tau} C^{<}(\tau,0)\right]\,. \tag{3.37}$$

In order to evaluate these correlation functions in energy representation, we imagine a directed virtual line which connects the external vertices. For the quantum dot, this line runs from c_σ to $c_\sigma^\dagger$, while for the metallic island is goes from $e^{-i\varphi}$ to $e^{i\varphi}$. Furthermore we assign an energy ω and drop a factor $(-i)$. Then we apply rules **1. - 5.** in which in rule **2.** the energy difference may further enclose the energy of the virtual line. A graphical representation is given in Fig. 3.9.

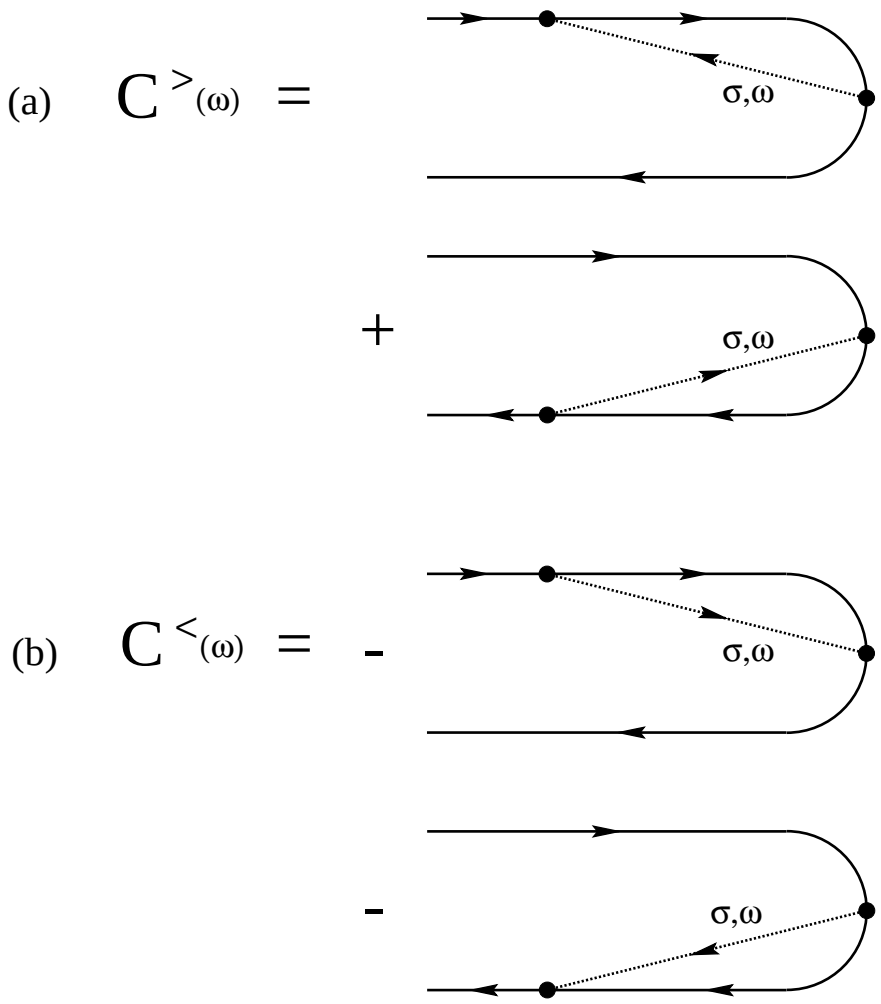

Figure 3.9: Graphical representation of the correlation functions in energy space. The internal vertices are not indicated here. Instead of summing up two diagrams one can take the imaginary part of one of them and then multiply with $2i$ (mirror rule).

An interesting quantity from a theoretical point of view is the spectral density

$$A(\omega) = \frac{1}{2\pi i}[C^<(\omega) - C^>(\omega)] \tag{3.38}$$

which describes the charge excitations of the system. We will see that within our

approximations all quantities of interest like the probability P_σ^{st}, the current I_r^{st} and the correlation functions $C^>, C^<$ can be related to the spectral density. Thus, its specific form which is related to energy renormalization and finite life-time broadening effects will be the central point of our analysis.

Chapter 4

Self-Energy and Stationary Distribution Probabilities

As we saw in the last chapter, the main task is now to calculate the self-energy Σ. This will be done in this chapter. First, we calculate the simplest irreducible self-energy diagrams. These contain only one tunneling line and describe therefore single electron tunneling. The next complicated irreducible self-energy diagrams consist of two tunneling lines. Here we recover cotunneling. Our goal, however, is to include resonant tunneling. We do this within an approximation. We find a systematic criterion which diagrams should be retained and summed.

4.1 Single Electron Tunneling

For single electron tunneling all tunneling processes occur incoherently, i.e. between two tunneling events, the density matrix is diagonal. In the diagrammatic language this means that tunneling lines are separated by free propagators. Therefore, there are no overlapping tunneling lines: each vertical line intersecting the diagram crosses at most one line. Transitions between diagonal states are described by a self-energy part $\Sigma^{(1)}$ with only one line. If the tunneling line connects two vertices on one propagator the initial and the final state coincide. If the line connects the two propagators, then an electron enters or leaves the island during the transition (examples are given on the left hand side of Figs. 3.1 and 3.4). This means we include those processes which are described by the the master equation with rates obtained by the golden rule in lowest order perturbation theory. According to the rules in Chapter 3, we find for the rates in the quantum dot case

$$\Sigma^{(1)}_{0,\sigma} = 2\pi i\gamma^{+}(\epsilon_0) \tag{4.1}$$

$$\Sigma^{(1)}_{\sigma,0} = 2\pi i\gamma^{-}(\epsilon_0) \tag{4.2}$$

$$\Sigma^{(1)}_{0,0} = -2\pi iM\gamma^{+}(\epsilon_0) \tag{4.3}$$

$$\Sigma^{(1)}_{\sigma,\sigma'} = -2\pi i\delta_{\sigma\sigma'}\gamma^{-}(\epsilon_0)\,. \tag{4.4}$$

For the metallic island we find

$$\Sigma^{(1)}_{n,n\pm1} = 2\pi i \alpha^{\pm}(\pm E^{\pm}_{ch}) \tag{4.5}$$

$$\Sigma^{(1)}_{n,n} = -2\pi i \sum_{\pm} \alpha^{\pm}(\pm E^{\pm}_{ch}) \tag{4.6}$$

with $E^{\pm}_{ch} = E_{ch}(n \pm 1) - E_{ch}(n)$.

4.2 Cotunneling

In situations in which single electron tunneling is suppressed by Coulomb blockade the lowest order contribution to the current arises due to cotunneling. The rate for a process in which an electron enters the island from the left lead and an electron leaves to the right one is described by diagrams with two overlapping lines. One line corresponds to tunneling through the left junction and goes from a vertex on the backward to a vertex on the forward propagator. The other one is associated with tunneling through the right junction and has the opposite direction (examples are given in the middle of Figs. 3.1 and 3.4). According to the rules in Chapter 3 rules we encounter three resolvents in the calculation of such a diagram. We sum up all contributions. With the help of the mirror rule we can combine always two diagrams to the imaginary part of one of them. After omitting the term $i\eta$ in the first and third resolvent, we see that the imaginary part of the second resolvent yields a delta-function which ensures energy conservation of the whole process. We find then for the rates the same expressions as with the golden rule in higher-order perturbation theory [23].

4.3 Resonant Tunneling

Until now, we have formulated the diagram rules for arbitrary states of the island. In the following, however, we assume strong Coulomb repulsion, i.e., E_C and U are very large for the metallic island and the quantum dot, respectively. This implies that only a few states of the island are involved: the charge states $n = 0, 1$ for the metallic island and dot empty or singly occupied with spin σ for the quantum dot. All other island states are associated with large energies, so that they are not involved. A diagram with such a higher energy state contains at least one resolvent with a very large denominator and therefore doesn't contribute. For this reason, we consider only diagrams with the "allowed" states.

The perturbative approach breaks down at low temperatures and voltages or for strong coupling of the island to the leads. Then resonant tunneling processes become important.

To account for their influence we have to find a systematic criterion which diagrams should be retained and summed. For this we note that during a tunneling

process the reservoirs contain an electron excitation. Two parallel tunneling lines imply two such excitations. Our criterion is that we take into account only those matrix elements of the total density matrix, i.e. reservoirs plus charge states, which differ at most by two excitations in the leads or (equivalently) in the metallic island. Graphically this means that any vertical line will cut at most two tunneling lines. Examples of contributing resonant tunneling processes are shown on the right hand side of Figs. 3.1 and 3.4).

The combination of the two restrictions, diagrams with at most two parallel tunneling lines in the two-charge-state problem, implies that no diagram contains *crossing* tunneling lines. In this case we can evaluate the irreducible self-energy analytically.

4.3.1 Quantum Dot

In the following, the index σ labels the singly occupied state with spin $\sigma = 1, \dots M$. The label χ additionally allows an empty dot, $\chi = 0, 1, \dots M$.

In order to evaluate the stationary probabilities from Eq. (3.26) with $\chi = 0$ we need $\Sigma_{\chi,0}$. This diagram is constructed by attaching the open tunneling lines of

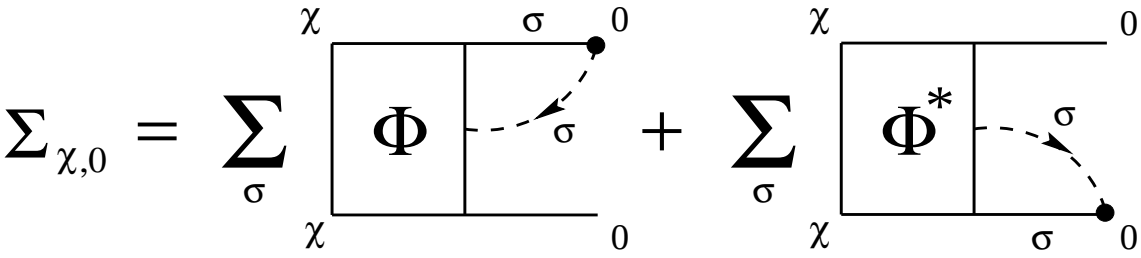

Figure 4.1: The irreducible self energy is obtained by attaching the open tunneling line of ϕ and ϕ^* to the upper and lower propagator.

ϕ and ϕ^* to the upper and lower propagator. Including mirror rule, we get (see Fig. 4.1)

$$\Sigma_{\chi,0} = 2i \,\mathrm{Im} \sum_r \sum_\sigma \int d\omega \; \phi^{\chi,\sigma}_{\chi,0}(r,\sigma,\omega)\,. \tag{4.7}$$

The diagram ϕ is constructed by iteration. The self-consistent equation for the diagram $\phi(\omega)$ reads (see Figs. 4.2 and 4.3)

$$\begin{aligned}\phi^{0,\sigma}_{0,0}(r,\sigma,\omega) = \pi^{\sigma,\sigma}_{0,0}(\omega) \Bigg[& \gamma^+_r(\omega) - \gamma^-_r(\omega) \sum_{r'} \int d\omega' \frac{1}{\omega - \omega' + i\eta} \, \phi^{*\,0,\sigma}_{0,0}(r',\sigma,\omega') \\ & - \gamma^+_r(\omega) \sum_{\sigma'} \sum_{r'} \int d\omega' \frac{1}{\omega - \omega' + i\eta} \, \phi^{*\,0,\sigma'}_{0,0}(r',\sigma',\omega') \Bigg]\end{aligned} \tag{4.8}$$

and

$$\phi^{\sigma',\sigma}_{\sigma',0}(r,\sigma,\omega) = \pi^{\sigma,\sigma}_{0,0}(\omega)\left[-\gamma^-_r(\omega)\delta_{\sigma\sigma'} - \gamma^-_r(\omega)\sum_{r'}\int d\omega' \frac{1}{\omega-\omega'+i\eta}\,\phi^{*\sigma',\sigma}_{\sigma',0}(r',\sigma,\omega')\right.$$
$$\left. - \gamma^+_r(\omega)\sum_{\sigma''}\sum_{r'}\int d\omega' \frac{1}{\omega-\omega'+i\eta}\,\phi^{*\sigma',\sigma''}_{\sigma',0}(r',\sigma'',\omega')\right] \quad (4.9)$$

We see that only one matrix element $\pi^{\sigma,\sigma}_{0,0}(\omega)$ of $\pi(\omega)$ is involved. Because of the

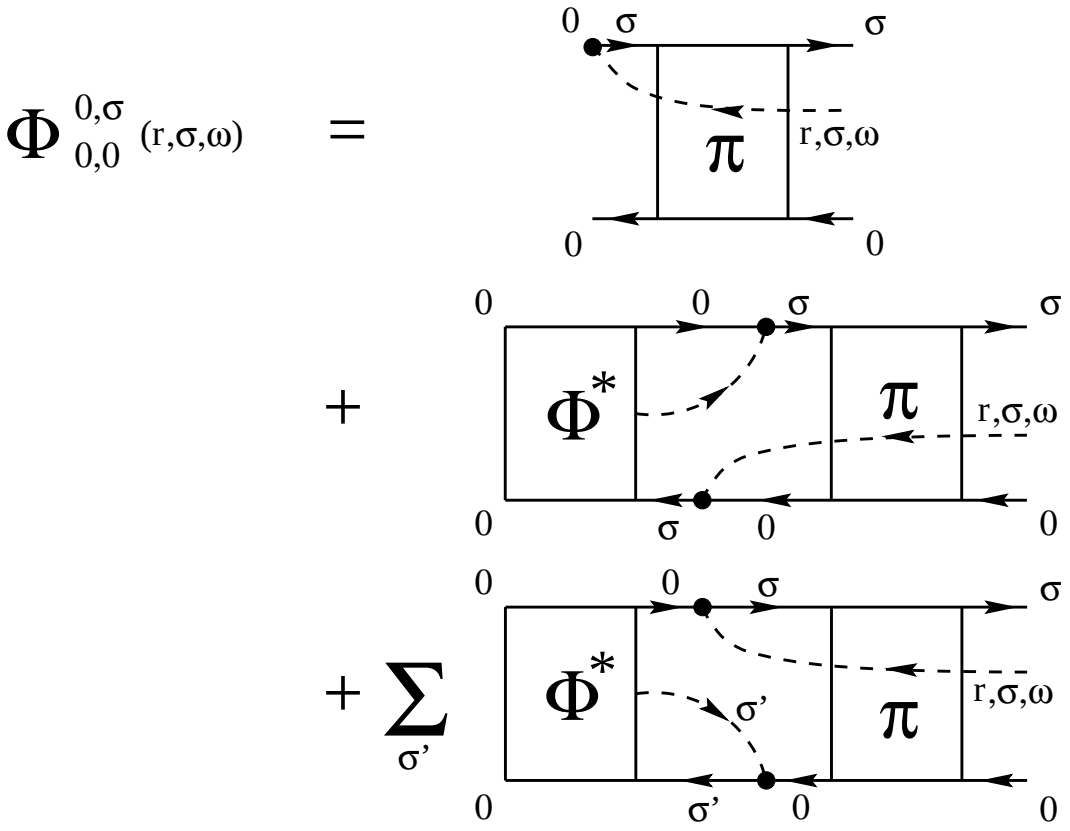

Figure 4.2: Graphical representation of the self-consistent equation for ϕ beginning with an empty dot state.

restriction to two charge states, only one matrix element $\sigma^{\sigma,\sigma}_{0,0}(\omega)$ of $\sigma(\omega)$ enters the Dyson equation (3.28). These matrix elements are independent of spin σ due to symmetry. We therefore drop the indices and deduce from Eq. (3.31)

$$\pi(\omega) = \frac{1}{\omega - \epsilon_0 - \sigma(\omega)} \quad (4.10)$$

for numbers and no more for matrices. Since at most two tunneling lines are allowed at once, the irreducible self-energy $\sigma(\omega)$ consists of only one tunneling lines. We

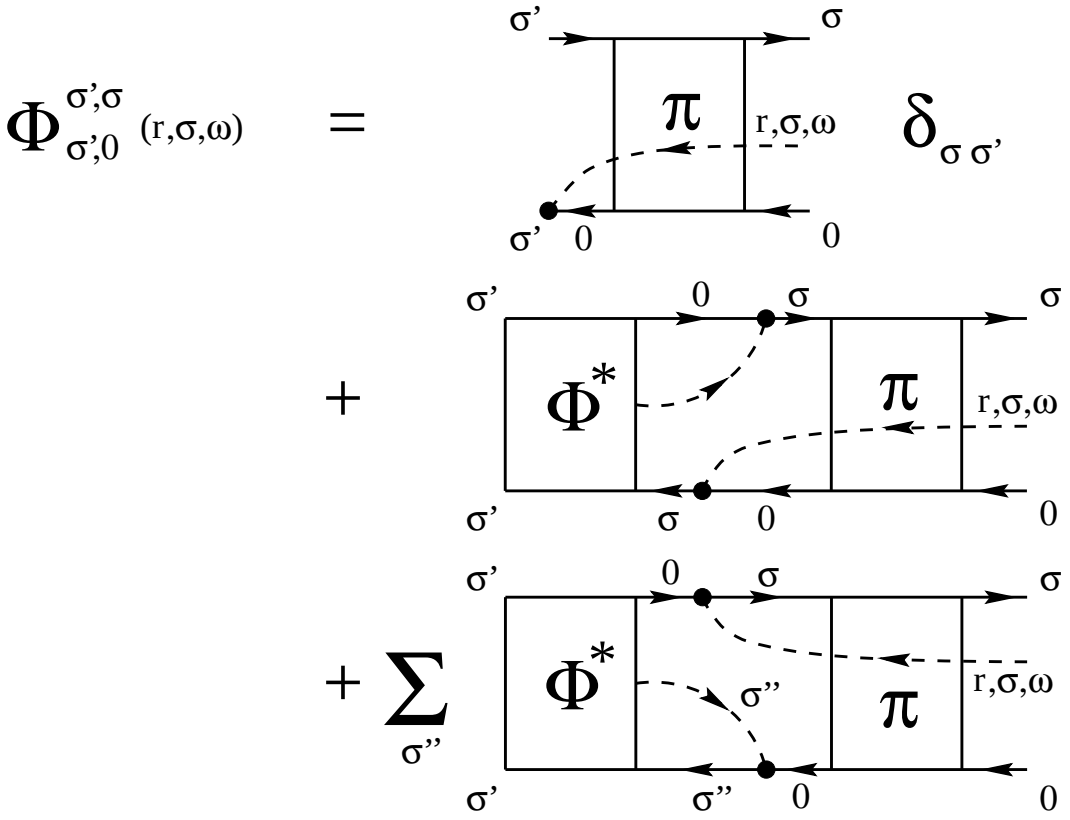

Figure 4.3: Graphical representation of the self-consistent equation for ϕ beginning with an occupied dot state.

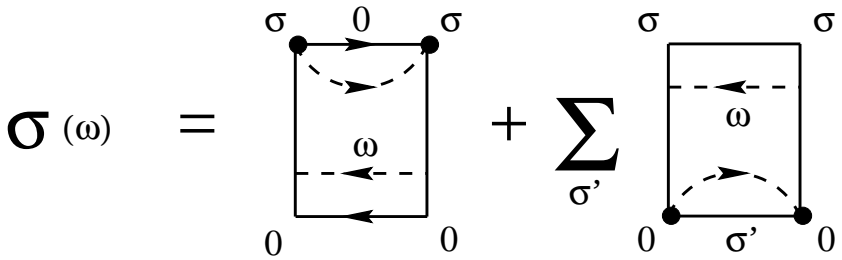

Figure 4.4: In our approximation, the diagram for the irreducible self-energy $\sigma(\omega)$ contains one tunneling line in addition to the backward running line.

calculate all contributions, which are depicted in Fig. 4.4, and get

$$\sigma(\omega) = \int d\omega' \frac{\gamma(\omega')}{\omega - \omega' + i\eta} \,. \tag{4.11}$$

Defining

$$\phi^+(\omega) = \sum_r \phi_{0,0}^{0,\sigma}(r,\sigma,\omega) \qquad \text{and} \qquad \phi^-(\omega) = \sum_r \sum_{\sigma'} \phi_{\sigma,0}^{\sigma,\sigma'}(r,\sigma',\omega) \tag{4.12}$$

which are again independent of σ, we get the integral equations

$$[\omega - \epsilon_0 - \sigma(\omega)]\phi^{\pm}(\omega) = \pm\gamma^{\pm}(\omega) - \gamma(\omega) \int d\omega' \frac{1}{\omega - \omega' + i\eta}\, \phi^{*\pm}(\omega') \tag{4.13}$$

with the solutions for the imaginary parts (see Appendix B)

$$\operatorname{Im} \phi^{\pm}(\omega) = \mp\pi \frac{\lambda^{\pm}}{\lambda} \gamma(\omega) |\pi(\omega)|^2 \tag{4.14}$$

with

$$\lambda^{\pm} = \int d\omega\, \gamma^{\pm}(\omega) |\pi(\omega)|^2 \qquad \text{and} \qquad \lambda = \int d\omega\, |\pi(\omega)|^2 \,. \tag{4.15}$$

The self-energies are then

$$\Sigma_{0,0} = -2\pi i M \frac{\lambda^+}{\lambda} \qquad \text{and} \qquad \Sigma_{\sigma,0} = 2\pi i \frac{\lambda^-}{\lambda} \tag{4.16}$$

and the solution of Eq. (3.26) reads

$$P_0^{st} = \lambda^- \qquad \text{and} \qquad P_\sigma^{st} = \lambda^+ \qquad \text{with} \qquad \lambda^- + M\lambda^+ = 1 \,. \tag{4.17}$$

4.3.2 Metallic Island

The calculations are exactly the same as for the quantum dot with $M = 1$. We only have to exchange the functions $\gamma_r^{\pm}(\omega)$ with $\alpha_r^{\pm}(\omega)$ and to take the corresponding functions $\pi(\omega)$ and $\sigma(\omega)$ (for simplicity, we do not use any index for distinction). Since there are no crossed diagrams or states with double occupancy, the fermionic nature of the tunneling lines in the quantum dot case has no effect.

Now, we denote the empty and singly occupied island state by $n = 0, 1$ respectively. The difference of the charging energies is $\Delta_0 = E_{ch}(1) - E_{ch}(0)$.

The irreducible self-energy part $\Sigma_{n,0}$ is given by (see Fig. 4.5 for illustration)

$$\Sigma_{n,0} = 2i \operatorname{Im} \sum_r \int d\omega\, \phi_{n,0}^{n,1}(r,\omega) \,. \tag{4.18}$$

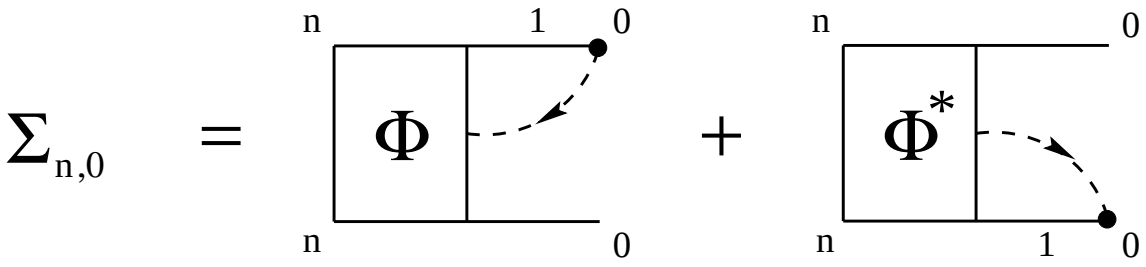

Figure 4.5: The irreducible self energy is obtained by attaching the open tunneling line of ϕ and ϕ^* to the upper and lower propagator.

The self-consistent equation for the diagram ϕ reads (its graphical representation is given in Figs. 4.6 and 4.7)

$$\phi^{0,1}_{0,0}(r,\omega) = \pi^{1,1}_{0,0}(\omega)\left[\alpha^+_r(\omega) - \alpha^-_r(\omega)\sum_{r'}\int d\omega' \frac{1}{\omega-\omega'+i\eta}\,\phi^{*0,1}_{0,0}(r',\omega') \right. \\ \left. - \alpha^+_r(\omega)\sum_{r'}\int d\omega' \frac{1}{\omega-\omega'+i\eta}\,\phi^{*0,1}_{0,0}(r',\omega')\right] \qquad (4.19)$$

and

$$\phi^{1,1}_{1,0}(r,\omega) = \pi^{1,1}_{0,0}(\omega)\left[-\alpha^-_r(\omega) - \alpha^-_r(\omega)\sum_{r'}\int d\omega' \frac{1}{\omega-\omega'+i\eta}\,\phi^{*1,1}_{1,0}(r',\omega') \right. \\ \left. - \alpha^+_r(\omega)\sum_{r'}\int d\omega' \frac{1}{\omega-\omega'+i\eta}\,\phi^{*1,1}_{1,0}(r',\omega')\right] . \qquad (4.20)$$

Like above, only one matrix element $\pi^{1,1}_{0,0}(\omega)$ of $\pi(\omega)$ and $\sigma^{1,1}_{0,0}(\omega)$ of $\sigma(\omega)$ plays a role. We therefore drop the indices and find (see Fig. 4.8)

$$\pi(\omega) = \frac{1}{\omega - \Delta_0 - \sigma(\omega)} \qquad \text{with} \qquad \sigma(\omega) = \int d\omega' \frac{\alpha(\omega')}{\omega-\omega'+i\eta}\,. \qquad (4.21)$$

Defining

$$\phi^+(\omega) = \sum_r \phi^{0,1}_{0,0}(r,\omega) \qquad \text{and} \qquad \phi^-(\omega) = \sum_r \phi^{1,1}_{1,0}(r,\omega)\,, \qquad (4.22)$$

we get the integral equations

$$[\omega - \Delta_0 - \sigma(\omega)]\phi^\pm(\omega) = \pm\alpha^\pm(\omega) - \alpha(\omega)\int d\omega' \frac{1}{\omega-\omega'+i\eta}\,\phi^{*\pm}(\omega') \qquad (4.23)$$

with the solutions for the imaginary parts (see Appendix B)

$$\mathrm{Im}\,\phi^\pm(\omega) = \mp\pi\frac{\lambda^\pm}{\lambda}\alpha(\omega)|\pi(\omega)|^2 \qquad (4.24)$$

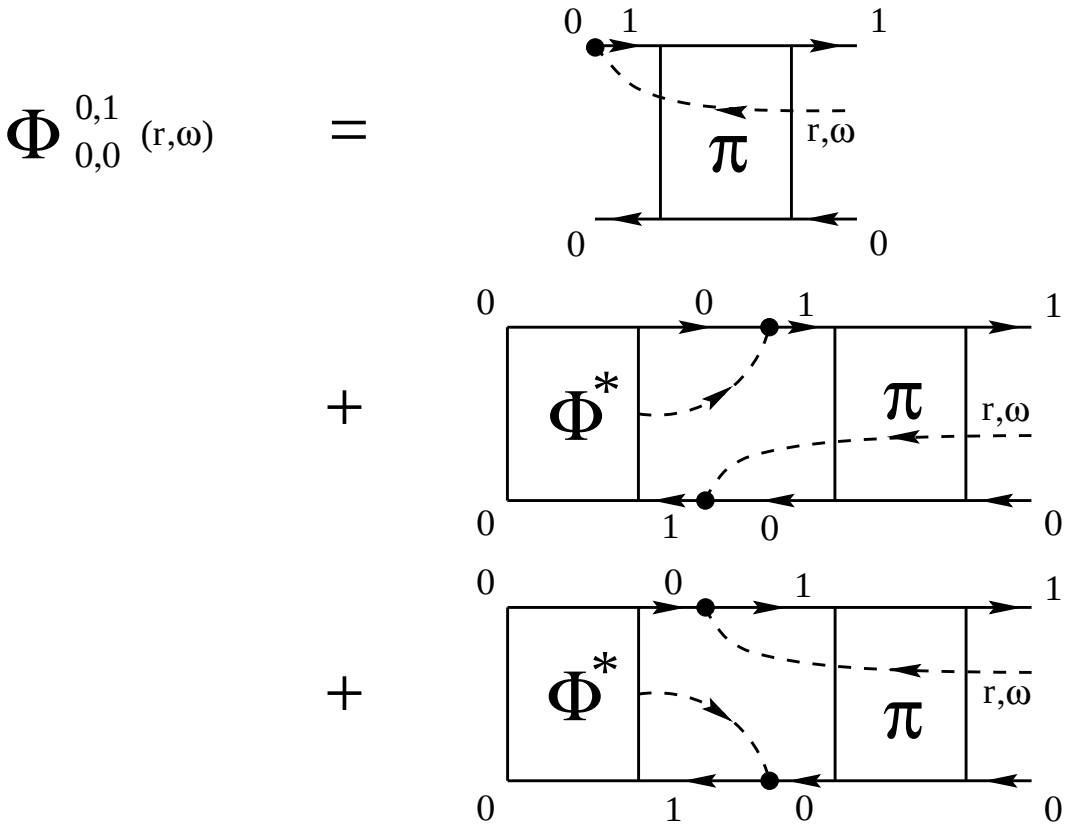

Figure 4.6: Graphical representation of the self-consistent equation for ϕ beginning with an empty island state.

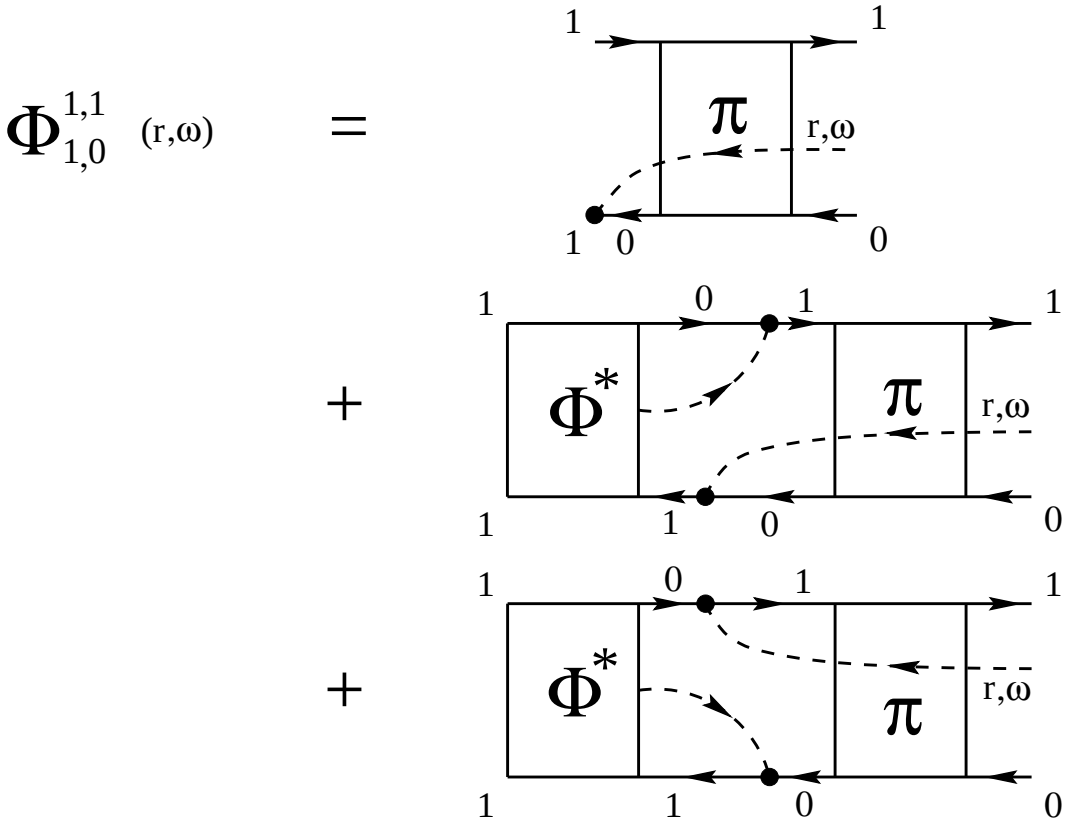

Figure 4.7: Graphical representation of the self-consistent equation for ϕ beginning with an occupied island state.

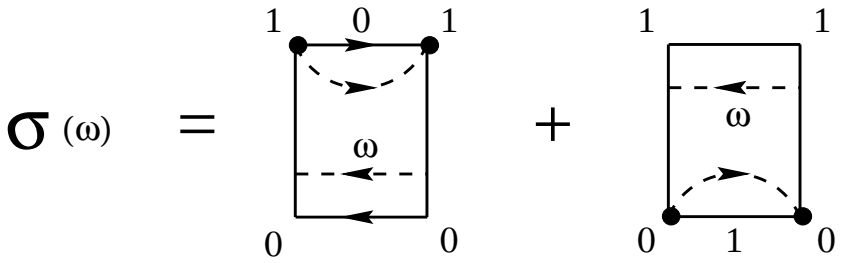

Figure 4.8: In our approximation, the diagram for the irreducible self-energy $\sigma(\omega)$ contains one tunneling line in addition to the backward running line.

with

$$\lambda^{\pm} = \int d\omega\, \alpha^{\pm}(\omega)|\pi(\omega)|^2 \qquad \text{and} \qquad \lambda = \int d\omega\, |\pi(\omega)|^2 \,. \tag{4.25}$$

The self-energies are then

$$\Sigma_{0,0} = -2\pi i \frac{\lambda^+}{\lambda} \qquad \text{and} \qquad \Sigma_{1,0} = 2\pi i \frac{\lambda^-}{\lambda} \tag{4.26}$$

and the solution of Eq. (3.26) reads

$$P_0^{st} = \lambda^- \qquad \text{and} \qquad P_1^{st} = \lambda^+ \qquad \text{with} \qquad \lambda^- + \lambda^+ = 1 \,. \tag{4.27}$$

Chapter 5

The Current and the Spectral Density

In this chapter, we calculate the current through the island. Formally, the expectation value of the corresponding operator can be written in terms of correlation functions of the nonequilibrium degrees of freedom. These, in turn, are related to the spectral density. The effects of resonant tunneling are described by this spectral density.

5.1 The Current

5.1.1 Quantum Dot

The current flowing through the barriers $r = L, R$ is defined by

$$I_r(t) = e\frac{d}{dt}\langle n_r(t)\rangle\,. \tag{5.1}$$

The time dependence of $n_r(t)$ in the Heisenberg picture is given by the equation of motion $\frac{d}{dt}\,n_r(t)_H = i\,[H, n_r]\,(t)_H$. Therefore, we obtain for Eq. (5.1)

$$I_r(t) = -ie\left\{\sum_{k\sigma} T_k^r \langle (a_{k\sigma r}^\dagger c_\sigma)(t)\rangle - h.c.\right\} \tag{5.2}$$

and for the stationary current

$$I_r^{st} = \lim_{t\to\infty} I_r(t) = \lim_{t_i\to-\infty} I_r(0). \tag{5.3}$$

The current is then an expectation value of a product of a dot and reservoir electron operator (see Fig. 5.1). Now, we repeat the procedure of expanding the propagator and tracing out the reservoirs. Due to Wick's theorem the reservoir electron operator gets coupled with an other reservoir electron operator within the propagators by

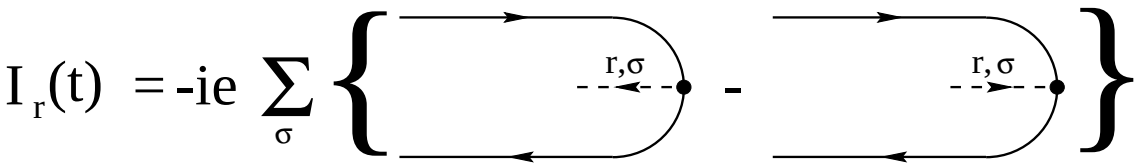

Figure 5.1: Graphical representation of the current I_r through lead r. Internal vertices are not indicated.

a tunneling line. We write out this tunneling line explicitly. The current is then written as an expectation value of a product of two dot electron operators at different times, i.e., we encounter now the correlation functions $C^{>}(t,t')$ and $C^{<}(t,t')$. In

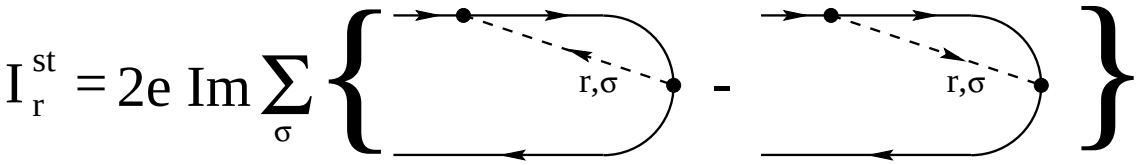

Figure 5.2: Graphical representation of the relation between the current and the correlation functions. Here, the line connecting the external vertices is a real one. Internal vertices are not indicated.

order to calculate the stationary current I_r^{st} we relate it to $C^{>}(\omega)$ and $C^{<}(\omega)$ as indicated in Fig. 5.2 which gives

$$I_r^{st} = -ieM \int d\omega \left\{ \gamma_r^+(\omega) C^{>}(\omega) + \gamma_r^-(\omega) C^{<}(\omega) \right\}. \tag{5.4}$$

The correlation functions can now be calculated from the diagrams shown in Figs. 5.3 and 5.4. We have to consider only the latest (i.e. rightmost) correlated part of the diagram. The processes before end up with probability P_χ^{st} in a diagonal state χ. We have used the same criterion as for the calculation of the density matrix with one exception. If a vertical line lies between the external vertices we allow a cut through at most one tunneling line. Here we have used the fact that such a vertical line will in addition always cut the virtual line connecting the external vertices. The sum of all these diagrams gives (where the mirror rule allows us to combine always two diagrams to the imaginary part of one of them)

$$C^{>}(\omega) = 2i\,\mathrm{Im}\left\{ P_0^{st}\,\pi(\omega) - M\,\pi(\omega) \int d\omega' \frac{P_0^{st}\phi^+(\omega')^* + P_\sigma^{st}\phi^-(\omega')^*}{\omega - \omega' + i\eta} \right\} \tag{5.5}$$

$$C^{<}(\omega) = -2i\,\mathrm{Im}\left\{ -P_\sigma^{st}\,\pi^*(\omega) + \pi^*(\omega) \int d\omega' \frac{P_0^{st}\phi^+(\omega') + P_\sigma^{st}\phi^-(\omega')}{\omega' - \omega + i\eta} \right\} \tag{5.6}$$

which yields with Eqs. (4.10), (4.11), (4.14), and (4.17)

$$C^{>}(\omega) = -2\pi i\,\gamma^-(\omega)\,|\pi(\omega)|^2 \tag{5.7}$$

$$C^{<}(\omega) = 2\pi i\,\gamma^+(\omega)\,|\pi(\omega)|^2 \tag{5.8}$$

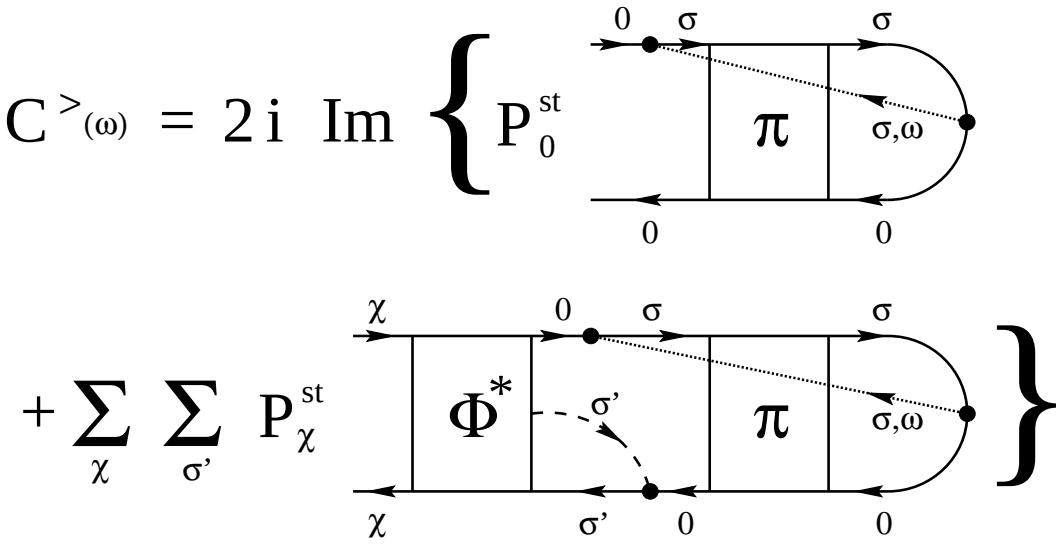

Figure 5.3: Graphical representation of $C^{>}(\omega)$ for the quantum dot.

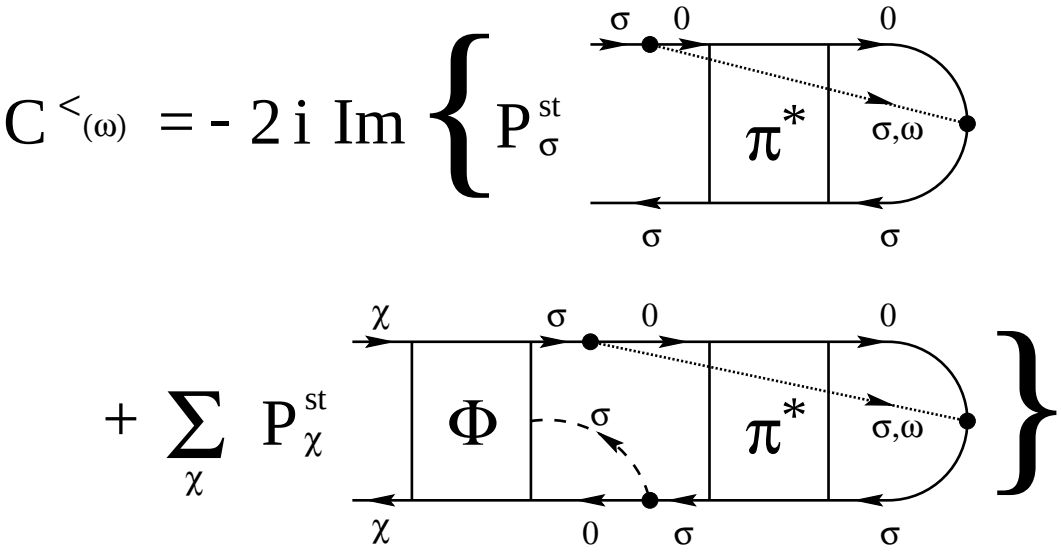

Figure 5.4: Graphical representation of $C^{<}(\omega)$ for the quantum dot.

and therefore

$$A(\omega) = \left[\gamma^+(\omega) + \gamma^-(\omega)\right] |\pi(\omega)|^2 \,. \tag{5.9}$$

Notice that $\int d\omega A(\omega) = P_0^{st} + P_\sigma^{st}$ which is not equal to 1 for $M \geq 2$. This is due to the fact that we only allow an empty or a singly occupied dot in all intermediate situations (see Section 5.2.1).

5.1.2 Metallic Island: Path-Integral Approach

For the metallic island we start like before with

$$I_r(t) = e\frac{d}{dt}\langle n_r(t)\rangle \tag{5.10}$$

and find after some algebra

$$I_r(t) = -ie\left\{\sum_{kqn} T_{kq}^{rn}\langle (a_{knr}^\dagger c_{qn})(t)\rangle - h.c.\right\} \,. \tag{5.11}$$

We can calculate this expression within the path-integral approach by adding a source term to the Hamiltonian

$$H(t) \;\rightarrow\; H(t) - ie\lambda(t)\sum_{kqn}\{T_{kq}^{rn} a_{knr}^\dagger(t) c_{qn}(t) - h.c.\} \tag{5.12}$$

and then taking the functional derivative of the propagator with respect to the source $\lambda(t)$:

$$I_r(t) = \left\langle T_K \frac{i\delta}{\delta\lambda(t)} \exp\left(-i\int_K dt' \left[H(t') - ie\lambda(t')\left\{\sum_{kqn} T_{kq}^{rn} a_{knr}^\dagger c_{qn} - h.c.\right\}\right]\right)\Big|_{\lambda\equiv 0}\right\rangle . \tag{5.13}$$

To account for the source term we modify the tunneling term by multiplying a factor $(1 \mp ie\lambda(t))$ to the tunneling amplitudes:

$$T \;\rightarrow\; T(1 - ie\lambda(t)) \tag{5.14}$$

$$T^* \;\rightarrow\; T^*(1 + ie\lambda(t)) \,. \tag{5.15}$$

The Hubbard-Stratonovich transformation, which introduces the collective variable φ leads to the same expressions as in Chapter 2 but with the replacements

$$e^{-i\varphi(t)} \;\rightarrow\; e^{-i\varphi(t)}(1 - ie\lambda(t)) \tag{5.16}$$

$$e^{i\varphi(t)} \;\rightarrow\; e^{i\varphi(t)}(1 + ie\lambda(t)) \,. \tag{5.17}$$

Due to the functional derivation the correlation functions $C^>$ and $C^<$ are involved. For a large number of channels N_{ch} the stationary current then reads

$$I_r^{st} = -ie\int d\omega \left\{\alpha_r^+(\omega) C^>(\omega) + \alpha_r^-(\omega) C^<(\omega)\right\} . \tag{5.18}$$

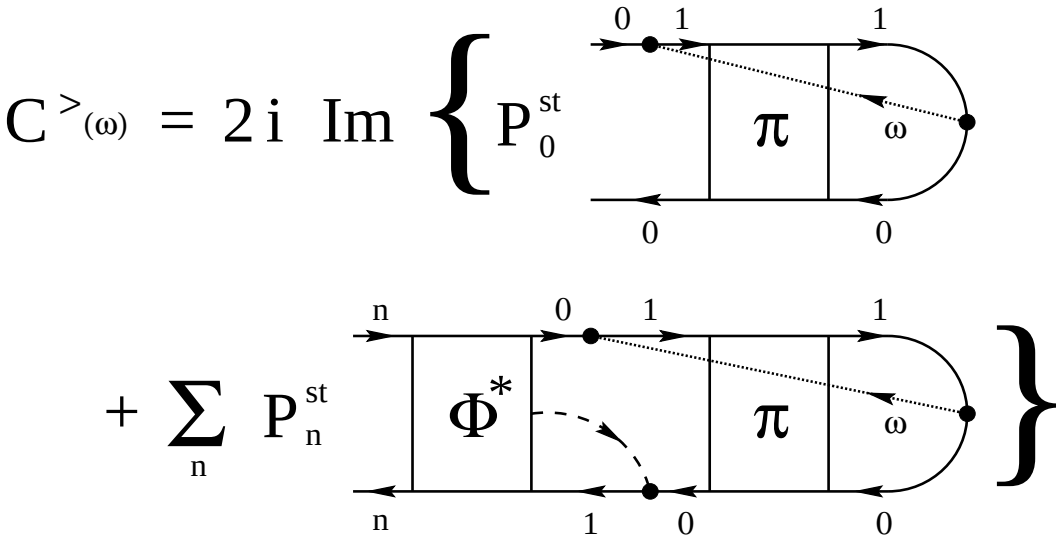

Figure 5.5: Graphical representation of $C^{>}(\omega)$ for the metallic island.

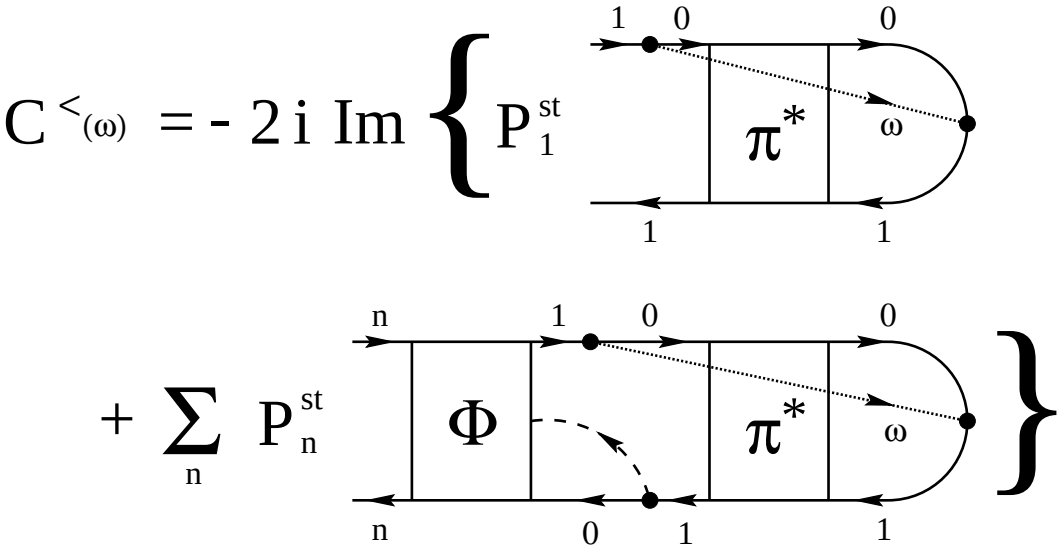

Figure 5.6: Graphical representation of $C^{<}(\omega)$ for the metallic island.

Note that for a small number of channels more complicated correlation functions occur as well, in which more than two exponentials $e^{\pm i\varphi}$ are involved.

The value of the correlation functions (for a graphical representation see Figs. 5.5 and 5.6) is within our approximation

$$C^{>}(\omega) = 2i\,\mathrm{Im}\left\{P_0^{st}\,\pi(\omega) - \pi(\omega)\int d\omega' \frac{P_0^{st}\phi^{+}(\omega')^{*} + P_1^{st}\phi^{-}(\omega')^{*}}{\omega - \omega' + i\eta}\right\} \tag{5.19}$$

$$C^{<}(\omega) = -2i\,\mathrm{Im}\left\{-P_1^{st}\,\pi^{*}(\omega) + \pi^{*}(\omega)\int d\omega' \frac{P_0^{st}\phi^{+}(\omega') + P_1^{st}\phi^{-}(\omega')}{\omega' - \omega + i\eta}\right\} \tag{5.20}$$

which yields with Eqs. (4.21), (4.24), and (4.27)

$$C^{>}(\omega) = -2\pi i\,\alpha^{-}(\omega)\,|\pi(\omega)|^2 \tag{5.21}$$

$$C^{<}(\omega) = 2\pi i\,\alpha^{+}(\omega)\,|\pi(\omega)|^2 \tag{5.22}$$

and therefore

$$A(\omega) = \alpha(\omega)|\pi(\omega)|^2 \tag{5.23}$$

with $\int d\omega A(\omega) = 1$.

5.1.3 Metallic Island: Operator Approach

Within the operator approach we work with a modified Hamiltonian, which includes operators φ in the tunneling term. In this case

$$I_r(t) = -ie\left\{\sum_{kqn} T_{kq}^{rn}\langle(a_{knr}^{\dagger}c_{qn}e^{-i\varphi})(t)\rangle - h.c.\right\}. \tag{5.24}$$

At this stage, we again expand the propagator and trace out the microscopic degrees of freedom. For a large number of channels N_{ch} the vertex at time t is coupled to only one other vertex, thus building a simple loop. Writing out this simple loop explicitly we relate the stationary current to the correlation functions and find

$$I_r^{st} = -ie\int d\omega\left\{\alpha_r^{+}(\omega)C^{>}(\omega) + \alpha_r^{-}(\omega)C^{<}(\omega)\right\}, \tag{5.25}$$

which the same result as in the previous section.

5.2 The Spectral Density

The physical quantities of interest, the stationary distribution and the current, as well as the correlation functions can be expressed in terms of the spectral density.

For the quantum dot we find:

$$
\begin{aligned}
A(\omega) &= \frac{1}{2\pi}\Gamma(\omega)|\pi(\omega)|^2 && (5.26)\\
P_0^{st} &= \int d\omega \frac{\sum_r \Gamma_r(\omega) f_r^-(\omega)}{\Gamma(\omega)} A(\omega) && (5.27)\\
P_\sigma^{st} &= \int d\omega \frac{\sum_r \Gamma_r(\omega) f_r^+(\omega)}{\Gamma(\omega)} A(\omega) && (5.28)\\
I_r^{st} &= \frac{e}{h} 2\pi M \int d\omega \sum_{r'} \frac{\Gamma_r(\omega)\Gamma_{r'}(\omega)}{\Gamma(\omega)} A(\omega)[f_{r'}^+(\omega) - f_r^+(\omega)] && (5.29)\\
C^>(\omega) &= -2\pi i \frac{\sum_r \Gamma_r(\omega) f_r^-(\omega)}{\Gamma(\omega)} A(\omega) && (5.30)\\
C^<(\omega) &= 2\pi i \frac{\sum_r \Gamma_r(\omega) f_r^+(\omega)}{\Gamma(\omega)} A(\omega)\,. && (5.31)
\end{aligned}
$$

In the following we assume a constant density of states of the dot electrons, i.e., $\Gamma_r(\omega) = \Gamma_r$ is energy-independent.

In order to write the results for the metallic island in a similar form we introduce the functions

$$
\begin{aligned}
\alpha_r(\omega) &= \alpha_r^+(\omega) + \alpha_r^-(\omega) && (5.32)\\
\alpha^\pm(\omega) &= \sum_r \alpha_r^\pm(\omega) && (5.33)\\
\alpha(\omega) &= \alpha^+(\omega) + \alpha^-(\omega) && (5.34)
\end{aligned}
$$

and use the identity

$$
\alpha_r^\pm(\omega) = \alpha_r(\omega) f_r^\pm(\omega)\,. \qquad (5.35)
$$

Then we find

$$
\begin{aligned}
A(\omega) &= \alpha(\omega)|\pi(\omega)|^2 && (5.36)\\
P_0^{st} &= \int d\omega \frac{\sum_r \alpha_r(\omega) f_r^-(\omega)}{\alpha(\omega)} A(\omega) && (5.37)\\
P_1^{st} &= \int d\omega \frac{\sum_r \alpha_r(\omega) f_r^+(\omega)}{\alpha(\omega)} A(\omega) && (5.38)\\
I_r^{st} &= \frac{e}{h} 4\pi^2 \int d\omega \sum_{r'} \frac{\alpha_r(\omega)\alpha_{r'}(\omega)}{\alpha(\omega)} A(\omega)[f_{r'}^+(\omega) - f_r^+(\omega)] && (5.39)\\
C^>(\omega) &= -2\pi i \frac{\sum_r \alpha_r(\omega) f_r^-(\omega)}{\alpha(\omega)} A(\omega) && (5.40)\\
C^<(\omega) &= 2\pi i \frac{\sum_r \alpha_r(\omega) f_r^+(\omega)}{\alpha(\omega)} A(\omega)\,. && (5.41)
\end{aligned}
$$

These results satisfy the conservation laws and sum rules. Current is conserved, i.e. $\sum_r I_r^{st} = 0$, and vanishes in equilibrium when $\mu_r = 0$. All probabilities are positive and the usual relationships between the correlation functions and the spectral density in equilibrium are reproduced.

In the following we choose a symmetric bias $\mu_L = -\mu_R = eV/2$. This is no loss of generality but can be always achieved by a shift of the parameters ϵ_0 and Δ_0.

5.2.1 Quantum Dot

The spectral density reads

$$A(\omega) = \frac{1}{2\pi} \frac{\Gamma}{[\omega - \epsilon_0 - \mathrm{Re}\,\sigma(\omega)]^2 + [\mathrm{Im}\,\sigma(\omega)]^2} \tag{5.42}$$

with

$$\mathrm{Re}\,\sigma(\omega) = (M-1) \sum_r \frac{\Gamma_r}{2\pi} \left[\ln\left(\frac{\beta E_C}{2\pi}\right) - \mathrm{Re}\,\psi\left(\frac{1}{2} + i\frac{\beta}{2\pi}(\omega - \mu_r)\right)\right] \tag{5.43}$$

$$\mathrm{Im}\,\sigma(\omega) = -\pi\gamma(\omega) = -\sum_r \frac{\Gamma_r}{2}[1 + (M-1) f_r(\omega)]\,. \tag{5.44}$$

To understand the effects of the resonant tunneling processes, we first consider the lower order contributions. We obtain these by expanding Eq. (5.42) with respect to Γ:

$$A(\omega) = A^{(0)}(\omega) + A^{(1)}(\omega) + \ldots\,. \tag{5.45}$$

In lowest order we recover single electron tunneling described by

$$A^{(0)}(\omega) = \frac{\gamma^+(\omega) + \gamma^-(\omega)}{\gamma(\omega)} \delta(\omega - \epsilon_0)\,. \tag{5.46}$$

This is the classical result. Possible processes are an electron entering or leaving the island. In lowest order their energy must match the energy of the dot level. This explains the delta-function.

The contribution of the next order is

$$A^{(1)}(\omega) = \frac{1}{2\pi} \frac{\Gamma}{(\omega - \epsilon_0)^2}\,, \tag{5.47}$$

which describes cotunneling.

For the derivation of Eq. (5.42) we took only those diagrams into account in which a vertical line will cut at most two tunneling lines. For $M = 1$, however, this constriction is no approximation. The sum of all more complicated contributions is exactly zero (see Appendix D). In this case Eq. (5.42) reduces to the Breit-Wigner formula

$$A(\omega) = \frac{1}{\pi} \frac{\Gamma/2}{(\omega - \epsilon_0)^2 + (\Gamma/2)^2} \qquad \text{for} \qquad M = 1\,. \tag{5.48}$$

The spectral density has a Lorentzian shape with a maximum at $\omega = \epsilon_0$ and a half-width $\Gamma/2$.

For $M \geq 2$ the spectral density Eq. (5.42) has a similar shape:

$$A(\omega) = \frac{1}{\pi} \frac{\Gamma/2}{\left[\omega - \epsilon(\omega)\right]^2 + \left[\sum_r \Gamma_r/2\{1 + (M-1) f_r(\omega)\}\right]^2} \,. \tag{5.49}$$

But now, the bare dot level energy ϵ_0 is renormalized by the real part of the self-energy. In the limit when one of the energies $k_B T, eV/2, |\omega|$ dominates the other ones, the renormalization shows a logarithmic dependence

$$\epsilon(\omega) = \epsilon_0 + (M-1) \sum_r \frac{\Gamma_r}{2\pi} \ln \frac{E_C}{\max\{2\pi k_B T, eV/2, |\omega|\}} \,, \tag{5.50}$$

which can be seen from Eq. (5.43). If ω is of the order of one of the chemical potentials μ_r, we can write this in the form

$$\epsilon(\omega) = \epsilon_0 + (M-1) \sum_r \frac{\Gamma_r}{2\pi} \ln \frac{E_C}{\max\{2\pi k_B T, |\omega - \mu_r|\}} \,. \tag{5.51}$$

Resonances in the spectral density lie at frequencies ω with $\omega - \epsilon(\omega) = 0$. One solution of this equation leads to the position of the charge excitation peak. In comparison to the bare level ϵ_0 its position is shifted to higher energies.

For a low lying level ϵ_0 the Anderson model can be mapped by a Schrieffer-Wolff transformation onto the Kondo model which describes scattering of electrons in a metal by the spin of magnetic impurities. At low temperatures, the interaction of the spin of the conductance electrons with the spin of the impurity leads to an increase of the resistivity (Kondo effect). In the Anderson model the Kondo effect shows up as an increase of the transmittivity through the dot, expressed by a spectral density with sharp resonances near the Fermi levels μ_r. This is clearly a nonperturbative effect. It cannot be understood within a perturbative approach, but requires the consideration of quantum fluctuations described here by resonant tunneling processes.

And indeed, at low temperatures and $\epsilon_0 < 0$ we find a solution of $\omega - \epsilon(\omega) = 0$ which leads to sharp Kondo resonances near the Fermi levels μ_r (see Fig. 5.7). They arise due to the fact that the logarithm in Eq. (5.51) diverges for $\omega = \mu_r$. The logarithmic terms are typical for the occurrence of Kondo physics.

Furthermore, the broadening, which is determined by the imaginary part of the self-energy, is energy dependent. The Fermi functions in Eq. (5.44) give rise to an asymmetric broadening (see Fig. 6.5).

An important ingredient of the occurrence of Kondo physics and the asymmetric broadening effect is that there is an asymmetry in the probabilities to realize an occupied or an unoccupied dot: For $M \geq 2$ the number of processes filling up the dot is $2M$ (an electron enters the dot from the left or the right lead and carries an

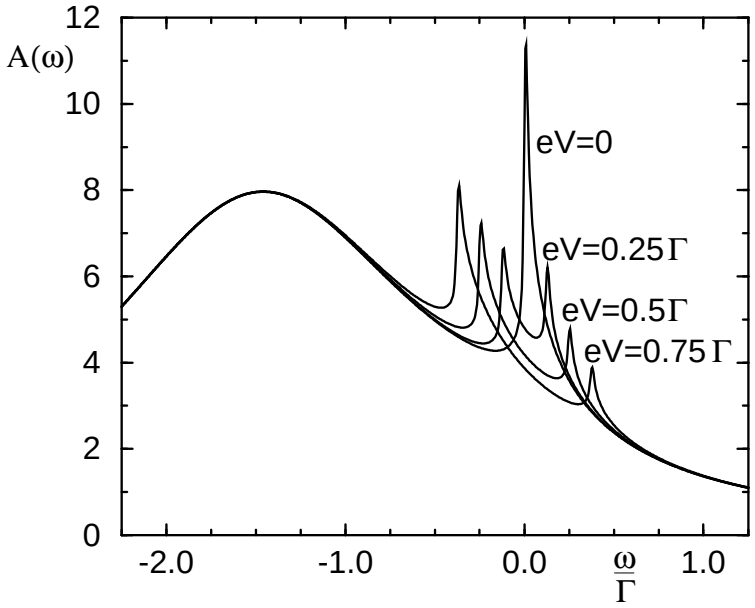

Figure 5.7: The spectral density for $M = 2$, $\Gamma_L = \Gamma_R = \Gamma/2$, $k_B T = 0.005\Gamma$, $\epsilon_0 = -2\Gamma$, and $E_C = 50\Gamma$ at different voltages. At $V = 0$ there is a Kondo resonance which splits at finite transport voltages.

arbitrary spin) while only 2 processes make an occupied dot empty (the electron with given spin leaves the dot).

We see from Eqs. (5.27) and (5.28) that $\int d\omega A(\omega) = P_0^{st} + P_\sigma^{st}$ which does not equal to 1 for $M \geq 2$. This is due to the fact that we only allow for an empty or a singly occupied dot in all intermediate situations. Higher occupation has been neglected. The energy of excitations in which higher occupancy is involved are of the order of U higher than those with at most single occupancy. Therefore, the spectral density should have additional charge excitation peaks at these higher energies. The integral of the spectral density then equals to one. Since we have performed the limit $U \to \infty$ before integration, the integral is less than one.

5.2.2 Metallic Island

Here, the spectral density is

$$A(\omega) = \frac{\alpha(\omega)}{[\omega - \Delta_0 - \mathrm{Re}\,\sigma(\omega)]^2 + [\mathrm{Im}\,\sigma(\omega)]^2} \tag{5.52}$$

with

$$\mathrm{Re}\,\sigma(\omega) \;=\; -\sum_r \alpha_0^r\,(\omega - \mu_r)\left[2\ln\left(\frac{\beta E_C}{2\pi}\right) - 2\mathrm{Re}\,\psi\left(i\frac{\beta}{2\pi}(\omega - \mu_r)\right)\right] \tag{5.53}$$

$$\mathrm{Im}\,\sigma(\omega) \;=\; -\pi\alpha(\omega)\,. \tag{5.54}$$

Similar to the quantum dot case we can expand Eq. (5.52) in α_0 and then recover for the lowest order contribution the single electron tunneling or classical result

$$A^{(0)}(\omega) = \delta(\omega - \Delta_0)\,. \tag{5.55}$$

The term of next order describes cotunneling

$$A^{(1)}(\omega) = \frac{\alpha(\omega)}{(\omega - \Delta_0)^2}\,. \tag{5.56}$$

In general, the self-energy $\sigma(\omega)$ implies renormalization and broadening effects. In the limit when one of the energies $k_BT, eV/2, |\omega|$ dominates the other ones, the self-energy reads due to Eqs. (5.53) and (5.54)

$$\sigma(\omega) = -2\sum_r \alpha_0^r\,\omega \ln\frac{E_C}{\max\{2\pi k_BT, eV/2, |\omega|\}} - i\pi\sum_r \alpha_0^r \max\{2k_BT, eV/2, |\omega|\}\,. \tag{5.57}$$

The real part of the self-energy is proportional to ω, in contrast to the quantum dot case, in which it was crucially given by the logarithm only. Therefore, in order to write the spectral density in a Lorentz form, we have to combine all terms which contain the factor ω. Introducing the renormalization factor Z with

$$Z^{-1} = 1 + 2\sum_r \alpha_0^r \ln\frac{E_C}{\max\{2\pi k_BT, eV/2, |\omega|\}}\,, \tag{5.58}$$

we obtain for Eq. (5.52)

$$A(\omega) = Z\frac{\tilde{\alpha}(\omega)}{[\omega - \tilde{\Delta}]^2 + [\pi\tilde{\alpha}(\omega)]^2}\,, \tag{5.59}$$

with

$$\tilde{\Delta} = Z\Delta_0 \qquad \text{and} \qquad \tilde{\alpha}(\omega) = Z\alpha(\omega)\,. \tag{5.60}$$

For dominating temperature k_BT or transport voltage eV (to be more precisely for $k_BT \geq |\omega|, eV/2$ or $eV/2 \geq |\omega|$ and $eV \gg k_BT$), Eq. (5.59) has the Lorentzian form looked for, in which the peak position as well as the broadening is renormalized by Z. Notice that this renormalization is multiplicative and not additive like in the quantum dot case. If the frequency $|\omega|$ is the dominant energy, i.e. $|\omega| \gg eV, k_BT$, further calculations yield

$$A(\omega) = \frac{|\omega|}{\Delta_0}\frac{\tilde{\Delta}\,\tilde{\alpha}_0}{\left(\omega - \tilde{\Delta}\right)^2 + \left(\pi\tilde{\Delta}\tilde{\alpha}_0\right)^2} \tag{5.61}$$

in which the renormalized parameters are now

$$\tilde{\Delta} = \frac{Z\Delta_0}{1 + \pi^2\tilde{\alpha}_0^2} \qquad \text{and} \qquad \tilde{\alpha}_0 = Z\sum_r \alpha_0^r\,. \tag{5.62}$$

Chapter 6

Results

The final results for the physical quantities of interest, the stationary distribution and the current, are given in Eqs. (5.27) - (5.29) and (5.37) - (5.39) of Section 5. They are related to the spectral density. In comparison to the result from lowest order perturbation theory, the "classical" result, there are renormalization and broadening effects. The renormalization is as well responsible for the occurrence of Kondo physics in the quantum dot case. All these effects are discussed in this chapter.

For all plots in this chapter we choose symmetric barriers $\alpha_0^L = \alpha_0^R$ and $\Gamma_L = \Gamma_R = \Gamma/2$. In the quantum dot case, we consider $M = 2$. Furthermore we take a symmetric bias $\mu_L = -\mu_R = eV/2$.

6.1 Average Charge on the Island

The average number of (excess) electrons on the island is given by $\langle n \rangle = M P_\sigma^{st}$ in the quantum dot case and $\langle n \rangle = P_1^{st}$ in the metallic case. Figures 6.1 and 6.2 show plots in the limit $k_B T \ll eV$ for the quantum dot and the metallic island. For comparison, the classical results are displayed as well.

In the quantum dot case, there are steps at the Fermi levels of the leads. These steps, which – in the classical limit – are smeared only by temperature (in the Figs. 6.1 and 6.2 we have chosen $T = 0$), are additionally washed out due to quantum fluctuations expressed by the imaginary part of the self-energy. Furthermore, the whole structure is shifted to lower energies. This indicates renormalization effects.

For systems with a metallic island, the classical result yields a linear decrease of the average charge between the Fermi levels. Also here, the sharp structure is washed out by quantum fluctuations, even at $T = 0$.

At $V = 0$, the single electron transistor becomes equivalent to the single electron box. In the classical limit, the average charge is then described by a step function which is smeared by temperature. The renormalization effects, however, lead to an anomalous temperature behaviour of the slope $\partial\langle n \rangle / \partial \Delta_0$ at $\Delta_0 = 0$ in the metallic

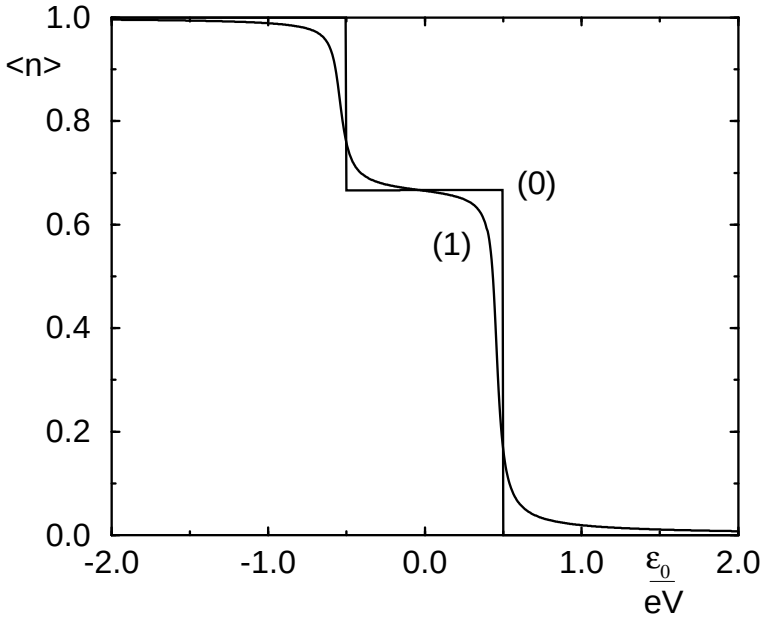

Figure 6.1: The average number of electrons in the dot as a function of the level position ϵ_0 normalized to the transport voltage eV for $M = 2$, $T = 0$, $\Gamma_L = \Gamma_R = \Gamma/2$, $eV = 20\Gamma$ and $E_C = 500\Gamma$. The step function (0) shows the classical result. Due to resonant tunneling processes the steps are smeared out and the whole curve is shifted to the left.

case. Neglecting the broadening, i.e. $\pi Z \sum_r \alpha_0^r \ll 1$, we find using Eq. (5.59)

$$\begin{aligned} \frac{\partial\langle n\rangle}{\partial\Delta_0}\Big|_{\Delta_0=0} &= \frac{\partial}{\partial\Delta_0}\int d\omega\, f(\omega) Z\delta(\omega - Z\Delta_0)\Big|_{\Delta_0=0} = -\frac{1}{4k_BT}Z^2 \\ &= -\frac{1}{4k_BT\left[1 + 2\sum_r \alpha_0^r \ln(\frac{E_C}{2\pi k_B T})\right]^2}\,. \end{aligned} \tag{6.1}$$

It is reduced compared to the classical result

$$\frac{\partial\langle n\rangle}{\partial\Delta_0}\Big|_{\Delta_0=0} = -\frac{1}{4k_BT}\,. \tag{6.2}$$

6.2 Conductance Oscillations

The current $I = I_R^{st} = -I_L^{st}$ through the system is given by Eqs. (5.29) and (5.39). In the classical limit it reads

$$I = \frac{e}{h} 2\pi M \frac{\Gamma_L\Gamma_R}{\sum_r \Gamma_r[1 + (M-1)f_r(\epsilon_0)]}[f_L(\epsilon_0) - f_R(\epsilon_0)] \tag{6.3}$$

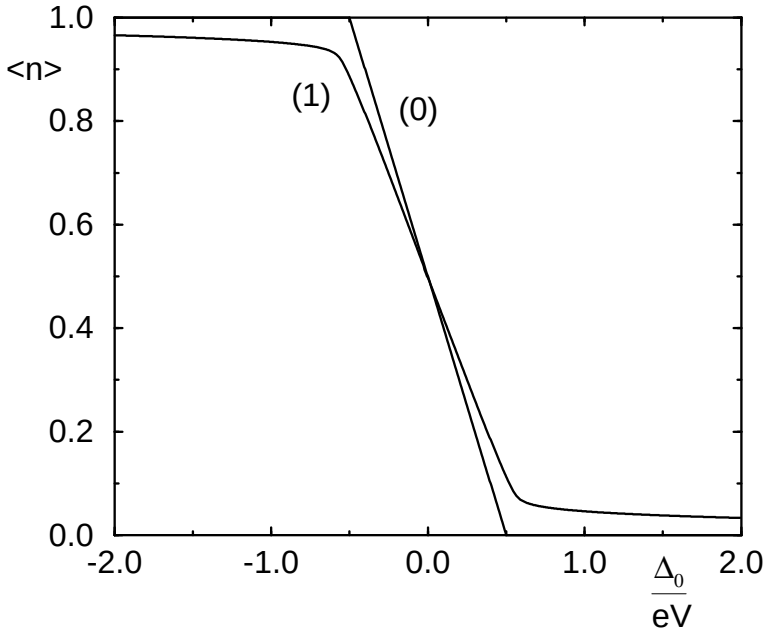

Figure 6.2: The average number of excess electrons on the metallic island as a function of the gap energy Δ_0 normalized to the transport voltage eV for $T = 0$, $\alpha_0^L = \alpha_0^R = 0.01$ and $E_C = 25eV$. The linear function (0) shows the classical result. Due to resonant tunneling processes the curve is smeared out.

for the quantum dot and

$$I = \frac{e}{h} 4\pi^2 \frac{\alpha_L(\Delta_0)\alpha_R(\Delta_0)}{\alpha(\Delta_0)} [f_L(\Delta_0) - f_R(\Delta_0)] \tag{6.4}$$

for the metallic island. The gate voltage dependence, i.e., the dependence on ϵ_0 or Δ_0 respectively, is determined by the larger of the energy scales k_BT or eV. If the transport voltage provides the dominant energy scale, transport is only possible within a window delimited by the Fermi levels of the leads. For the quantum dot, the current is constant within this window. In the metallic case, the structure is described by a parabola. For the other limit, i.e., if the temperature dominates over the transport voltage, we get a peak with a width in the order of k_BT.

This will be modified due to renormalization and broadening effects. But instead of considering the current, we examine the differential conductance

$$G = \frac{\partial I}{\partial V}\,, \tag{6.5}$$

which will show more pronounced signature of quantum fluctuations.

In this section we consider its gate voltage dependence. (Notice that the derivative is performed with respect to an other variable, the transport voltage.)

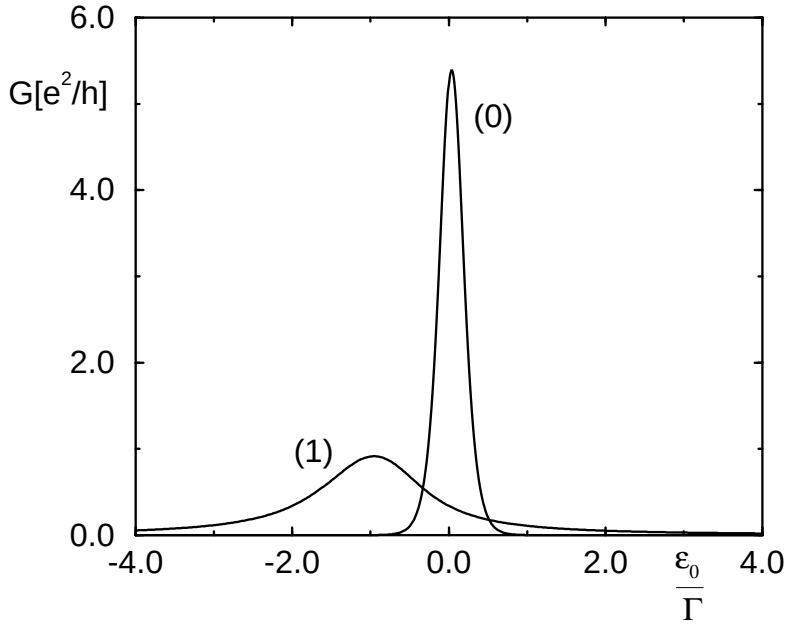

Figure 6.3: The differential conductance in linear response ($V = 0$) for the quantum dot as a function of the level position ϵ_0 with $M = 2$, $\Gamma_L = \Gamma_R = \Gamma/2$, $k_B T = 0.1\Gamma$ and $E_C = 100\Gamma$. In the classical limit (0) the peak width is given by temperature. Due to resonant tunneling processes, the peak width is determined by the intrinsic broadening Γ and the peak position is shifted to the left.

6.2.1 Linear Response

In the linear response regime, i.e. at $V = 0$, we derive from Eqs. (5.29) and (5.39).

$$G = -\frac{e^2}{h} 2\pi M \int d\omega \frac{\Gamma_L \Gamma_R}{\Gamma} A(\omega) f'(\omega)\Big|_{V=0} \tag{6.6}$$

for the quantum dot and

$$G = -\frac{e^2}{h} 4\pi^2 \int d\omega \frac{\alpha_L(\omega)\alpha_R(\omega)}{\alpha(\omega)} A(\omega) f'(\omega)\Big|_{V=0} \tag{6.7}$$

for the metallic island. The derivative of the Fermi function confines the integration variable within the regime $|\omega| \leq k_B T$. We therefore get a single peak.

Figure 6.3 shows the curve for a quantum dot. We see as an effect of the renormalization that the peak is shifted to lower energies in comparison to the classical result. Since the broadening of the spectral density is of the order Γ and the width of the derivative of the Fermi function is $k_B T$, the larger one of these two energy scales determines the width of the conductance peak. In Fig. 6.3, the intrinsic broadening

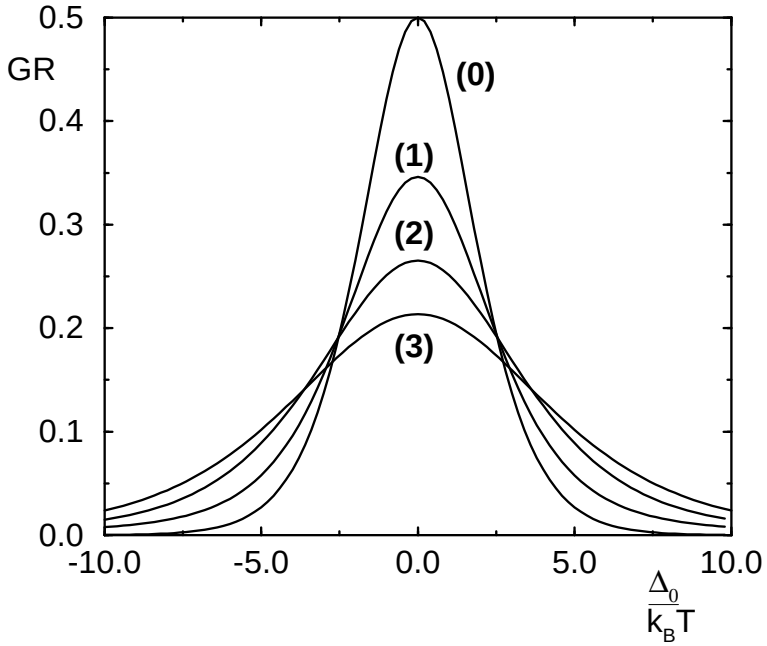

Figure 6.4: The differential conductance in linear response ($V = 0$) for the metallic island as a function of the gap energy Δ_0 normalized to the temperature k_BT with $\alpha_0^L = \alpha_0^R = 0.05$ and (1) $k_BT/E_C = 0.1$, (2) $k_BT/E_C = 0.01$ and (3) $k_BT/E_C = 0.001$. For comparison, (0) shows the classical result, which is independent of the temperature k_BT.

Γ is the larger one. Therefore, the peak width is enlarged and the peak height is reduced compared to the classical result.

Some plots with different values of k_BT are depicted for the metallic case in Fig. 6.4. The broadening of the spectral density is of the order $\pi Z \sum_r \alpha_0^r k_BT$. For $\pi Z \sum_r \alpha_0^r \ll 1$, we can neglect this compared to the broadening of the derivative of the Fermi function, which is of the order of k_BT. Therefore, we normalized the x-axis to k_BT. The deviations from the classical result are traced back to the renormalization of Δ_0. They are explained as follows: Using $\int d\Delta_0 A(\Delta_0) = 1$ and $\int dx\ x/\sinh x = \pi^2/2$ [44] we find for symmetric barriers with resistances $R_L = R_R = R/2$ that the integral

$$R \int d\Delta_0 G(\Delta_0) = \frac{\pi^2}{4} k_BT \tag{6.8}$$

is proportional to k_BT. For $\pi Z \sum_r \alpha_0^r \ll 1$ we calculate the height of the conductance peak using $A(\omega) = Z\delta(\omega - Z\Delta_0)$ and find

$$RG(\Delta_0 = 0) = \frac{1}{2} Z \tag{6.9}$$

which depends logarithmically on k_BT. Therefore, the normalized width γ of the structure, given by

$$\gamma = \frac{1}{k_BT}\frac{\int d\Delta_0 G(\Delta_0)}{G(\Delta_0=0)} = \frac{\pi^2}{2}\frac{1}{Z} = \frac{\pi^2}{2}\left[1 + 2\sum_r \alpha_0^r \ln\frac{E_C}{2\pi k_BT}\right], \tag{6.10}$$

increases with decreasing temperature.

Finally, we would like to remark, that the peak height and width can be calculated analytically even without neglecting the broadening. The integral in Eq. (6.7) yields (using Eq. (5.59)) for the maximum value of the linear conductance

$$RG(\Delta_0=0) = \frac{1}{2}Z\left[\frac{1}{2} - \frac{1}{\pi}\arctan\left(\frac{(\pi Z\sum_r \alpha_0^r)^2 - 1}{2\pi Z\sum_r \alpha_0^r}\right)\right] \tag{6.11}$$

and therefore for the width

$$\gamma = \frac{\pi^2}{2}\frac{1}{Z}\left[\frac{1}{2} - \frac{1}{\pi}\arctan\left(\frac{(\pi Z\sum_r \alpha_0^r)^2 - 1}{2\pi Z\sum_r \alpha_0^r}\right)\right]^{-1}. \tag{6.12}$$

It is clear that for $\pi Z\sum_r \alpha_0^r \ll 1$ these results reduce to Eqs. (6.9) and (6.10).

6.2.2 Nonlinear Response

In the opposite limit, i.e. T=0, the transport voltage provides the relevant energy scale. The conductance is then given by

$$G = \frac{e}{h}2\pi M\frac{\partial}{\partial V}\int_{-eV/2}^{eV/2} d\omega \frac{\Gamma_L\Gamma_R}{\Gamma}A(\omega)\Big|_{T=0} \tag{6.13}$$

for the quantum dot and

$$G = \frac{e}{h}4\pi^2\frac{\partial}{\partial V}\int_{-eV/2}^{eV/2} d\omega \frac{\alpha_L(\omega)\alpha_R(\omega)}{\alpha(\omega)}A(\omega)\Big|_{T=0} \tag{6.14}$$

for the metallic island.

Figure 6.5 shows the curve for the quantum dot case. The main contribution to the conductance comes from the derivation of the integration limits. Therefore, we find two peaks with distance eV. They are shifted to the left in comparison to the classical case. This is an effect of the renormalization. In the classical limit the width of the peaks is determined by temperature, i.e., at $T = 0$ there are delta-peaks. Due to the broadening of the spectral density by the intrinsic broadening Γ, the width is now given by the larger one of k_BT and Γ. In Fig. 6.5 we have chosen $\Gamma > k_BT$.

In Chapter 5 we recognized, that the imaginary part of the self-energy $\sigma(\omega)$, which describes the broadening of the spectral density, contains the Fermi functions $f_r(\omega)$. In consequence, it is always smaller at higher energies. This leads to a

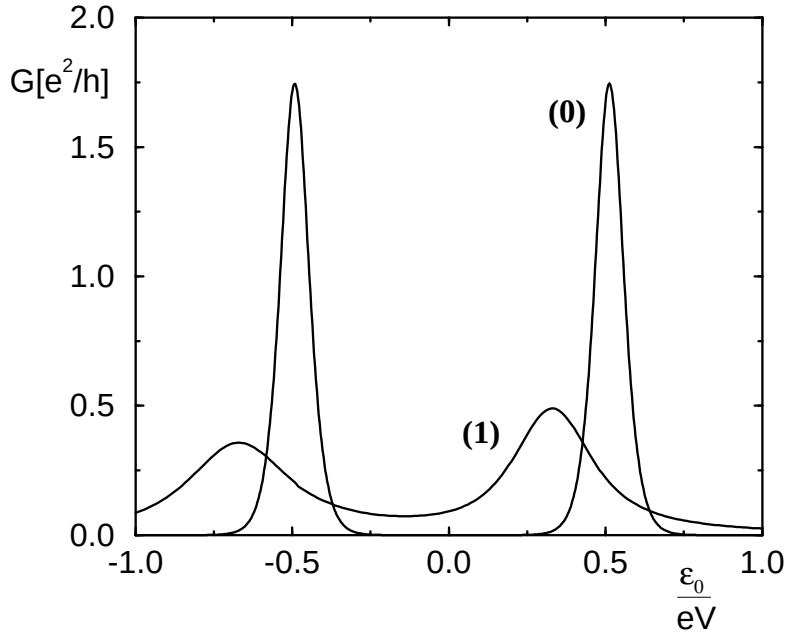

Figure 6.5: The differential conductance in nonlinear response for the quantum dot as a function of the level position ϵ_0 with $M = 2$, $\Gamma_L = \Gamma_R = \Gamma/2$, $eV = 5\Gamma$, $k_BT = 0.15\Gamma$ and $E_C = 500\Gamma$. For comparison, (0) shows the classical result, in which the width of the peaks is given by temperature. Due to resonant tunneling processes, the width of the peaks is determined by the intrinsic broadening Γ and Fermi functions which give rise to an asymmetric broadening. Furthermore, the peak positions are shifted to the left.

classically unexpected asymmetry of the peak heights. The peak near $\epsilon_0 = eV/2$ is less broadened and therefore higher than the peak near $\epsilon_0 = -eV/2$.

Figure 6.6 shows some plots with different values of eV for the metallic island. Again we have normalized the x-axis to the dominating energy scale, which is here transport voltage. In the classical limit we get a structure with the width eV and vertical steps at the edges. These steps are washed out due to renormalization effects, even at zero temperature. In analogy to the previous section we calculate with the help of $\int d\Delta_0 A(\Delta_0) = 1$ the integral

$$R \int d\Delta_0 G(\Delta_0) = \frac{eV}{3}\,, \tag{6.15}$$

which is proportional to eV. As a typical height of the conductance curve we choose $G(\Delta_0 = 0)$. For $\pi Z \sum_r \alpha_0^r \ll 1$ we can again use $A(\omega) = Z\delta(\omega - Z\Delta_0)$ which implies

$$RG(\Delta_0 = 0) = \frac{1}{2}Z\,. \tag{6.16}$$

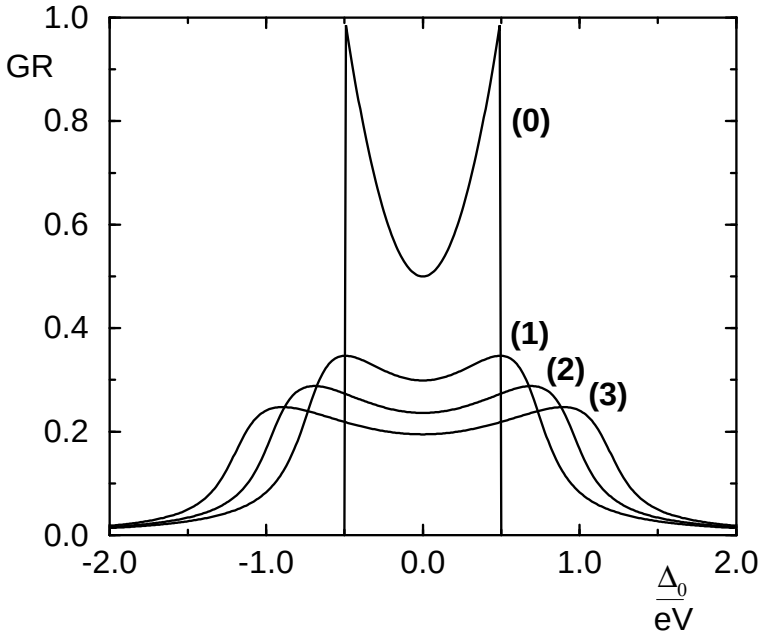

Figure 6.6: The differential conductance in nonlinear response for the metallic island as a function of the gap energy Δ_0 normalized to the transport voltage eV with $\alpha_0^L = \alpha_0^R = 0.05$, $T = 0$ and (1) $eV/E_C = 0.1$, (2) $eV/E_C = 0.01$ and (3) $eV/E_C = 0.001$. For comparison, (0) shows the classical result, which is independent of the transport voltage eV.

Now it depends logarithmically on eV. The normalized width of the structure

$$\gamma = \frac{1}{eV}\frac{\int d\Delta_0 G(\Delta_0)}{G(\Delta_0 = 0)} = \frac{2}{3}\frac{1}{Z} = \frac{2}{3}\left[1 + 2\sum_r \alpha_0^r \ln\frac{E_C}{eV/2}\right] \tag{6.17}$$

then increases with decreasing transport voltage.

6.3 Zero-Bias Anomalies

In this section we examine the transport (bias) voltage dependence of the conductance for the quantum dot with $M \geq 2$. As we saw in Section 5, the bare dot level is renormalized by $\mathrm{Re}\,\sigma(\omega)$, which depends logarithmically on temperature and transport voltage. Due to this logarithmic term, the conductance shows an anomalous behaviour at zero bias $eV = 0$.

For a low lying renormalized level ϵ, we find the well-known [11, 12, 41] zero-bias maximum (see Fig. 6.7), which can be traced back to the behaviour of the Kondo resonances near the Fermi levels: A finite transport voltage leads to a splitting of

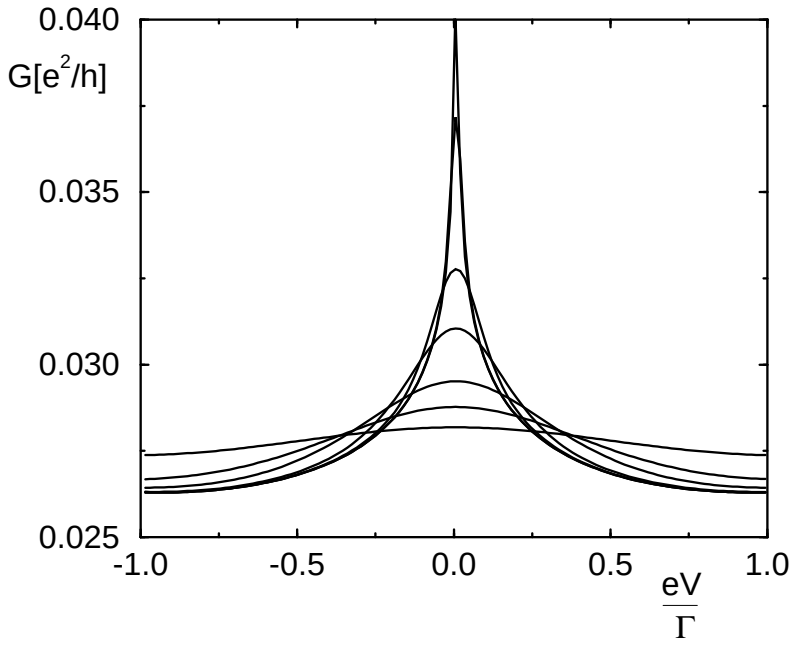

Figure 6.7: The differential conductance as a function of the transport voltage eV for the quantum dot with a low lying energy level ($\epsilon_0 = -5\Gamma$) shows a zero-bias maximum. For decreasing temperatures the peak height increases. We have chosen $k_BT/\Gamma = 0.0005$, $k_BT/\Gamma = 0.005$, $k_BT/\Gamma = 0.025$, $k_BT/\Gamma = 0.05$, $k_BT/\Gamma = 0.1$, $k_BT/\Gamma = 0.15$ and $k_BT/\Gamma = 0.25$, while $M = 2$, $\Gamma_L = \Gamma_R = \Gamma/2$, and $E_C = 50\Gamma$.

the Kondo peak (see Fig. 5.7). Therefore, there is an overall decrease of the spectral density in the range $|\omega| < eV$ with increasing transport voltage.

If the renormalized level lies above the Fermi levels, i.e. $\epsilon > 0$, the whole structure (see Fig. 6.8) is inverted compared to the $\epsilon < 0$ case although the Kondo peak at zero energy is absent. The contributions of single electron tunneling and cotunneling lead, compared to resonant tunneling, only to a weak bias voltage dependence of the differential conductance. This shows clearly that the influence of the logarithmic terms in $\sigma(\omega)$ are still important. They lead to an overall increase of the spectral density near zero energy with increasing transport voltage (see Fig. 6.9). The reason is that the logarithmic peaks in $\mathrm{Re}\,\sigma(\omega)$ decrease with increasing transport voltage and approach the value of $\omega - \epsilon_0$ if ϵ_0 is large enough. Thus the value of $|\omega - \epsilon_0 - \mathrm{Re}\,\sigma(\omega)|$ decreases which in turn increases $|\pi(\omega)|$ and the spectral density $A(\omega)$.

The occurrence of zero-bias minima is known for Kondo scattering from magnetic impurities [36]. They have been observed in recent experiments [37] and have been interpreted as 2-channel Kondo scattering from atomic tunneling systems [38, 39] or by tunneling into a disordered metal [40]. Here we see that zero-bias minima can also arise due to resonant tunneling via local impurities if the level position is high enough to enter the mixed valence regime. A comparison of the scaling behavior of

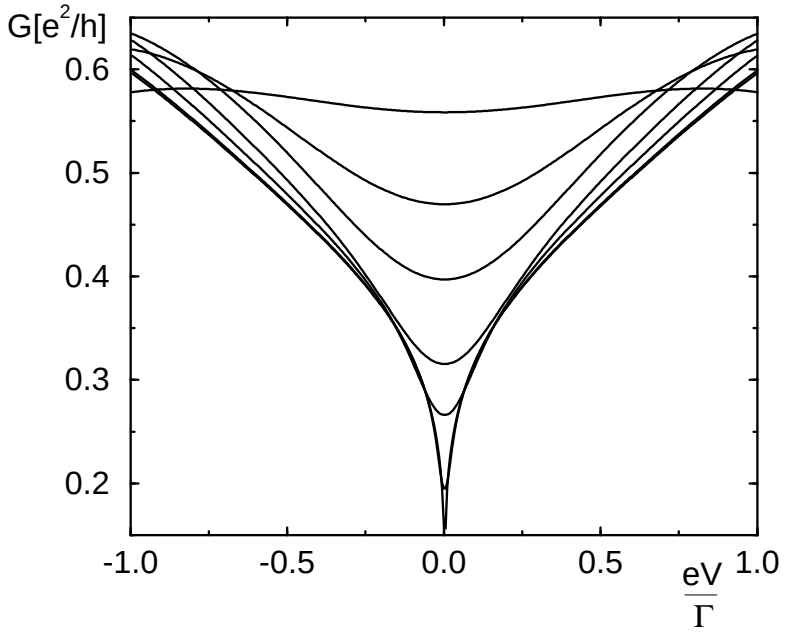

Figure 6.8: The differential conductance as a function of the transport voltage eV for the quantum dot with a renormalized energy level above the Fermi levels ($\epsilon_0 = 0$) shows a zero-bias minimum. For decreasing temperatures the minimum decreases. We have chosen $k_BT/\Gamma = 0.25$, $k_BT/\Gamma = 0.15$, $k_BT/\Gamma = 0.1$, $k_BT/\Gamma = 0.05$, $k_BT/\Gamma = 0.025$, $k_BT/\Gamma = 0.005$ and $k_BT/\Gamma = 0.0005$, while $M = 2, \Gamma_L = \Gamma_R = \Gamma/2$, and $E_C = 50\Gamma$.

the conductance as function of temperature and transport voltage (see Fig. 6.10) as well as the temperature dependence of the linear conductance (see Fig. 6.11) with recent experiments of Ralph & Buhrman [37], who measured transport properties through a quantum point contact, shows a quite remarkable coincidence. In order to explain the signal strength, however, one would need a large number of quantum dots in the sample of [37], for which there seems to be no experimental indication.

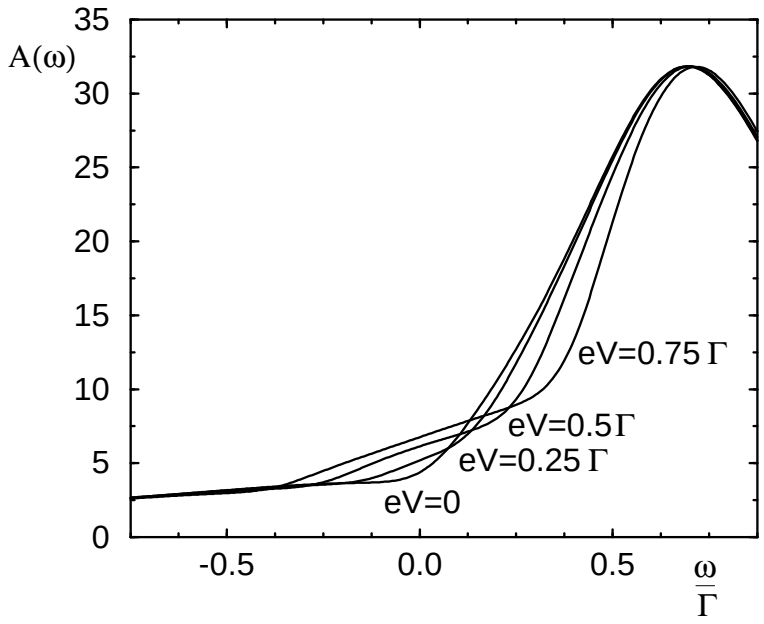

Figure 6.9: The spectral density for $M = 2$, $\Gamma_L = \Gamma_R = \Gamma/2$, $k_BT = 0.05\Gamma$, $\epsilon_0 = 0$ and $E_C = 50\Gamma$ at different voltages. Increasing voltage leads to an overall decrease of the spectral density in the range $|\omega| < eV$.

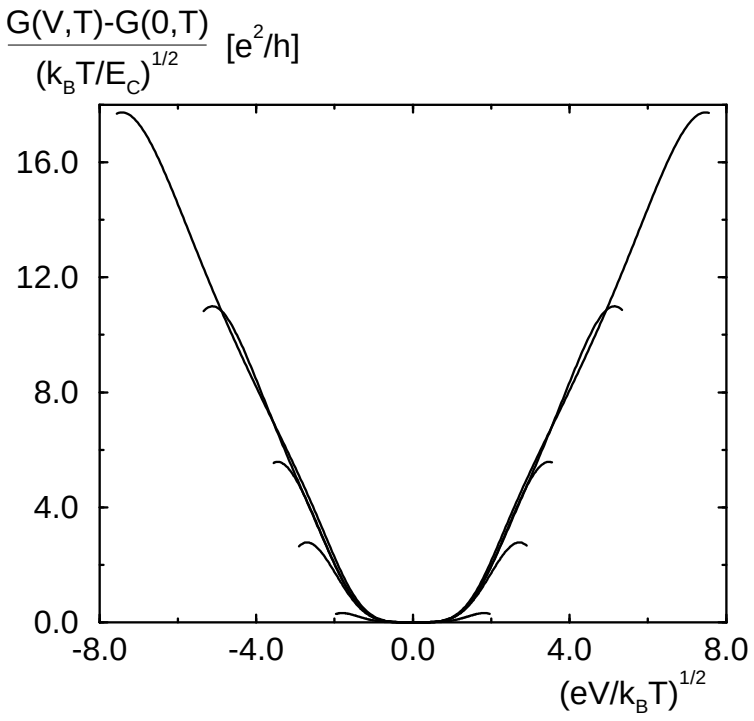

Figure 6.10: The rescaled curves of Fig. 6.8 collapse onto one curve.

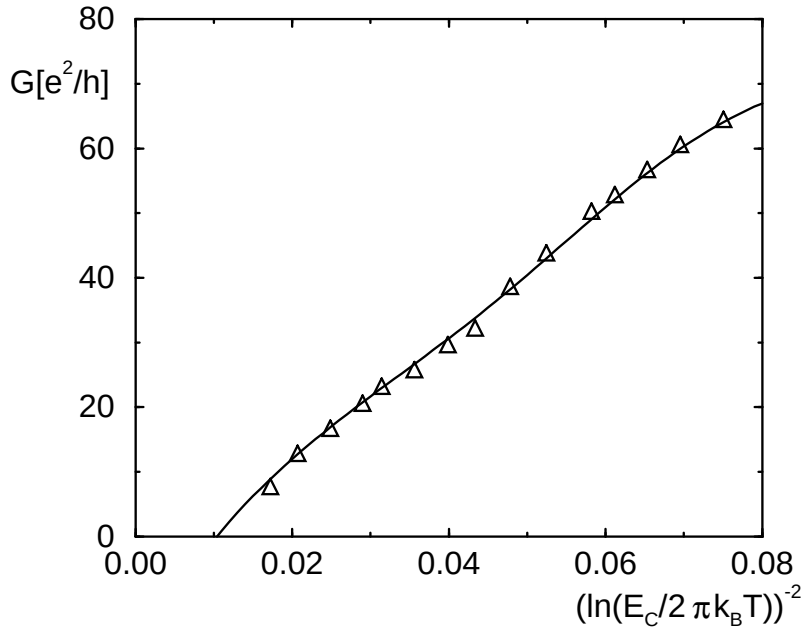

Figure 6.11: The temperature dependence of the linear conductance (solid lines) coincides with experimental data from [37] (triangles).

Chapter 7

Boson-Assisted Tunneling

The development of the diagrammatic technique is not restricted to the systems considered in this work so far. Instead, it is possible to extend the method to other and more complex systems. As an example we examine in this chapter the quantum dot with a coupling of the dot electrons to a bosonic mode with frequency ω_q, representing phonons, photons or fluctuations of the electrodynamic environment. In the diagrammatic language, the coupling to the bosons introduces a new type of lines, boson lines, connecting all vertices in the diagrams. We calculate the spectral density and the current in leading order. The spectral density shows a multiplet of Kondo peaks split by boson frequencies and transport voltage. Furthermore, the conductance as a function of the gate voltage has satellite peaks. Finally, the zero-bias anomalies are completed by satellite maxima and minima.

7.1 Hamiltonian and Density Matrix

We consider the Hamiltonian

$$H = H_L + H_R + H_D + H_{T,L} + H_{T,R} \tag{7.1}$$

in which H_L, H_R, $H_{T,L}$ and $H_{T,R}$ are the same as in Chapter 2. The dot is characterized by

$$H_D = \epsilon_0' \sum_\sigma n_\sigma + U_0' \sum_{1\le\sigma<\sigma'\le M} n_\sigma n_{\sigma'} + \sum_q \omega_q d_q^\dagger d_q + \sum_\sigma n_\sigma \sum_q g_q (d_q + d_q^\dagger) \tag{7.2}$$

in which ϵ_0' is the bare level energy and U_0' denotes the Coulomb repulsion. In addition to the terms describing the purely electronic part the Hamiltonian contains terms representing the kinetic energy of the bosons and the coupling to the dot electrons with electron-boson coupling g_q. This Hamiltonian can be rewritten after a unitary transformation [42] defined by

$$V = \exp\left(-i \sum_\sigma n_\sigma \varphi\right) \qquad \text{and} \qquad \varphi = i \sum_q \frac{g_q}{\omega_q} (d_q^\dagger - d_q)\,. \tag{7.3}$$

We get

$$\bar{H} = VHV^{-1} = \sum_{r=L,R} \bar{H}_r + \bar{H}_D + \sum_{r=L,R} \bar{H}_{T,r} \tag{7.4}$$

with

$$\bar{H}_r = H_r \tag{7.5}$$

and

$$\bar{H} = \epsilon_0 \sum_\sigma n_\sigma + U_0 \sum_{1\le\sigma<\sigma'\le M} n_\sigma n_{\sigma'} + \sum_q \omega_q d_q^\dagger d_q \tag{7.6}$$

and

$$\bar{H}_{T,r} = \sum_{k\sigma} \left(T_k^r a_{k\sigma r}^\dagger c_\sigma e^{i\varphi} + h.c. \right) . \tag{7.7}$$

Due to the electron-boson interaction the level position and the Coulomb repulsion are renormalized,

$$\epsilon_0 = \epsilon_0' - \sum_q \frac{g_q^2}{\omega_q} \qquad \text{and} \qquad U_0 = U_0' - 2\sum_q \frac{g_q^2}{\omega_q} , \tag{7.8}$$

and the tunneling part contains now phase factors $e^{\pm i\varphi}$. The initial density matrix for the dot is assumed to factorize into an electronic and a bosonic part

$$\rho_0^D = \rho_0^{D,el} \rho_0^{D,bos} \tag{7.9}$$

in which the boson part is given by the equilibrium density matrix

$$\rho_0^{D,bos} = \frac{1}{Z_0^{bos}} \exp\left[-\beta \sum_q \omega_q d_q^\dagger d_q \right] . \tag{7.10}$$

7.2 Diagrammatic Expansion

The only part of the system which is not in equilibrium are the electrons in the dot. Anything else, i.e. the lead electrons and the bosons, can be traced out. In order to develop the diagrammatic language we expand the propagator with respect to the tunneling Hamiltonian. The trace over the electron operators is performed in the same way as before. But now, the trace over the boson operators gives rise to an additional factor of the form

$$C_{bos}(t_1, t_1', t_2, t_2', \ldots, t_m, t_m') = \langle T_K \left[e^{-i\varphi(t_1)} e^{i\varphi(t_1')} e^{-i\varphi(t_2)} e^{i\varphi(t_2')} \ldots e^{-i\varphi(t_m)} e^{i\varphi(t_m')} \right] \rangle \tag{7.11}$$

in which we denote by (t_i, t_i') the pair of times which is connected by a tunneling line running from t_i' to t_i. Since φ is linear in the boson operators, we get

$$C_{bos}(t_1, t_1', t_2, t_2', \ldots, t_m, t_m') = \prod_{i<j} P^K(t_i, t_j)^{-1} \prod_{i<j} P^K(t_i', t_j')^{-1} \prod_{i,j} P^K(t_i, t_j') \tag{7.12}$$

with

$$P^K(t,t') = e^{\langle T_K \varphi(t)\varphi(t')\rangle} e^{-\langle\varphi\varphi\rangle} . \tag{7.13}$$

The last expression depends on the ordering of t and t' with respect to the Keldysh contour. We write $P^K(t,t') = P^+(t,t')$ if $t < t'$ and $P^K(t,t') = P^-(t,t')$ if $t > t'$ on the Keldysh contour. In the stationary limit, $P^\pm(t,t') = P^\pm(t-t')$ depends only on the difference of the times $t - t'$,

$$P^\pm(t) = e^{\langle\varphi(0)\varphi(\pm t)\rangle} e^{-\langle\varphi(0)\varphi(0)\rangle} , \tag{7.14}$$

and we can define the Fourier transform

$$P^\pm(\omega) = \frac{1}{2\pi}\int dt e^{i\omega t} P^\pm(t) , \tag{7.15}$$

which describes the probability for an electron to absorb (for $P^+(\omega)$) or emit (for $P^-(\omega)$) the boson energy ω. In the diagrammatic language, we represent the factors P^K by boson lines connecting each vertex with each other.

7.3 Self-Energy, Current and Spectral Density

For further calculation, however, we include only boson lines between vertices which are already connected by tunneling lines, i.e.

$$C_{bos}(t_1,t_1',t_2,t_2',\ldots,t_m,t_m') \approx \prod_{i=1}^{m} P^K(t_i,t_i') . \tag{7.16}$$

This amounts to a dressing of the tunneling lines. We can then draw the same diagrams as we did without bosons. Only the value of the tunneling line $\gamma_r^\pm(\omega)$ changes. It is now a convolution of the value given in Chapter 3 and the bosonic factors $P^\pm$:

$$\gamma_r^\pm(\omega) = \frac{1}{2\pi}\int d\omega'\, \Gamma_r(\omega') f_r^\pm(\omega') P^\pm(\omega-\omega') . \tag{7.17}$$

We are then able to perform the analytic resummation exactly in the same way as in Chapters 4 and 5. But now, the self-energy (4.11)

$$\sigma(\omega) = \int d\omega' \frac{M\gamma^+(\omega') + \gamma^-(\omega')}{\omega - \omega' + i\eta} \tag{7.18}$$

contains the new values for $\gamma^\pm(\omega)$.

The approximation, while neglecting many diagrams, describes well the spectral density of the dot at resonance points. The reason is that the position and value of the peaks of the spectral density are determined by a self-energy σ which is calculated here in lowest order perturbation theory in Γ including the bosons. Higher order contributions are small for high tunnel barriers.

After the unitary transformation, the definition for the Green's functions reads

$$C^{>}(t,t') = -i\langle (c_\sigma e^{i\varphi})(t)_{\bar{H}} (c_\sigma^\dagger e^{-i\varphi})(t')_{\bar{H}} \rangle \tag{7.19}$$

$$C^{<}(t,t') = i\langle (c_\sigma^\dagger e^{-i\varphi})(t')_{\bar{H}} (c_\sigma e^{i\varphi})(t)_{\bar{H}} \rangle \,. \tag{7.20}$$

In the stationary limit, we get

$$C^{>}(\omega) = -2\pi i \int d\omega' \gamma^{-}(\omega') |\pi(\omega')|^2 P^{-}(\omega - \omega') \tag{7.21}$$

$$C^{<}(\omega) = 2\pi i \int d\omega' \gamma^{+}(\omega') |\pi(\omega')|^2 P^{+}(\omega - \omega') \,. \tag{7.22}$$

Note, that the functions $\gamma(\omega)$ already contain a P–function and the Green's functions consist of a further convolution with a P–function. The spectral density $A(\omega) = [C^{<}(\omega) - C^{>}(\omega)]/(2\pi i)$ is then given by

$$A(\omega) = \int d\omega' \left[\gamma^{+}(\omega') P^{+}(\omega - \omega') + \gamma^{-}(\omega') P^{-}(\omega - \omega') \right] |\pi(\omega')|^2 \,. \tag{7.23}$$

For the relation between the stationary current flowing into reservoir r and the spectral density we recover Eq. (5.29)

$$I_r^{st} = \frac{e}{h} 2\pi M \int d\omega \sum_{r'} \frac{\Gamma_r \Gamma_{r'}}{\Gamma} A(\omega) [f_{r'}^{+}(\omega) - f_r^{+}(\omega)] \,. \tag{7.24}$$

The difference to other approaches in the $M = 1$ case [31, 32, 33, 34] is clearly displayed by the effect of the self-energy $\sigma(\omega)$ which determines the position of the maxima of the spectral density (7.23) via $|\pi(\omega)|^2$. In all previous works, $\sigma(\omega)$ has been approximated by a constant. We find here, that the energy dependence of $\sigma(\omega)$ cannot been neglected if the temperature $k_B T$ and the typical frequency ω_B of the bosons are smaller than Γ. To derive this analytically, we consider now a one-mode environment, the Einstein model with one boson frequency $\omega_q = \omega_B$.

7.4 Einstein Model

Defining $g = \sum_q g_q^2/\omega_B^2$ we obtain

$$P^{\pm}(\omega) = \sum_n p_n \delta(\omega \pm n\omega_B) \,, \tag{7.25}$$

in which

$$p_n = e^{-g(1+2N_0(\omega_B))} e^{n\omega_B/2k_B T_B} I_n(2gN_0(\omega_B) e^{\omega_B/2k_B T_B}) \tag{7.26}$$

is the probability for the emission of n bosons with frequency ω_B. Here, $N_0(\omega_B)$ is the Bose function, and I_n denotes the modified Bessel functions. The temperature

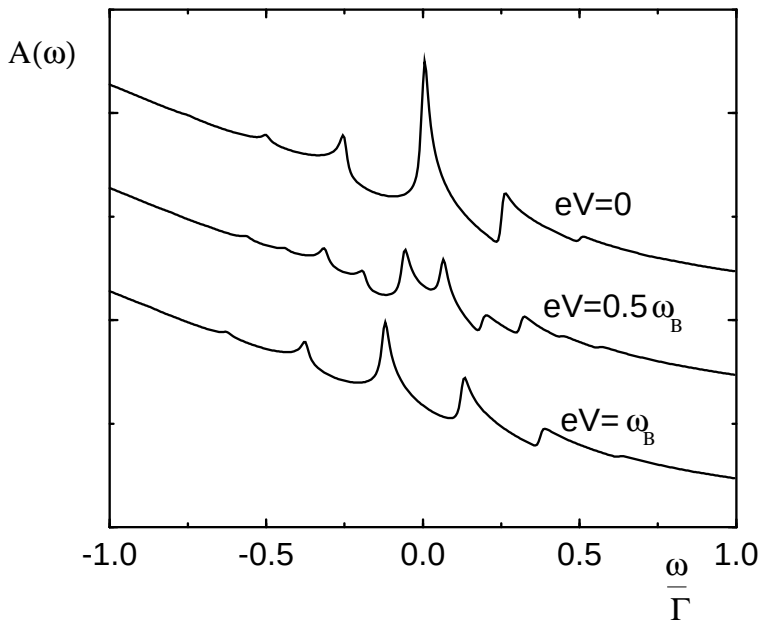

Figure 7.1: The spectral density for $M = 2$, $\Gamma_L = \Gamma_R = \Gamma/2$, $k_BT = k_BT_B = 0.005\Gamma$, $\epsilon = -2\Gamma$, $g = 0.2$, $\omega_B = 0.25\Gamma$ and $E_C = 50\Gamma$ at different voltages. For $V = 0$ there are resonances at multiples of ω_B, which split at finite bias voltage.

of the boson bath is T_B. In real experiments it can be different from the electron temperature T. The calculation of the spectral density yields

$$A(\omega) = \sum_n \frac{p_n\gamma^+(\omega + n\omega_B) + p_{-n}\gamma^-(\omega + n\omega_B)}{\left[\omega + n\omega_B - \epsilon_0 - \mathrm{Re}\,\sigma(\omega + n\omega_B)\right]^2 + \left[\mathrm{Im}\,\sigma(\omega + n\omega_B)\right]^2} \tag{7.27}$$

with

$$\begin{aligned}\mathrm{Re}\,\sigma(\omega) &= \sum_n (Mp_n - p_{-n}) \sum_r \frac{\Gamma_r}{2\pi}\Big[\ln\left(\frac{\beta E_C}{2\pi}\right) \\ &\qquad -\mathrm{Re}\,\psi\left(\frac{1}{2} + i\frac{\beta}{2\pi}(\omega + n\omega_B - \mu_r)\right)\Big] \qquad (7.28)\\ \mathrm{Im}\,\sigma(\omega) &= -\pi \sum_n Mp_n\gamma^+(\omega + n\omega_B) + p_{-n}\gamma^-(\omega + n\omega_B). \qquad (7.29)\end{aligned}$$

Here $\psi(z) = d[\ln\Gamma(z)]/dz$ denotes the digamma function, and we have again chosen a Lorentzian cut-off at E_C in the energy integrals. The real part of σ shows not only a logarithmic dependence on energy $|\omega|$, electron temperature k_BT and transport voltage eV but also on the boson frequency ω_B. These logarithmic terms lead to a multiplet of Kondo peaks split by transport voltage and boson frequency for $M \geq 2$ or $p_n \neq p_{-n}$. Hence we anticipate logarithmic singularities not only for the

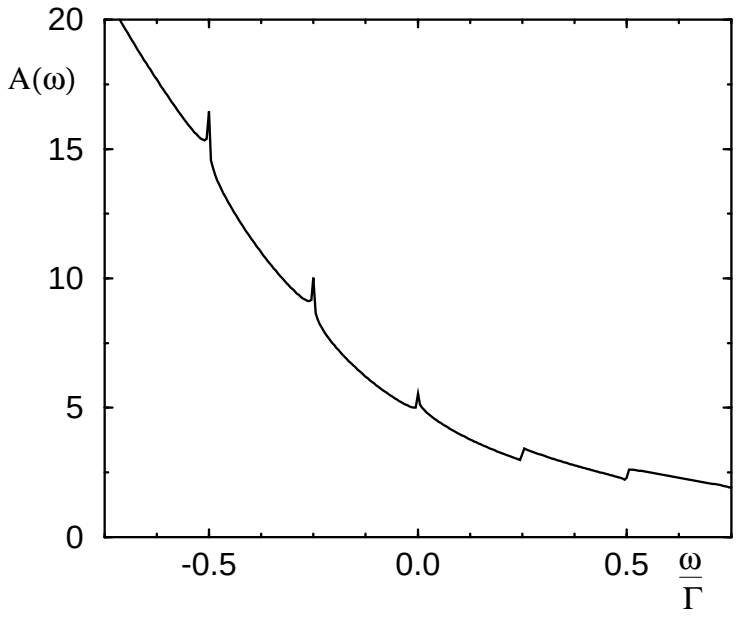

Figure 7.2: The spectral density for $M = 1$, $\Gamma_L = \Gamma_R = \Gamma/2$, $k_B T = 0.00005\Gamma$, $k_B T_B = 0.5\Gamma$, $V = 0$, $\epsilon = -\Gamma$, $g = 0.5$, $\omega_B = 0.25\Gamma$ and $E_C = 50\Gamma$.

degenerate case $M \geq 2$ (see Fig. 7.1) but also for a single dot level without spin ($M = 1$) since the probabilities for absorption and emission of bosons are different (see Fig. 7.2). This is an important difference to the case of classical time-dependent fields [12] in which both probabilities are equal.

7.5 Results

Figure 7.1 shows a typical series of pictures for the spectral density at different voltages for a low lying level ϵ_0. Without bias and $M = 2$, we obtain the usual Kondo peak near the Fermi level (which we choose as zero energy). Due to emission of bosons, there are now additional resonances at multiples of ω_B. At finite transport voltage, all peaks split and decrease in magnitude.

Kondo peaks in the case $M = 1$ are displayed in Fig. 7.2.

The resonances in the spectral density are most pronounced in the nonlinear differential conductance as function of the transport voltage V. Figure 7.3 shows the differential conductance for a low lying level ϵ_0. As usual we find a zero-bias maximum [11, 12, 41] since the splitting of the Kondo peak leads to an overall decrease of the spectral density in the energy range $|\omega| < eV$ (see Fig. 5.7). Due to emission of bosons we observe, furthermore, a set of symmetric satellite maxima. They can be traced back to the fact that pairs of Kondo peaks can merge if the

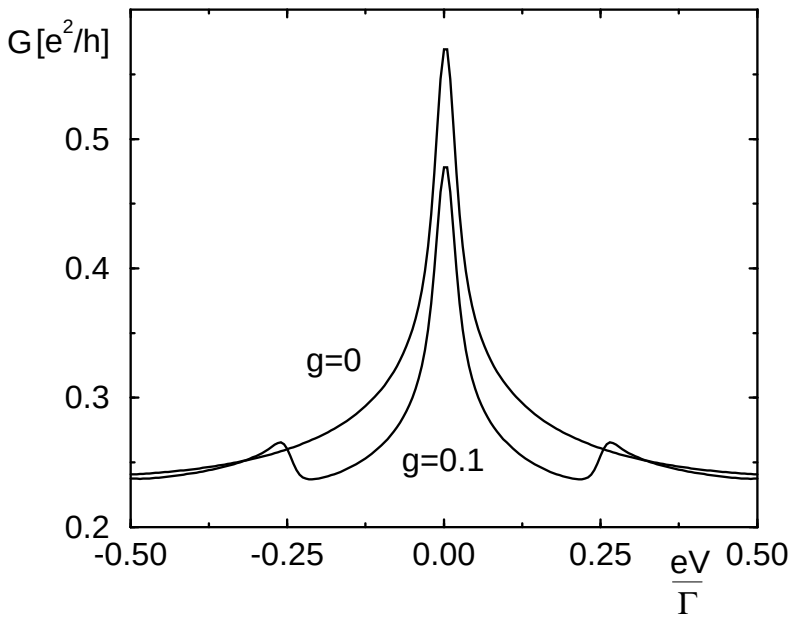

Figure 7.3: The differential conductance vs. bias voltage for $M = 2, \Gamma_L = \Gamma_R = \Gamma/2$, $k_B T = k_B T_B = 0.005\Gamma$, $\epsilon = -2\Gamma$, $\omega_B = 0.25\Gamma$ and $E_C = 50\Gamma$. The curves show a maximum at zero bias and satellite maxima at multiples of ω_B for a finite electron-boson coupling.

transport voltage is given by multiples of the boson frequency (see Fig. 7.1). This gives rise to pronounced Kondo peaks at $\omega = \pm eV/2$ and thus to an increase of the spectral density with transport voltage near these points.

The differential conductance for ϵ_0 near zero energy is shown in Fig. 7.4 with and without bosons. As described in Chapter 6, we find that the zero-bias maximum in the $\epsilon_0 < 0$ case is inverted to a zero-bias minimum. In the presence of bosons we obtain satellite steps at $|eV| = m\omega_B$.

Finally, we investigate the differential conductance at fixed transport voltage as a function of the position of the dot level, which experimentally can be varied by changing the gate voltage V_G coupled capacitively to the dot. Figure 7.5 shows the classically expected pair of peaks at $|\epsilon_0| = eV/2$ together with satellites between the main peaks (due to emission and absorption) and peaks for $|\epsilon_0| > eV/2$ (only due to absorption of bosons).

The imaginary part of $\sigma(\omega)$ gives rise to a classically unexpected asymmetry of the peak heights. The peak at $\epsilon_0 = eV/2$ is larger than the one at $\epsilon_0 = -eV/2$ since $|\mathrm{Im}\,\sigma(\omega)|$ is always smaller at higher energies (except for the $M = 1$ case in which particle-hole symmetry holds). This demonstrates a significant effect due to the broadening of the spectral density by quantum fluctuations.

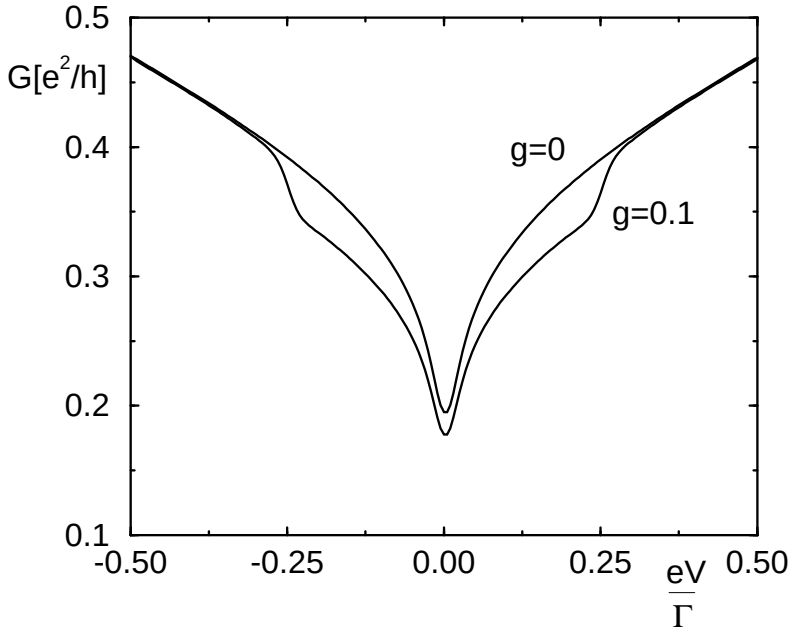

Figure 7.4: The differential conductance vs. bias voltage for $M = 2, \Gamma_L = \Gamma_R = \Gamma/2$, $k_BT = k_BT_B = 0.005\Gamma$, $\epsilon = 0$, $\omega_B = 0.25\Gamma$ and $E_C = 50\Gamma$. The curves show a minimum at zero bias and steps at multiples of ω_B for a finite electron-boson coupling.

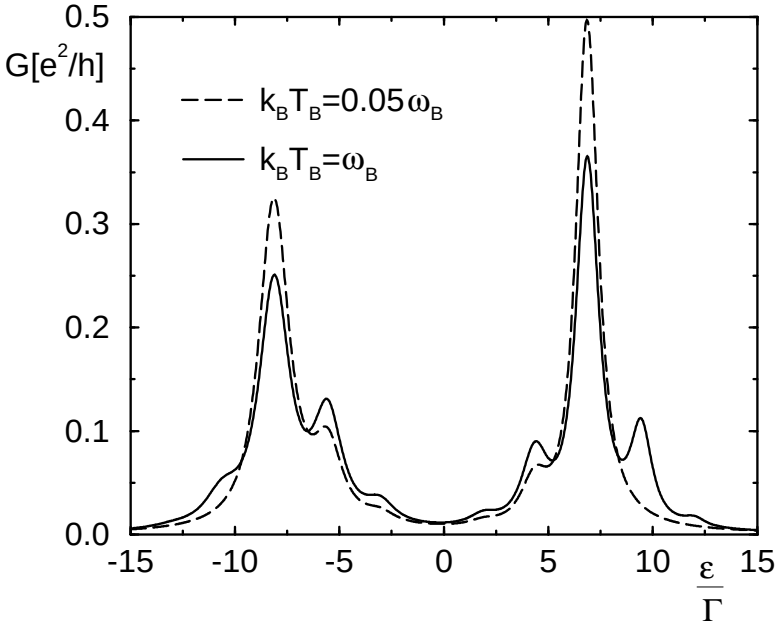

Figure 7.5: The differential conductance as a function of ϵ for $M = 2$, $\Gamma_L = \Gamma_R = \Gamma/2$, $k_BT = 0.125\Gamma$, $eV = 15\Gamma$, $g = 0.3$, $\omega_B = 2.5\Gamma$ and $E_C = 250\Gamma$.

Chapter 8

Summary and Outlook

In this work, we have studied low-temperature quantum transport through a single electron transistor in non-equilibrium.

A description of the single electron transistor was given in Chapter 2. The concept of charging energy provides a qualitative description of the transport properties and explains Coulomb oscillations and Coulomb blockade. Different processes contribute to the current. We distinguished single electron tunneling which is described in lowest-order perturbation theory, from higher-order processes such as cotunneling and resonant tunneling, in which several tunneling events occur in a coherent way. For strong coupling between the island and the leads, resonant tunneling becomes important. The purpose of this work was to examine this influence on transport properties.

A more detailed understanding of the transport properties requires a specification of the excitation spectrum of the island. We considered two limiting cases: (i) a quantum dot with a discrete excitation spectrum, in which elastic tunneling processes dominate, and (ii) a metallic island with a continuous one, in which the main contribution is due to inelastic tunneling processes. After introducing the standard tunneling Hamiltonian for each case, we studied the time-evolution of the density matrix which is determined by a propagator. Because the full density matrix contains much more information than necessary for a description of transport processes, we traced out all microscopic degrees of freedom and obtained a reduced density matrix in the remaining variables (in the metallic case the number of excess electrons and in the quantum dot case the number of excess electrons and the spin). We expressed the reduced propagator in terms of these remaining variables using an operator approach and, alternatively, a real-time path-integral approach for the metallic case.

The next task was then to evaluate the reduced propagator. This was done in Chapter 3. To do so we expanded the reduced propagator in the tunneling part of the Hamiltonian. We visualized each term of the expansion by a diagram and derived a set of rules how to translate it into an analytic expression. Within this diagrammatic language, the propagator can be expressed as an iteration in the form

of a Dyson equation by irreducible self-energy parts. In the stationary limit, we found a Master equation for the distribution function of the island states and saw that the irreducible self-energy parts play the role of the transition rates.

In Chapter 4 we identified the corresponding diagrams with single electron tunneling, cotunneling and resonant tunneling processes. For single electron tunneling and cotunneling the diagrammatic rules led to the well known transition rates obtained in perturbation theory. In situations in which the system is near the resonance points, processes dominate in which only two island states are involved. In this case, we were able to evaluate resonant tunneling analytically within a conserving approximation.

The physical quantities of interest, the average charge on the island and the current through the system, can be expressed in terms of the spectral density. These final results, followed by a discussion how resonant tunneling processes influence the spectral density, were presented in Chapter 5. We encountered an energy-dependent self-energy. Its real part yields a renormalization of the system parameters and is responsible for the existence of Kondo physics in the quantum dot case. The imaginary part represents a finite life-time broadening.

In Chapter 6 we considered the effect of the quantum fluctuations on the average charge and the differential conductance. The structures in the plots showing the average charge and the differential conductance as a function of the gate voltage are washed out. Furthermore, the renormalization of the energy level in the quantum dot case leads, in comparison to the result from lowest order perturbation theory, to a shift of the whole curve to negative energies. In nonlinear response, we found a classically unexpected asymmetry of the peak heights in the differential conductance through the quantum dot. The effect of Kondo physics is clearly displayed in the plots of the differential conductance as a function of the transport voltage. For a low-lying energy level there is a well known zero-bias maximum due to sharp resonances in the spectral density. Interestingly, however, we found for an energy level near or above the Fermi levels a reduction of the conductance at low voltages, i.e., a zero-bias minimum.

An extension of our diagrammatic technique to a more complex system was presented in Chapter 7, in which, as an example, a quantum dot with bosonic interactions was considered. The bosons lead to a splitting of the Kondo peaks and give rise to side peaks in the differential conductance. Furthermore, the zero-bias extrema are accompanied by side extrema. Remarkably, we found Kondo peaks due to different emission and absorption probabilities of the bosons even in the case of a nondegenerate level.

Because the method described in this work is very general it should easily be possible to consider in future works other generalizations such as metallic islands with bosonic interactions or superconducting electrodes and examine the influence of resonant tunneling in these systems.

Finally, it would be interesting to include tunneling processes in which more than two island states are involved. This would allow a description of the situation

far away from the resonance points as well as give a more accurate description of the situation near the resonances. Furthermore, the Zeeman splitting of the energy levels in the quantum dot due to an applied magnetic field could then be accounted for. In this case, however, it is no longer possible to derive analytical formulas for the current and the average charge. Instead, numerical work is required.

In conclusion, we find that the diagrammatic technique presented here provides a general tool for the description of a variety of systems not only in the perturbative, but also in the nonperturbative regime. The study of resonant tunneling allows a systematic description of quantum fluctuations and, furthermore, reveals interesting physical effects.

Appendix A

Calculation of the Effective Action

As described in Chapter 2, we model the single electron transistor with a continuous spectrum on the island by the tunneling Hamiltonian

$$H = \sum_{r=L,R} \sum_{kn} \epsilon_{knr} a^\dagger_{knr} a_{knr} + \sum_{qn} \epsilon_{qn} c^\dagger_{qn} c_{qn} + \frac{e^2}{2C} \left(\sum_{qn} c^\dagger_{qn} c_{qn} - n_x \right)^2 + \sum_{r=L,R} \sum_{kqn} \left(T^{rn}_{kq} a^\dagger_{knr} c_{qn} + h.c. \right) . \tag{A.1}$$

The propagator is given by

$$\mathbf{1} = T_K \exp\left(-i \int_K dt H(t) \right) . \tag{A.2}$$

In order to handle the interaction, we perform a Hubbard-Stratonovich transformation. It introduces a collective variable, the phase $\varphi(t)$, which is the quantum mechanical conjugate of the number of electrons $n(t)$ on the island. Using Gaussian (path) integrals, we write

$$T_K \exp\left(-i \int_K dt\, H_{ch}(t) \right) = \int \mathcal{D}[V(t)] T_K \exp\left\{ i \int_K dt \left(\frac{C}{2} V(t)^2 + e \left[\sum_{qn} c^\dagger_{qn} c_{qn} - n_x \right] V(t) \right) \right\} . \tag{A.3}$$

The capacitive interaction between electrons is replaced in this way by an interaction of the electrons with the fluctuating macroscopic field $V(t)$, the electrostatic potential of the island. We introduce the phase $\varphi(t)$ by defining

$$V(t) \equiv -\frac{\dot{\varphi}(t)}{e} . \tag{A.4}$$

Now, we perform a unitary time-dependent transformation

$$H \rightarrow U^\dagger H U - i U^\dagger \frac{\partial}{\partial t} U \tag{A.5}$$

$$\text{with} \qquad U = \exp\left[-i \varphi(t) \sum_{qn} c^\dagger_{qn} c_{qn} \right] . \tag{A.6}$$

Due to this transformation we obtain for the island electron operators

$$c_{qn}^{\dagger} \rightarrow c_{qn}^{\dagger} e^{i\varphi(t)} \tag{A.7}$$

$$c_{qn} \rightarrow c_{qn} e^{-i\varphi(t)} \, . \tag{A.8}$$

After this step we trace out the microscopic degrees of freedom. Thus, only the variable of interest, the collective variable φ remains. The reduced propagator then reads

$$\Pi = \mathrm{tr}\left[\rho_0 T_K \exp\left(-i\int_K dt H(t)\right)\right] = \int \mathcal{D}[\varphi(t)] W[\varphi(t)] \exp\left(iS_{ch}[\varphi(t)]\right) \, . \tag{A.9}$$

The term $W[\varphi(t)]$ describes the noninteracting electrons in the leads and the island and, furthermore, the tunneling,

$$W[\varphi(t)] = \mathrm{tr}\left\{\rho_0 T_K \exp\left[-i\int_K dt \sum_{r=L,R}\sum_{kn} \epsilon_{knr} a_{knr}^{\dagger} a_{knr} - i\int_K dt \sum_{qn} \epsilon_{qn} c_{qn}^{\dagger} c_{qn} \right.\right.$$
$$\left.\left. -i\int_K dt \sum_{r=L,R}\sum_{kqn} \left(T_{kq}^{rn} a_{knr}^{\dagger} c_{qn} e^{-i\varphi(t)} + h.c.\right)\right]\right\} \, . \tag{A.10}$$

The occurrence of $e^{\pm i\varphi(t)}$ in the tunneling term indicates the coupling of the electrons to the collective variable. The charging energy is described by

$$S_{ch}[\varphi(t)] = \int_K dt \left(\frac{C}{2}\left(\frac{\dot{\varphi}(t)}{e}\right)^2 + n_x \dot{\varphi}(t)\right) \, , \tag{A.11}$$

which is independent of the microscopic degrees of freedom.

The exponent in $W[\varphi(t)]$ is bilinear in the electron operators. Therefore, it is possible to perform the trace, and we get [43]

$$W[\varphi(t)] = \exp\left(\mathrm{tr}\ln \hat{G}^{-1}(\varphi)\right) / \exp\left(\mathrm{tr}\ln \hat{G}_0^{-1}\right) \tag{A.12}$$

with

$$\hat{G}^{-1}(\varphi) = \hat{G}_0^{-1} - \hat{T}(\varphi) \tag{A.13}$$

in which $\hat{G}(\varphi)$ is the Green's function including tunneling, while $\hat{G}_0$ denotes the free Green's function and $\hat{T}(\varphi)$ describes the tunneling. These terms are written as 3×3 matrices (corresponding to the three electron reservoirs):

$$\hat{G}_0 = \mathrm{diag}\left(G_{0L}, G_{0R}, G_{0I}\right) \tag{A.14}$$

and

$$\hat{T}(\varphi) = \begin{pmatrix} 0 & 0 & T_L(\varphi) \\ 0 & 0 & T_R(\varphi) \\ T_L^*(\varphi) & T_R^*(\varphi) & 0 \end{pmatrix} \, . \tag{A.15}$$

Each element, in turn, is a matrix with matrix elements labeled by the electron states k or q, the channel index n and times t and t':

$$\begin{aligned}
(G_{0r})_{kn}(t,t') &= -i\langle T_K a_{knr}(t) a^\dagger_{knr}(t')\rangle \\
&= \pm i e^{-i\epsilon_{knr}(t-t')} f_r^\pm(\epsilon_{knr}) \qquad \text{for } r = L,R \qquad \text{(A.16)} \\
(G_{0I})_{qn}(t,t') &= -i\langle T_K c_{qn}(t) c^\dagger_{qn}(t')\rangle \\
&= \pm i e^{-i\epsilon_{qn}(t-t')} f^\pm(\epsilon_{qn}) \qquad \text{(A.17)} \\
(T_r)_{kqn}(t,t') &= T^{rn}_{kq} e^{-i\varphi}\delta(t-t') \qquad \text{for } r = L,R\,, \qquad \text{(A.18)}
\end{aligned}$$

in which $f^+(\epsilon) = 1/[\exp(\beta\epsilon)+1]$ is the Fermi distribution, $f^-(\epsilon) = 1 - f(\epsilon)$ and $f_r^\pm(\epsilon) = f^\pm(\epsilon - \mu_r)$. For $t < t'$ with respect to the closed time path we take the upper sign of $\pm$ and for $t' > t$ the lower one. The trace in Eq. (A.12) is the trace over all these indices as well as over the 3×3 matrix. By reducing the fraction, expanding the logarithm in $\hat{G}_0\hat{T}(\varphi)$ and omitting all odd powers of the expansion (since their trace equals to zero) we conclude from Eq. (A.12)

$$W[\varphi(t)] = \exp\left[-\mathrm{tr}\sum_{m=1}^{\infty}\frac{1}{2m}\left(\hat{G}_0\hat{T}(\varphi)\right)^{2m}\right]. \qquad \text{(A.19)}$$

The trace over the 3×3 matrix yields

$$\begin{aligned}
\frac{1}{2m}\,\mathrm{tr}\left(\hat{G}_0\hat{T}(\varphi)\right)^{2m} = \frac{1}{m}\,\mathrm{tr}\sum_{r_1=L,R}\cdots\sum_{r_m=L,R} & G_{0r_1}T_{r_1}(\varphi)G_{0I}T^*_{r_2}(\varphi) \\
& G_{0r_2}T_{r_2}(\varphi)G_{0I}T^*_{r_3}(\varphi) \\
& \cdots \\
& G_{0r_m}T_{r_m}(\varphi)G_{0I}T^*_{r_1}(\varphi)\,. \qquad \text{(A.20)}
\end{aligned}$$

Performing the trace over the electron states k and q, the channel index n and the times, we find

$$\begin{aligned}
\ln(W[\varphi(t)]) = -\sum_{m=1}^{\infty}\sum_{r_1=L,R}\cdots\sum_{r_m=L,R}(2\pi)^{2m-1}\int_K dt_1\int_K dt'_1\ldots\int_K dt_m\int_K dt'_m \\
\underset{t_1<t_2\,,\ldots,\,t_m}{} \\
\alpha^K_{r_1,\ldots,r_m}(t_1,t'_1,\ldots,t_m,t'_m)e^{i\varphi(t_1)}e^{-i\varphi(t'_1)}\ldots e^{i\varphi(t_m)}e^{-i\varphi(t'_m)} \qquad \text{(A.21)}
\end{aligned}$$

in which $\alpha^K_{r_1,\ldots,r_m}(t_1,t'_1,\ldots,t_m,t'_m)$ contains m reservoir and m island Green's functions. In the diagrammatic language, each Green's function is given by a line connecting two vertices. The whole expression is then a closed loop with alternating reservoir and island lines (see Fig. 3.2). The condition $t_1 < t_2,\ldots,t_m$ on the Keldysh contour ensures that each term corresponds to a topological different diagram. The direction of the line, i.e. the time-ordering of the connected vertices, determines the sign of $\pm$ in Eqs. (A.16) and (A.17). We indicate the corresponding sign of the reservoir lines by σ and that of the island by η and write

$$\alpha^K_{r_1,\ldots,r_m}(t_1,t'_1,\ldots,t_m,t'_m) = i^{2m}(-1)^{c+1}\alpha^{\sigma_1,\eta_1,\ldots,\sigma_m,\eta_m}_{r_1,\ldots,r_m}(t_1,t'_1,\ldots,t_m,t'_m) \qquad \text{(A.22)}$$

in which $(-1)^{c+1} = \sigma_1\eta_1 \ldots \sigma_m\eta_m$ is obtained by counting the number c of crossing lines and

$$\alpha^{\sigma_1,\eta_1,\ldots,\sigma_m,\eta_m}_{r_1,\ldots,r_m}(t_1,t_1',\ldots,t_m,t_m') = \frac{1}{(2\pi)^{2m-1}}$$
$$\int d\epsilon_1 \int dE_1 \ldots \int d\epsilon_m \int dE_m e^{-i\epsilon_1(t_1-t_1')} e^{-iE_1(t_1'-t_2)} \ldots e^{-i\epsilon_m(t_m-t_m')} e^{-iE_m(t_m'-t_1)}$$
$$\alpha^{\sigma_1,\eta_1,\ldots,\sigma_m,\eta_m}_{r_1,\ldots,r_m}(\epsilon_1,E_1,\ldots,\epsilon_m,E_m) \qquad \text{(A.23)}$$

with

$$\alpha^{\sigma_1,\eta_1,\ldots,\sigma_m,\eta_m}_{r_1,\ldots,r_m}(\epsilon_1,E_1,\ldots,\epsilon_m,E_m) = \sum_n \sum_{k_1 q_1} \ldots \sum_{k_m q_m}$$
$$f^{\sigma_1}_{r_1}(\epsilon_1) T^{r_1 n}_{k_1 q_1} \delta(\epsilon_1 - \epsilon_{k_1 n r_1}) f^{\eta_1}(E_1) T^{*\,r_2 n}_{k_2 q_1} \delta(E_1 - \epsilon_{q_1 n})$$
$$f^{\sigma_2}_{r_2}(\epsilon_2) T^{r_2 n}_{k_2 q_2} \delta(\epsilon_2 - \epsilon_{k_2 n r_2}) f^{\eta_2}(E_2) T^{*\,r_3 n}_{k_3 q_2} \delta(E_2 - \epsilon_{q_2 n})$$
$$\ldots$$
$$f^{\sigma_m}_{r_m}(\epsilon_m) T^{r_m n}_{k_m q_m} \delta(\epsilon_m - \epsilon_{k_m n r_m}) f^{\eta_m}(E_m) T^{*\,r_1 n}_{k_1 q_m} \delta(E_m - \epsilon_{q_m n}) \; . \qquad \text{(A.24)}$$

The simplest loops consist of two lines with energies ϵ and E. One energy integration in Eq. (A.23) can be performed without encountering the exponentials including the times. We therefore replace the simple loop by a single line carrying the energy $\omega = \epsilon - E$ by defining

$$\alpha^{\pm}_r(\omega) = \int dE \; \alpha^{\pm,\mp}_r(\omega + E, E) \; . \qquad \text{(A.25)}$$

Assuming constant tunneling matrix elements $T^{rn} = T^{rn}_{kl}$ and neglecting the energy dependences of the density of states $N^n_r(\epsilon), N^n_I(E)$ in the leads and the island, we obtain

$$\alpha^{\pm}_r(\omega) = \pm\alpha^r_0 \frac{\omega - \mu_r}{\exp[\pm\beta(\omega - \mu_r)] - 1} \qquad \text{(A.26)}$$

in which

$$\alpha^r_0 = \sum_n |T^{rn}|^2 N^n_r(0) N^n_I(0) = \frac{1}{4\pi^2}\frac{R_K}{R_r} \qquad \text{(A.27)}$$

is the ratio of the quantum resistance $R_K = h/e^2$ to the tunneling resistance R_r of barrier r.

Appendix B

Solution of the Integral Equation

In this appendix, we calculate the imaginary part $\mathrm{Im}\,\phi(\omega)$, when $\phi(\omega)$ satisfies the integral equation

$$[\pi(\omega)]^{-1}\phi(\omega) = h(\omega) - \gamma(\omega)\int d\omega' \frac{1}{\omega - \omega' + i\eta}\phi^*(\omega') \tag{B.1}$$

with inhomogeneity $h(\omega)$,

$$\pi(\omega) = \frac{1}{\omega - \epsilon - \sigma(\omega)} \qquad \text{and} \qquad \sigma(\omega) = \int d\omega' \frac{\gamma(\omega')}{\omega - \omega' + i\eta}\,. \tag{B.2}$$

The relation $\frac{1}{x+i\eta} = P\left(\frac{1}{x}\right) - i\pi\delta(x)$, in which P denotes Cauchy's principal value, implies $\mathrm{Im}\,[\pi(\omega)]^{-1} = -\mathrm{Im}\,\sigma(\omega) = \pi\gamma(\omega)$. The imaginary part of Eq. (B.1) is an integral equation for $\mathrm{Im}\,\phi(\omega)$:

$$[\omega - \epsilon - \mathrm{Re}\,\sigma(\omega)]\mathrm{Im}\,\phi(\omega) = \gamma(\omega)P\int d\omega' \frac{1}{\omega - \omega'}\,\mathrm{Im}\,\phi(\omega')\,. \tag{B.3}$$

The function $\sigma(\omega)$ and therefore $\pi(\omega)$ as well is an analytic function in the upper complex half plane and decays fast enough for $|\omega| \to \infty$, so that the Kramers-Kronig relation yields

$$\pi(\omega) = -\frac{1}{i\pi}P\int d\omega' \frac{\pi(\omega')}{\omega - \omega'}\,. \tag{B.4}$$

The ansatz $\mathrm{Im}\,\phi(\omega) = c\,\mathrm{Im}\,\pi(\omega)$ satisfies Eq. (B.3), which is proved as follows:

$$\begin{aligned}[\omega - \epsilon - \mathrm{Re}\,\sigma(\omega)]\mathrm{Im}\,\pi(\omega) &= \mathrm{Re}\,[\pi(\omega)]^{-1}\,\mathrm{Im}\,\pi(\omega) = \\ -\mathrm{Im}\,[\pi(\omega)]^{-1}\,\mathrm{Re}\,\pi(\omega) &= \gamma(\omega)P\int d\omega' \frac{1}{\omega - \omega'}\,\mathrm{Im}\,\pi(\omega')\,.\end{aligned} \tag{B.5}$$

To determine the constant c, we multiply Eq. (B.1) by $\pi(\omega)/\gamma(\omega)$, integrate over ω and take the imaginary part. We get

$$\int d\omega\,\frac{\mathrm{Im}\,\phi(\omega)}{\gamma(\omega)} = \int d\omega\,\frac{\mathrm{Im}\,\pi(\omega)}{\gamma(\omega)}h(\omega) - \mathrm{Im}\int d\omega\,\pi(\omega)\int d\omega' \frac{1}{\omega - \omega' + i\eta}\phi^*(\omega')\,. \tag{B.6}$$

The integration over a function which is analytical in the upper complex half plane and decays fast enough for $|\omega| \to \infty$ gives zero and therefore the third term vanishes. Using the ansatz, we can evaluate the constant c and finally find the imaginary part of the solution of Eq. (B.1) as

$$\text{Im}\,\phi(\omega) = -\pi \frac{\int d\omega' h(\omega')|\pi(\omega')|^2}{\int d\omega' |\pi(\omega')|^2} \gamma(\omega)|\pi(\omega)|^2 \,. \tag{B.7}$$

Appendix C

Calculation of $\sigma(\omega)$

Here, we give a sketch of the calculation of $\sigma(\omega)$.

C.1 Quantum Dot

The self-energy is given by $\sigma(\omega) = \sum_{r=L,R} \sigma_r(\omega)$ with

$$\sigma_r(\omega) = M\sigma_r^+(\omega) + \sigma_r^-(\omega) \qquad \text{and} \qquad \sigma_r^\pm(\omega) = \int d\omega' \frac{\gamma_r^\pm(\omega')}{\omega - \omega' + i\eta}\,. \tag{C.1}$$

In order to make these integrals convergent, we introduce a Lorentzian cutoff

$$D_r(\omega) = \frac{E_C^2}{(\omega - \mu_r)^2 + E_C^2} \tag{C.2}$$

with $E_C = U/2$. After doing so, the integrand decays fast enough for $|\omega| \to \infty$ to close the integration contour in the upper or lower complex half plane and apply Cauchy's Theorem by collecting all residua.

In the following, we calculate two linear combinations of $\sigma_r^+(\omega)$ and $\sigma_r^-(\omega)$. One of them can be easily evaluated by closing the integration contour in the lower half plane, where there is a pole at $\omega' = \mu_r - iE_C$:

$$\sigma_r^+(\omega) + \sigma_r^-(\omega) = \frac{\Gamma_r}{2\pi} \int d\omega' D_r(\omega') \frac{1}{\omega - \omega' + i\eta} = \frac{\Gamma_r}{2} D_r(\omega) \left(\frac{\omega - \mu_r}{E_C} - i \right)\,. \tag{C.3}$$

For the other one, we choose

$$\sigma_r^+(\omega) - \sigma_r^-(\omega) = -\frac{\Gamma_r}{2\pi} \int d\omega' D_r(\omega') \frac{\tanh[\frac{\beta}{2}(\omega - \mu_r)]}{\omega - \omega' + i\eta}\,. \tag{C.4}$$

The integrand has poles at $\omega' = \mu_r \pm iE_C$, at $\omega' = \omega + i\eta$ and at $\omega' = \omega_m \equiv (2m+1)\pi i/\beta + \mu_r$ for $m = 0, \pm 1, \pm 2, \ldots$.

Closing the integration contour in the upper and lower half plane and taking the average of these two terms, Cauchy's Theorem yields

$$\sigma_r^+(\omega) - \sigma_r^-(\omega) = \frac{i\Gamma_r}{2}\left\{ D_r(\omega)\left[\tanh\left(\frac{\beta}{2}(\omega-\mu_r)\right) - \tanh\left(i\frac{\beta}{2}E_C\right)\right] \right. \\ \left. -\frac{2}{\beta}\sum_{m=0}^{\infty}\left[D_r(\omega_m)\frac{1}{\omega-\omega_m} - D_r(\omega_{-m-1})\frac{1}{\omega-\omega_{-m-1}}\right]\right\} . \tag{C.5}$$

We use the digamma function $\psi(z) = d[\ln\Gamma(z)]/dz$ and its representation [45]

$$\psi(x) - \psi(y) = \sum_{m=0}^{\infty}\left(-\frac{1}{m+x} + \frac{1}{m+y}\right) . \tag{C.6}$$

Furthermore, we use $\psi(z^*) = [\psi(z)]^*$ and $\psi(\frac{1}{2} - z) = \psi(\frac{1}{2} + z) + i\pi\tanh(i\pi z)$ and arrive at

$$\sigma_r^+(\omega) - \sigma_r^-(\omega) = \frac{\Gamma_r}{2\pi}D_r(\omega)\left\{2\psi\left(\frac{1}{2}+\frac{\beta E_C}{2\pi}\right) - 2\mathrm{Re}\,\psi\left(\frac{1}{2}+i\frac{\beta}{2\pi}(\omega-\mu_r)\right) \right. \\ \left. +i\pi\tanh\left(\frac{\beta}{2}(\omega-\mu_r)\right)\right\} . \tag{C.7}$$

The sum and the difference of Eqs. (C.3) and (C.7) leads to the result

$$\sigma_r^{\pm}(\omega) = \frac{\Gamma_r}{2\pi}D_r(\omega)\left\{\pm\psi\left(\frac{1}{2}+\frac{\beta E_C}{2\pi}\right) \mp \mathrm{Re}\,\psi\left(\frac{1}{2}+i\frac{\beta}{2\pi}(\omega-\mu_r)\right) \right. \\ \left. +\pi\frac{\omega-\mu_r}{2E_C} - i\pi f_r^{\pm}(\omega)\right\} \tag{C.8}$$

and therefore

$$\sigma_r(\omega) = \frac{\Gamma_r}{2\pi}D_r(\omega)\left\{(M-1)\psi\left(\frac{1}{2}+\frac{\beta E_C}{2\pi}\right) - (M-1)\mathrm{Re}\,\psi\left(\frac{1}{2}+i\frac{\beta}{2\pi}(\omega-\mu_r)\right) \right. \\ \left. +(M+1)\pi\frac{\omega-\mu_r}{2E_C} - i\pi\left[1+(M-1)f_r(\omega)\right]\right\} . \tag{C.9}$$

The cutoff parameter E_C dominates always over all other energies. In the limit $E_C \gg \max\{\omega, k_BT, eV\}$ the self-energy reduces to

$$\sigma_r(\omega) = \frac{\Gamma_r}{2\pi}\left\{(M-1)\ln\left(\frac{\beta E_C}{2\pi}\right) - (M-1)\mathrm{Re}\,\psi\left(\frac{1}{2}+i\frac{\beta}{2\pi}(\omega-\mu_r)\right) \right. \\ \left. -i\pi\left[1+(M-1)f_r(\omega)\right]\right\} . \tag{C.10}$$

C.2 Metallic Island

The self-energy now reads $\sigma(\omega) = \sum_{r=L,R} \sigma_r(\omega)$ with

$$\sigma_r(\omega) = \sigma_r^+(\omega) + \sigma_r^-(\omega) \qquad \text{and} \qquad \sigma_r^\pm(\omega) = \int d\omega' \frac{\alpha_r^\pm(\omega')}{\omega - \omega' + i\eta} \,. \tag{C.11}$$

For the calculation, we again make use of the cutoff

$$D_r(\omega) = \frac{E_C^2}{(\omega - \mu_r)^2 + E_C^2} \,. \tag{C.12}$$

In order to determine $\sigma_r^+(\omega)$ and $\sigma_r^-(\omega)$, we consider two linear combinations. One of them can be easily evaluated by closing the integration contour in the lower half plane, where there is a pole at $\omega' = \mu_r - iE_C$:

$$\sigma_r^+(\omega) - \sigma_r^-(\omega) = -\int d\omega' D_r(\omega') \alpha_0^r \frac{\omega' - \mu_r}{\omega - \omega' + i\eta} = \pi \alpha_0^r D_r(\omega) \left[E_C + i(\omega - \mu_r) \right] . \tag{C.13}$$

In this work, we need only an other one, namely

$$\sigma_r^+(\omega) + \sigma_r^-(\omega) = \int d\omega' D_r(\omega') \frac{\alpha_0^r (\omega - \mu_r) \coth[\frac{\beta}{2}(\omega - \mu_r)]}{\omega - \omega' + i\eta} \,. \tag{C.14}$$

The integrand has poles at $\omega' = \mu_r \pm iE_C$, at $\omega' = \omega + i\eta$ and at $\omega' = \omega_m \equiv 2m\pi i/\beta + \mu_r$ for $m = \pm 1, \pm 2, \ldots$.

Closing the integration contour in the upper and lower half plane and taking the average of these two terms, Cauchy's Theorem yields

$$\begin{aligned} \sigma_r(\omega) = -i\pi\alpha_0^r \Bigg\{ & D_r(\omega)(\omega - \mu_r) \left[\coth\left(\frac{\beta}{2}(\omega - \mu_r) \right) - \coth\left(i\frac{\beta}{2} E_C \right) \right] \\ & - \frac{2}{\beta} \sum_{m=0}^{\infty} \left[D_r(\omega_m) \frac{\omega_m - \mu_r}{\omega - \omega_m} - D_r(\omega_{-m}) \frac{\omega_{-m} - \mu_r}{\omega - \omega_{-m}} \right] \Bigg\} \,. \end{aligned} \tag{C.15}$$

Also here, we use the digamma function $\psi(z)$ and its property $\psi(-z) = \psi(1+z) + i\pi \coth(i\pi z)$ and arrive at

$$\begin{aligned} \sigma_r(\omega) = -\alpha_0^r D_r(\omega)(\omega - \mu_r) \Bigg\{ & \psi\left(\frac{\beta E_C}{2\pi} \right) + \psi\left(1 + \frac{\beta E_C}{2\pi} \right) \\ & - 2\mathrm{Re}\, \psi\left(i\frac{\beta}{2\pi}(\omega - \mu_r) \right) + i\pi \coth\left(\frac{\beta}{2}(\omega - \mu_r) \right) \Bigg\} \,. \end{aligned} \tag{C.16}$$

In the limit $E_C \gg \max\{\omega, k_B T, eV\}$ the self-energy reduces to

$$\begin{aligned} \sigma_r(\omega) = -\alpha_0^r(\omega - \mu_r) \Bigg\{ & 2\ln\left(\frac{\beta E_C}{2\pi} \right) - 2\mathrm{Re}\, \psi\left(i\frac{\beta}{2\pi}(\omega - \mu_r) \right) \\ & + i\pi \coth\left(\frac{\beta}{2}(\omega - \mu_r) \right) \Bigg\} \,. \end{aligned} \tag{C.17}$$

Appendix D

Quantum Dot with One Non-Degenerate Level

All results in this work are calculated by summing a certain class of diagrams: any vertical line will cut at most two tunneling lines. The contribution of other diagrams is neglected. For the quantum dot with one non-degenerate level, however, the sum of all more complicated diagrams is exactly zero. This can be seen in the following way:

Take such a more complicated diagram. Consider the rightmost place with three tunneling lines (see Fig. D.1). There is a vertex, where a tunneling line enters from or leaves to the left. Furthermore, two tunneling lines pass, one of them running from the left to right, and one running from the right to the left. Up to the next vertex on the right, the upper and lower propagator is labeled by the same state $n = 0$ or $n = 1$. Thus, the resolvent between these two vertices contains no term for the dot energy. Now we construct a new diagram by changing the position of these two vertices from the lower to the upper propagator and vice versa (see Fig. D.1). Due to this procedure, the absolute value of the diagram is not changed. The number of crossings of tunneling lines, however, increases or decreases by 1, which induces a factor -1. Therefore, the sum of both diagrams is exactly zero. Consequently, all formulas for the quantum dot presented in this work are no approximation for the non-degenerate case but are exact results, and for the spectral density, we recover the well-known Breit-Wigner formula.

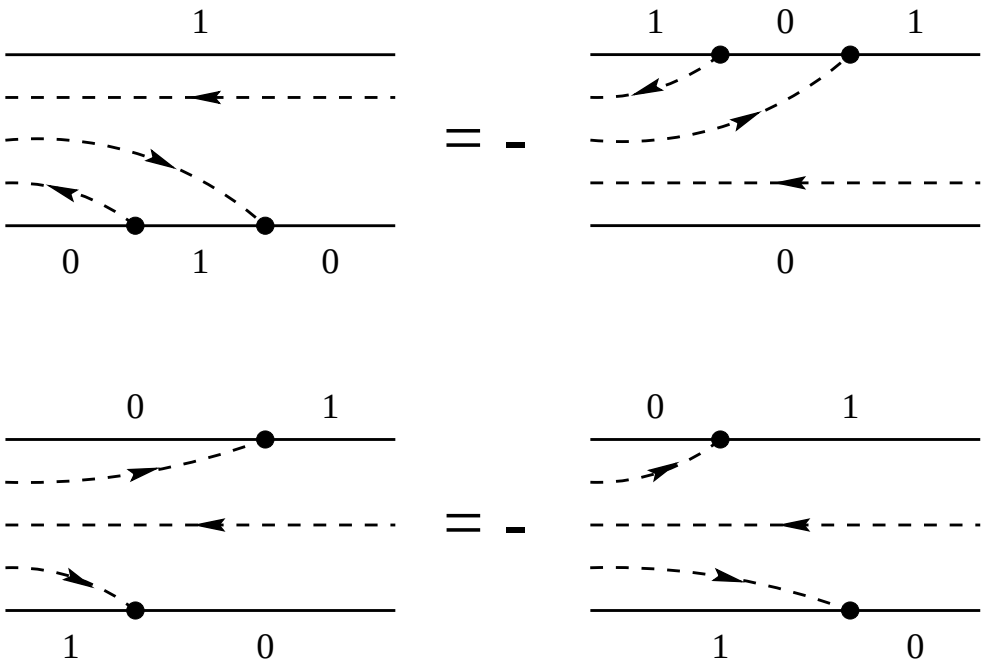

Figure D.1: Changing the position of the two vertices gives a new possible diagram and implies a minus sign.

Appendix E

Deutsche Zusammenfassung

Elektronischer Quantentransport durch mesoskopische Inseln war Gegenstand ausgedehnter experimenteller und theoretischer Untersuchungen. Er umfaßt den Transport durch diskrete Energieniveaus in Quantenpunkten sowie den Transport durch ein Kontinuum von Energieniveaus in kleinen metallischen Inseln. Ein Quantenpunkt ist in strukturierten zweidimensionalen Elektronengasen (2 DEG) in Halbleiter-Heterostrukturen wie z.B. GaAs/$Al_xGa_{1-x}As$ realisiert. Kürzlich ist es möglich geworden, Tunnelsysteme mit ultrakleinen Metallpartikeln herzustellen, die diskrete elektronische Zustände zeigen.

Modellsysteme sind die Elektronenbox und der Einzelelektronentransistor. Die Box besteht aus einer kleinen Insel, die über einen Tunnelkontakt an eine Zuleitung gekoppelt ist. Sie ist zusätzlich kapazitiv an eine Spannungsquelle, das Gate, gekoppelt. Der Einzelelektronentransistor besteht aus einer kleinen Insel, die über Tunnelkontakte an zwei Zuleitungen gekoppelt ist. Eine angelegte Transportspannung treibt einen Strom durch das System. Auch hier ist die Insel kapazitiv an eine Gate-Spannungsquelle gekoppelt. Die geringe Größe des Systems führt zu einer kleinen Inselkapazität C. Die Coulomb-Wechselwirkung der Elektronen auf der Insel wird deshalb relevant. Diese Wechselwirkung wird durch die elektrostatischen Energie des Gesamtsystems, der *Ladungsenergie* $E_{ch}(n) = E_C(n - n_x)^2$ mit $E_C \equiv e^2/2C$, beschrieben. Die Ladungsenergie hängt von der Zahl der Überschußelektronen n auf der Insel und der kontinuierlich veränderbaren Variablen n_x ab, die mit Hilfe der Gatespannung gesteuert werden kann. Bei tiefen Temperaturen richtet sich die Zahl der Überschußelektronen auf der Insel so ein, daß die Ladungsenergie minimal ist. Sie erhöht sich daher stufenweise mit zunehmender Gatespannung um je eins.

In Störungstheorie niedrigster Ordnung sind Tunnelprozesse nur möglich, wenn entweder die Temperatur oder die Transportspannung ausreichend ist, um den Energieunterschied zweier benachbarter Ladungszustände zu überwinden. Der Transport bei niedrigen Temperaturen und Spannungen (d.h. für $k_BT \ll E_C$ und $eV \ll E_C$) hängt deshalb stark von der Gatespannung ab. Er kann erlaubt oder unterdrückt (*Coulomb Blockade*) sein. Der differentielle Leitwert als Funktion von der Gatespannung zeigt daher in linearer Antwort eine Reihe von Peaks (*Coulomb Oszilla-*

tionen). In nichtlinearer Antwort, d.h. für größere Transportspannungen, zeigen diese Peaks zusätzliche Strukturen.

Eine Beschreibung von sequentiellem Tunneln mit Hilfe einer Master-Gleichung ist ausreichend, solange die Kopplung der Zuleitungen an die Insel schwach und Temperatur und Transportspannung nicht zu klein sind. Dann findet der Transport als Abfolge unkorrelierter Prozesse statt. In einem Prozeß tunnelt ein Elektron von der Zuleitung mit dem höherem elektrochemischen Potential auf die Insel. Danach geht, in einem zweiten Prozeß, ein Elektron von Insel auf die Zuleitung mit dem niedrigeren elektrochemischen Potential. Auf diese Weise wird ein Elektron nach dem anderen transferiert. Dabei werden zwei benachbarte Ladungszustände miteinbezogen. Die zu den Prozessen gehörigen Raten erhält man in Störungstheorie niedrigster Ordnung in den Tunnelamplituden. Die Master-Gleichung erlaubt uns dann, die Wahrscheinlichkeit für verschiedene Inselzustände und den Strom durch das System zu berechnen.

Im allgemeinen sollten Quantenfluktuationen und kohärente Prozesse höherer Ordnung betrachten werden. Dies beinhaltet "Cotunneln", bei dem in einem kohärenten Prozeß zweiter Ordnung Elektronen über einen virtuellen Zustand der Insel direkt von einer Zuleitung zur anderen tunneln und so die Coulomb Blockade umgehen. Weiterhin spielt "Resonanztunneln" eine Rolle. Es beinhaltet kohärente Prozesse mit beliebig vielen Tunnelereignissen in beiden Kontakten. Im Vergleich zum wohlbekannten Resonanztunneln eines einzelnen Elektrons stößt man hier auf zwei Schwierigkeiten. Zum einen beeinhalten metallische Systeme mit kontinuierlichem Anregungsspektrum viele Elektronen, so daß mit überwältigender Wahrscheinlichkeit verschiedene Elektronenzustände in den verschiedenen Übergängen eines kohärenten Prozesses involviert sind. Zum anderen ist der Einfluß der Coulomb Wechselwirkung stark und kann deshalb nicht in Störungstheorie behandelt werden.

Wir unterscheiden zwei Klassen von Tunnelprozessen höherer Ordnung: bleibt nach dem Gesamtprozeß keine Elektron-Loch-Anregung auf der Insel zurück, so nennen wir ihn *elastisch*, andernfalls *inelastisch*. Während in metallischen Systemen inelastische Prozesse dominieren, sind in Quantenpunkten mit großem Niveauabstand elastische Prozesse wichtiger.

Der Quantenpunkt mit nur einem Energieniveau ist äquivalent zum Anderson-Modell. Liegt das Niveau weit unterhalb der Ferminiveaus der Zuleitungen, so kann das Anderson-Modell mittels einer Schrieffer-Wolff-Transformation auf das Kondo-Modell abgebildet werden, welches die Streuung von Elektronen in einem Metall an dem Spin einer magnetischen Störstelle beschreibt. Für tiefe Temperaturen führt die Wechselwirkung des Spins der Leitungselektronen mit dem Spin der Störstelle zu einem Anstieg des Widerstandes (Kondo-Effekt). Im Anderson-Modell zeigt sich der Kondo-Effekt in der Erhöhung der Transmittivität durch den Quantenpunkt, was durch eine Spektraldichte mit scharfen Resonanzen an den Fermi-Niveaus der Zuleitungen ausgedrückt wird. Das Verständnis diese Effekts erfordert eine Untersuchung jenseits der Störungstheorie, d.h. erst Resonanztunnelprozesse geben eine ausreichende Erklärung.

Eine Beschreibung, die eine systematische Klassifikation all dieser Prozesse erlaubt, ist notwendig. Im Fall eines einzelnen Energieniveaus sollte auch die Beschreibung des Kondo-Effekts, verallgemeinert auf Nichtgleichgewichtssituationen, beinhaltet sein.

Der Zweck dieser Arbeit ist es, eine systematische diagrammatische Technik zu entwickeln, um die Prozesse des Einzelelektronentunnelns, Cotunnelns und Resonanztunnelns zu identifizieren und ihren Einfluß auf die Transporteigenschaften des Einzelelektronentransistors zu untersuchen. Die Beschreibung des Systems basiert auf einem Standard-Tunnel-Hamiltonoperator. Wir betrachten den reduzierten Propagator, der die Zeitentwicklung der Dichtematrix bestimmt. Dabei verwenden wir eine Vielteilchen-Expansions-Methode. Für metallische Systeme benutzen wir einen alternativen Zugang in einer Realzeit-Pfadintegral-Darstellung. Letztere ist von der Untersuchung eines an ein Bad harmonischer Oszillatoren gekoppelten Quantensystems und der Beschreibung von Elektronentunneln bekannt.

Die Quantenfluktuationen, die durch Resonanztunnelprozesse repräsentiert werden, beeinflussen die Spektraldichte, die die Anregungen des Systems beschreibt. Real- und Imaginärteil einer energieabhängigen Selbstenergie bewirken Renormierungs- und Verbreiterungseffekte. Es zeigt sich Kondo-Physik, was durch logarithmische Singularitäten im Realteil der Selbstenergie angezeigt wird. Die uns interessierenden physikalischen Größen, die Wahrscheinlichkeitsverteilung der Inselzustände und der Strom durch das System können in Abhängigkeit von der Spektraldichte ausgedrückt werden. Sie zeigen daher auch Renormierungs- und Verbreiterungseffekte.

Diese Arbeit gliedert sich wie folgt:

In Kapitel 2 wird eine Beschreibung des Einzelelektronentransistors sowie ein qualitatives Bild seiner Transporteigenschaften wird in Kapitel 2 gegeben. Wir führen den Tunnel-Hamiltonoperator für die beiden Grenzfälle eines diskreten und eines kontinuierlichen Anregungsspektrums ein.

In Kapitel 3 entwickeln wir den reduzierten Propagator nach dem Tunnelanteil des Hamiltonoperators und beschreiben jeden Term der Entwicklung mit Hilfe einer diagrammatischen Sprache. Alle erwähnten Tunnelprozesse können mit entsprechenden Diagrammen in Beziehung gebracht werden.

In Kapitel 4 und Kapitel 5 leiten wir analytische Formeln für die Spektraldichte und damit auch für die mittlere Inselladung und den Strom durch das System ab. Dazu verwenden wir ein systematisches Kriterium, um die wichtigste Klasse von Diagrammen auszuwählen und all diese Beiträge aufzusummieren.

Der Einfluß von Renormierungs- und Verbreiterungseffekten auf die interessierenden physikalischen Größen wird in Kapitel 6 diskutiert. Ein Ergebnis ist, daß die Schaubilder der mittleren Inselladung und des differentiellen Leitwerts als Funktion von der Gatespannung ausgewaschen sind. Außerdem ist für Systeme mit diskreten Energieniveaus die gesamte Kurve verschoben. In diesem Fall führen die Quantenfluktuationen auch zum Kondo-Effekt. Wir sehen für ein tiefliegendes Energieniveau scharfe Resonanzen an den Ferminiveaus. Sie führen zu einem Anstieg des Leitwerts

bei verschwindender Transportspannung (Zero-Bias Maximum). Interessanterweise finden wir jedoch für ein Energieniveau nahe bei oder oberhalb der Ferminiveaus, daß die logarithmischen Terme im Realteil der Selbstenergie weiterhin wichtig sind und zu einer Inversion der gesamten Struktur im Leitwert, d.h. einem Zero-Bias Minimum, führen.

Die hier vorgestellte diagrammatische Technik ist sehr allgemein und kann daher auch auf komplexere Systeme angewendet werden. In Kapitel 7 diskutieren wir beispielhaft eine Ausdehnung der Methode auf einen Quantenpunkt mit bosonischen Wechselwirkungen. Die Bosonen bewirken eine weitere Aufspaltung der Kondo-Peaks, der Leitwert als Funktion der Gatespannung zeigt neue Seitenpeaks, und die Zero-Bias Extrema werden durch Nebenextrema vervollständigt. Bemerkenswerterweise finden wir aufgrund der unterschiedlichen Emissions- und Absorptionswahrscheinlichkeit der Bosonen selbst im Fall eines nichtentarteten Niveaus Kondo-Peaks.

In den Anhängen werden einige technische Details bezüglich der Herleitung der effektiven Wirkung für metallische Systeme, der Lösung der in Kapitel 4 auftauchenden Integralgleichung, der Berechnung der Selbstenergie und des Spezialfalls eines Quantenpunktes mit einem nichtentarteten Niveau präsentiert.

Bibliography

[1] D.V. Averin and K.K. Likharev, in *Mesoscopic Phenomena in Solids*, ed. B.L. Altshuler et al. (Elsevier, 1991), p. 173

[2] *Single Charge Tunneling*, NATO ASI Series **294**, H. Grabert and M.H. Devoret, eds., (Plenum Press, 1992)

[3] Z. Phys. B **85**, 317 (1991), special issue on single charge tunneling

[4] D.V. Averin, A.N. Korotkov, and K.K. Likharev, Phys. Rev. B **44**, 6199 (1991)

[5] C.W.J. Beenakker, Phys. Rev. B **44**, 1646 (1991)

[6] L.I. Glazman and K.A. Matveev, JETP Lett **48**, 445 (1988)

[7] C. Bruder and H. Schoeller, Phys. Rev. Lett. **72**, 1076 (1994)

[8] T.K. Ng and P.A. Lee, Phys. Rev. Lett. **61**, 1768 (1988)

[9] L.I. Glazman and M.E. Raikh, JETP Lett. **47**, 452 (1988)

[10] S. Hershfield, J.H. Davies, and J.W. Wilkins, Phys. Rev. Lett. **67**, 3720 (1991)

[11] Y. Meir, N.S. Wingreen, and P.A. Lee, Phys. Rev. Lett. **70**, 2601 (1993); N.S. Wingreen and Y. Meir, Phys. Rev. B **49**, 11040 (1994)

[12] M.H. Hettler and H. Schoeller, Phys. Rev. Lett. **74**, 4907 (1995)

[13] P. Gueret, N. Blank, R. Germann, and H. Rothuizen, Phys. Rev. Lett. **68**, 1896 (1992)

[14] A.T. Johnson, L.P. Kouwenhoven, W. de Jong, N.C. van der Vaart, C.J.P.M. Harmans, and C.T. Foxon, Phys. Rev. Lett. **69**, 1592 (1992)

[15] E.B. Foxman, P.L. McEuen, U. Meirav, N.S. Wingreen, Y. Meir, P.A. Belk, N.R. Belk, M.A. Kastner, and S.J. Wind, Phys. Rev. B **47**, 10020 (1993)

[16] J. Weis, R.J. Haug, K. v. Klitzing, and K. Ploog, Phys. Rev. B **46**, 12837 (1992)

[17] D.C. Ralph, C.T. Black and M. Tinkham, Phys. Rev. Lett. **74**, 3241 (1995)

[18] G. Schön and A.D. Zaikin, Phys. Rep. **198**, 237 (1990)

[19] D.S. Golubev and A.D. Zaikin, Phys. Rev. B **50**, 8736 (1994)

[20] H. Grabert, Phys. Rev. B **50**, 17364 (1994)

[21] G. Falci, G. Schön and G.T. Zimanyi, Phys. Rev. Lett. **74**, 3257 (1995)

[22] H. Schoeller and G. Schön, Phys. Rev. B **50**, 18436 (1994)

[23] D.V. Averin and Yu.V. Nazarov, Chapter 6 in Ref. [2]

[24] J. König, H. Schoeller, G. Schön, and R. Fazio in *Quantum Dynamics of Submicron Structures*, ed. H. A. Cerdeira, B. Kramer and G. Schön, NATO ASI Series **E 291** (Kluwer, Dordrecht, 1995), p.221

[25] J. König, H. Schoeller, and G. Schön, Europhys. Lett. **31**, 31 (1995)

[26] J. König, H. Schoeller, and G. Schön, to be published in Festkörperprobleme

[27] J. König, H. Schoeller, and G. Schön, submitted to Phys. Rev. Lett.

[28] R.P. Feynman and F.L. Vernon, Ann. Phys. (N.Y.) **24**, 118 (1963)

[29] A.O. Caldeira and A.J. Leggett, Ann. Phys. (N.Y.) **149**, 374 (1983)

[30] U. Eckern, G. Schön and V. Ambegaokar, Phys. Rev. B **30**, 6419 (1984)

[31] N.S. Wingreen, K.W. Jacobsen, and J.W. Wilkins, Phys. Rev. Lett. **61**, 1396 (1988)

[32] L.I. Glazman and R.I. Shekhter, Sov. Phys. JETP **67**, 163 (1988)

[33] M. Jonson, Phys. Rev. B **39**, 5924 (1989)

[34] H.T. Imam, V.V. Ponomarenko, and D.V. Averin, Phys. Rev. B **50**, 18288 (1994)

[35] J. Stampe and H. Schoeller, unpublished.

[36] A.G.M. Jansen, A.P. van Gelder, P. Wyder, and S. Strassler, J. Phys. F **11**, L15 (1981)

[37] D.C. Ralph and R.A. Buhrman, Phys. Rev. Lett. **69**, 2118 (1992);
D.C. Ralph and R.A. Buhrman, Phys. Rev. B **69**, 3554 (1995)

[38] D.C. Ralph, A.W.W. Ludwig, J. von Delft and R.A. Buhrman, Phys. Rev. Lett. **72**, 1064 (1994).

[39] M.H. Hettler, J. Kroha, and S. Hershfield, Phys. Rev. Lett. **73**, 1967 (1994).

[40] N.S. Wingreen, B.L. Altshuler and Y. Meir, unpublished.

[41] D.C. Ralph and R.A. Buhrman, Phys. Rev. Lett. **72**, 3401 (1994).

[42] G.D. Mahan, *Many-Particle Physics*, (Plenum, 1990).

[43] H. Kleinert, Fortschritte der Physik **26**, 565 (1978)

[44] I.S. Gradstein und I.M. Ryshik, *Summen-, Produkt- und Integraltafeln*, (Verlag Harri Deutsch, 1981)

[45] M. Abramowitz and I. Stegun, *Handbook of Mathematical Functions*, Dover Publ. Inc.